Laboratory Experiments on Bentonite Samples: FY16 Progress

Fuel Cycle Research & Development

Prepared for
U.S. Department of Energy
Used Fuel Disposition Campaign
Ruth M. Tinnacher
Christophe Tournassat
James A. Davis

Lawrence Berkeley National Laboratory
August 2016

FCRD-UFD-2016-000627
LBNL-1006053

Revision 2
12/20/2012

APPENDIX E

FCT DOCUMENT COVER SHEET [1]

Name/Title of Deliverable/Milestone/Revision No.	Laboratory Experiments on Bentonite Samples: FY16 Progress
Work Package Title and Number	DR Crystalline Disposal R&D – LBNL FT-16LB08030304
Work Package WBS Number	1.02.08.03.03
Responsible Work Package Manager	Liange Zheng (signature on file) (Name/Signature)

Date Submitted 08/22/2016

Quality Rigor Level for Deliverable/Milestone[2]	☒ QRL-3	☐ QRL-2	QRL-1 ☐ Nuclear Data	☐ Lab/Participant QA Program (no additional FCT QA requirements)

This deliverable was prepared in accordance with Lawrence Berkeley National Laboratory
(Participant/National Laboratory Name)

QA program which meets the requirements of
☒ DOE Order 414.1 ☐ NQA-1-2000 ☐ Other

This Deliverable was subjected to:

☒ Technical Review ☐ Peer Review

Technical Review (TR)

Review Documentation Provided

☐ Signed TR Report or,
☐ Signed TR Concurrence Sheet or,
☒ Signature of TR Reviewer(s) below

Peer Review (PR)

Review Documentation Provided

☐ Signed PR Report or,
☐ Signed PR Concurrence Sheet or,
☐ Signature of PR Reviewer(s) below

Name and Signature of Reviewers

Patricia Fox (signature on file)

NOTE 1: *Appendix E should be filled out and submitted with the deliverable. Or, if the PICS:NE system permits, completely enter all applicable information in the PICS:NE Deliverable Form. The requirement is to ensure that all applicable information is entered either in the PICS:NE system or by using the FCT Document Cover Sheet.*

NOTE 2: *In some cases there may be a milestone where an item is being fabricated, maintenance is being performed on a facility, or a document is being issued through a formal document control process where it specifically calls out a formal review of the document. In these cases, documentation (e.g., inspection report, maintenance request, work planning package documentation or the documented review of the issued document through the document control process) of the completion of the activity along with the Document Cover Sheet is sufficient to demonstrate achieving the milestone. If QRL 1, 2, or 3 is not assigned, then the Lab/Participant QA Program (no additional FCT QA requirements box must be checked, and the work is understood to be performed, and any deliverable developed, in conformance with the respective National Laboratory/Participant, DOE- or NNSA-approved QA Program.*

PROJECT SUMMARY

The long-term management of nuclear waste requires a systematic understanding of the underlying processes controlling the release and transport of radioactive contaminants in the environment. The potential mobility of uranium(VI) is especially important, since uranium is the primary component in spent nuclear fuel, and the release of other radioisotopes will be driven by uranium dissolution and its diffusive transport away from the fuel matrix.

For many nuclear waste storage scenarios, bentonite and clays are either the host rock media, or the proposed backfill material in Engineered Barrier Systems (EBS), in close contact with waste containers. Hence, accurate predictions of uranium(VI) transport behavior in the near- and far-fields will be dependent on a realistic conceptual understanding of uranium(VI) diffusion in clays and bentonite close to the source term.

Uranium(VI) mobility on the field-scale is ultimately controlled by the parameters and processes effective at micro- and nanometer scales. First, uranium(VI) sorption onto bentonite and sodium-montmorillonite, its major mineralogical clay component, is an important, and potentially limiting, process affecting uranium(VI) fluxes (the mass of U(VI) transferred across cross-sectional area of the bentonite barrier over a specific time-period) and contaminant retardation. Second, the small-scale diffusion-accessible porosities of montmorillonite will largely determine the magnitude of uranium(VI) fluxes across the EBS. A prediction of uranium(VI) adsorption and diffusion processes in clay-rich media, however, is complicated by: (1) the complexity of the mineralogical structure of montmorillonite clay, in terms of its pore-size distributions, diffusion-accessible porosities, and available surface site types, and (2) the complex uranium(VI) solution speciation, which can include cationic, neutral, and anionic species, depending on chemical solution conditions.

Clay particles consist of stacks of negatively-charged smectite layers. This leads to two types of porosities: (1) large pores *between* clay particles, with little influence of electric-double-layer forces, and (2) very thin interlayer spaces *within* individual clay particles, where diffusion is impacted by surface charge and ionic strength. Furthermore, these two porous regimes provide different surface environments for contaminant sorption reactions. Electrostatic and hydration forces only are thought to govern *cation exchange reactions in interlayer spaces*, whereas chemical bonding with surface ligands is dominant for *surface complexation reactions at edge sites* of clay particles. Finally, a *'spillover' effect* may occur, where the electrostatic surface potential of basal cation exchange sites influences the surface potential of neighboring edge sites.

As sorption and diffusion processes are expected to take place differently in these two porosity volumes, this essentially creates two 'small-scale diffusion pathways', where each one becomes dominant under different system conditions. For instance, at high pH a partial or full exclusion of anions from negatively charged clay interlayer spaces could decrease the effective 'anion-accessible' porosity and diffusive flux under steady state conditions, while at low pH the 'surface diffusion' of weakly-adsorbed cations could increase the overall flux.

Changes in chemical solution composition (e.g., pH, calcium and bicarbonate concentrations, etc.) and temperature have to be expected across the EBS and as a function of time. These gradients can be caused by the presence of calcite impurities in the bentonite buffer, the vicinity of the EBS to concrete barriers or radiation heat released by nuclear waste packages. Variations in these parameters could dramatically affect uranium(VI) solution speciation, the type of clay surface sites predominantly involved in uranium(VI) sorption reactions, and the clay porosity accessible for uranium(VI) diffusion. Hence, predictive transport models need to be capable to include the potential impacts of these variable parameters on uranium(VI) sorption and diffusion behavior.

With regard to uranium-montmorillonite sorption models, simple models based on constant or a randomly sampled normal distribution of K_D values (sorption distribution constants) are not sufficient to capture the

system complexities, and the interdependencies between the various parameters and processes described above. In contrast, more complex surface complexation 'sub-models' can link chemical solution conditions with uranium solution speciation, clay surface properties and relevant sorption reactions, while still allowing for a calculation of K_D values at specific system conditions for incorporation into 'higher-level' performance models.

Previous U(VI)-montmorillonite adsorption and modeling studies have typically expanded classical surface complexation models, initially developed for simple oxides, to include both cation exchange and surface complexation reactions. With this approach, however, the unique characteristics of electrostatic surface potentials at montmorillonite edge sites, the spillover effect described above, and its effects on variable surface site characteristics as a function of chemical solution conditions, have not been taken into account. Nevertheless, given the importance of uranium(VI) sorption reactions for its overall diffusive transport behavior, a realistic representation of the U(VI)-montmorillonite system is needed in order to minimize the number of fitting parameters in diffusion models.

A second relevant process that could substantially lower U(VI) diffusive fluxes across the EBS, is the exclusion of anionic U(VI) solution species from montmorillonite interlayer spaces leading to a smaller diffusion-accessible porosity for uranium(VI). Anion exclusion effects in U(VI)-montmorillonite systems have been previously discussed in the literature, but no direct, experimental evidence from through-diffusion experiments has been reported until now.

Given these research needs, the primary goal of this study is to improve the understanding of U(VI) sorption and diffusion behavior in sodium-montmorillonite in order to support the development of realistic conceptual models describing these processes in performance assessment models while (1) accounting for potential changes in system conditions over time and space, (2) avoiding overly conservative transport predictions, and (3) using a minimum number of fitting parameters.

Our main objectives for FY 2016 included the following:

1. Develop a new type of U(VI)-montmorillonite surface complexation model that specifically accounts for the spillover effect (described above), and allows for a prediction of U(VI) sorption over a range of chemical solution conditions with a minimum number of fitting parameters. This model will be used to simulate U(VI) sorption behavior in U(VI)-montmorillonite diffusion models.
2. Complete a set of two, parallel uranium(VI) through-diffusion experiments, started during FY 2015, to investigate the relevance of a full or partial exclusion of anionic U(VI) solution species from sodium-montmorillonite interlayer spaces at alkaline pH. This was an approximately 20-week experiment with regard to the pH pre-equilibration of clay and the actual diffusion steps, followed by additional time commitments for the detailed characterization of the chemical composition of sample solutions. The latter is required for the later simulation of U(VI) solution speciation in diffusion models.

With regard to the first objective, a series of U(VI) – Na-montmorillonite batch adsorption experiments had been conducted as a function of pH, and with variable U(VI), Ca, and dissolved carbonate concentrations over the past fiscal years. Based on these experimental datasets, a new type of surface complexation model (SCM) was developed for montmorillonite that specifically accounts for the spillover effect using the edge surface speciation model by Tournassat et al. (2016a). This SCM allows for a prediction of U(VI) adsorption under varying chemical conditions with a minimum number of fitting parameters, not only for our own experimental results, but also for a number of other, previously published data sets. The model agreed well with many of these datasets without introducing a second site type or including the formation of ternary U(VI)-carbonato surface complexes. The model predictions were greatly impacted by utilizing analytical measurements of dissolved inorganic carbon (DIC) concentrations in individual sample solutions rather than assuming solution equilibration with a specific partial pressure of CO_2, even when the gas phase was laboratory air. Because of the formation of strong

aqueous U(VI)-carbonate solution complexes, the measurement of DIC concentrations was even important for systems set up in the 'absence' of CO_2, due to low levels of CO_2 contamination during the experiment.

For the second objective, U(VI) diffusion experiments at alkaline pH were continued until a sufficient number of data points had been collected under steady-state conditions for U(VI) diffusive flux. Sample solutions were characterized in terms of (1) solution pH, (2) U(VI) solution concentrations, (3) Gran alkalinity (carbonate concentrations), and (4) the concentration levels of other metals that could influence U(VI) solution speciation or indicate clay degradation over the course of the experiment. Last, a kinetic sorption experiment was started (currently ongoing) in order to characterize U(VI) sorption kinetics at the specific chemical conditions of U(VI) diffusion experiments.

Current results from parallel uranium(VI) through-diffusion experiments in Na-montmorillonite at two, slightly different, alkaline pH conditions (target pH 8.75 and 8.95), indicate a relevance of anion exclusion effects, the full or partial exclusion of anionic uranium(VI) solution species from clay interlayer spaces. Such exclusion affects the diffusion-accessible porosity for uranium(VI) species predominant under these chemical solution conditions, as well as the resulting uranium(VI) diffusive fluxes. Based on the literature we have reviewed, this is the first time this phenomenon has been experimentally demonstrated in a through-diffusion experiment. Hence, this result will have a profound impact on conceptual models describing the diffusive transport behavior of uranium(VI) in montmorillonite and bentonite.

Also, uranium(VI) sorption reactions were shown to be relevant for contaminant retardation in diffusion experiments, even at alkaline target pH values of 8.75 and 8.95, where uranium(VI) sorption is low compared to other pH conditions. Despite the similarity of these pH conditions in the parallel diffusion experiments, different degrees of uranium(VI) retardation could be observed in the two systems. Additionally, we also observed different, *apparent* kinetic limitations for uranium(VI) sorption reactions as a function of pH, which was indicated by varying time-frames required to reach steady-state conditions for uranium diffusive fluxes. The latter suggests that kinetic limitations for one or more reaction step(s) in the overall sorption process are dependent on chemical solution conditions, e.g., as could be the case for a rate-limited dissociation of uranium(VI) solution complexes prior to the formation of uranium(VI) surface complexes. Uranium(VI) sorption kinetics at alkaline pH are currently under experimental investigation.

All of these results, as well as the series of experimentally-determined uranium(VI) sorption and diffusion parameters, support the development of realistic conceptual models describing uranium(VI) mobility in nuclear waste repositories, and provide direct input parameters for later performance assessment models.

TABLE OF CONTENTS

LIST OF FIGURES

LIST OF TABLES

ACRONYMS

BET	Brunauer–Emmett–Teller (method for surface area measurements)
DIC	Dissolved Inorganic Carbon
EBS	Engineered Barrier Systems
EDL	Electric Double Layer
EPA	Environmental Protection Agency
EXAFS	Extended X-ray Absorption Fine Structure
FEBEX	Full-scale Engineered Barriers Experiment
FY	Fiscal Year
HLRW	High Level Radioactive Waste
HTO	Tritiated Water
IAEA	International Atomic Energy Agency
ICP-MS	Inductively Coupled Plasma Mass Spectrometer
LBNL	Lawrence Berkeley National Laboratory
LIFS	Laser-induced Fluorescence Spectroscopy
LOQ	Limit of Quantification
MCL	Maximum Contaminant Level
MDL	Method Detection Limit
ML	Minimum Level
MQW	Milli-Q Water
NEA, OECD	Nuclear Energy Agency, Organisation for Economic Co-operation and Development
NIH	National Institute of Health
SCM	Surface Complexation Model
SWy-2	Standardized Na-montmorillonite source clay from Wyoming, provided by the Clay Minerals Society

THIS PAGE INTENTIONALLY LEFT BLANK

1. INTRODUCTION AND RESEARCH MOTIVATION

Due to mining, milling and fuel processing operations, numerous sites have been contaminated with uranium in the past, with 38 proposed or final Superfund sites on the Environmental Protection Agency (EPA) National Priority List in the U.S. alone (NIH, 2016). In the future, the long-term storage of nuclear waste has the potential to create additional sources of uranium contamination affecting subsurface environments and drinking water resources, since spent nuclear fuel consists to approximately 95% of uranium. Chemically-induced, acute effects of uranium in humans, such as an inflammation of the kidneys (nephritis), have been reported (Hursh and Spoor, 1973), while chronic health effects and carcinogenicity are less well understood (World Health Organization, 2004). At this point in time, the World Health Organization has proposed a provisional guideline value of 15 µg uranium L^{-1} in drinking water (World Health Organization, 2004); the current U.S. EPA Maximum Contaminant Level (MCL) is set at 30 µg uranium L^{-1} (U.S. EPA, 2001). Hence, a sound scientific understanding of uranium mobility is needed in order to evaluate risks to humans and the environment, to optimize the management of nuclear waste and to take appropriate remediation actions if necessary.

While the U.S. has not yet decided on the geologic media for its long-term nuclear waste repository, in most scenarios, bentonite and clays are either the host rock media or the proposed backfill material in the engineered barrier systems (EBS) in close proximity to waste containers (Tournassat et al. 2015b). From a mineralogical perspective, sodium-montmorillonite clay is the major component of bentonite, and largely responsible for bentonite properties relevant for contaminant mobility. Given the low porosity and permeability, and the swelling properties of montmorillonite, diffusion is expected to be the primary transport mechanism in engineered barrier systems. Hence, accurate predictions of uranium(VI) transport behavior in the near- and far-fields will be dependent on a realistic conceptual understanding of uranium(VI) diffusion in clays and bentonite close to the source term.

Uranium(VI) mobility on the field-scale is ultimately controlled by the parameters and processes effective at micro- and nanometer scales. First, uranium(VI) sorption onto bentonite and sodium-montmorillonite is an important, and potentially limiting, process affecting uranium(VI) fluxes and contaminant retardation. Second, the small-scale diffusion-accessible porosities of montmorillonite will largely determine the magnitude of uranium(VI) fluxes across the EBS. A prediction of uranium(VI) adsorption and diffusion processes in clay-rich media, however, is complicated by: (1) the complex uranium(VI) solution speciation, which can include cationic, neutral, and anionic species, depending on chemical solution conditions, and (2) the complexity of the mineralogical structure of montmorillonite clay, in terms of its pore-size distributions, diffusion-accessible porosities, and available surface site types.

First, with regard to solution speciation, uranium can exist at oxidation states of IV or VI, but U(VI) is the most relevant oxidation state in most surface waters and in oxic groundwaters (Choppin, 2006). In reducing environments, the low solubility of U(IV) mineral phases greatly decreases uranium mobility. Furthermore, numerous studies have demonstrated the impacts of pH, bicarbonate and calcium concentrations on U(VI) solution speciation, adsorption and transport behavior (Davis et al. 2004; Curtis et al. 2006; Fox et al. 2006; Hartmann et al. 2008; Yabusaki et al. 2008; Ma et al. 2010; Kerisit et al. 2010; Bradbury and Baeyens 2011; Joseph et al. 2011).

Potential changes in chemical solution conditions and contaminant solution speciation over time and space are especially relevant for uranium, given the long half-lives of uranium isotopes and complex transport pathways in engineered barrier systems and the natural environment. For instance, in nuclear waste repositories, pore-water pH is buffered at values between 7 and 8 in the bentonite backfill material of the EBS surrounding waste canisters and/or in the clay host-rock (Muurinen and Lehikoinen 1999; Bradbury and Baeyens 2003; Wersin 2003; Wersin et al. 2004; Tournassat et al. 2015c). However, more alkaline pH conditions are expected in close proximity to steel canisters (pH 8 – 11) due to corrosion processes (Bildstein and Claret, 2015), as well as in cementitious leachates at bentonite-concrete boundaries (pH>13 for Ordinary Portland Cement and pH 9 – 11 for low alkali cement) due to the chemical degradation of cement (Savage et al. 1992; Gaucher and Blanc 2006; Gaboreau et al. 2012b; Milodowski et al. 2016). Furthermore, dissolved calcium concentrations may also vary over time and

space due to the progressive degradation of cement-based engineered barriers, the specific calcite contents in clay host rocks or changing concentrations in carbonate minerals along transport pathways (Hartmann et al. 2008; Gaboreau et al. 2012a; Adinarayana et al. 2013).

These chemical gradients in waste scenarios are important for the fate and transport of uranium, since U(VI) aqueous speciation is very complex and controls the extent and processes behind U(VI) adsorption reactions (e.g., cation exchange versus surface complexation reactions), as well as the U(VI) diffusion-accessible porosities and diffusion pathways (e.g., anion exclusion from clay interlayer spaces for anions versus 'surface diffusion' along basal cation exchange sites for cations). For instance, the uranyl cation (UO_2^{2+}) typically dominates speciation at low pH, while neutral and anionic U(VI)-hydroxyl and carbonate complexes become predominant at higher pH conditions. In a dilute U(VI) solution at pH 7 in the absence of carbonate, the predominant U(VI) species is the neutral $UO_2(OH)_2^0$. In comparison, for the same solution in equilibrium with atmospheric CO_2, the predominant species is the anion $(UO_2)_2CO_3(OH)_3^-$ (for a 1 µM solution). However, groundwater solutions are typically in equilibrium with partial pressures of CO_2 at 1% or greater, and may contain considerable concentrations of calcium due to the presence of carbonate minerals. At 1% CO_2, pH 7 and in the *absence* of Ca, U(VI) solution speciation is dominated by the anion $UO_2(CO_3)_2^{2-}$ (Figure 1-1). For a comparable solution in equilibrium with calcite, the predominant U(VI) species is the neutral $Ca_2UO_2(CO_3)_3^0$ (Figure 1-2).

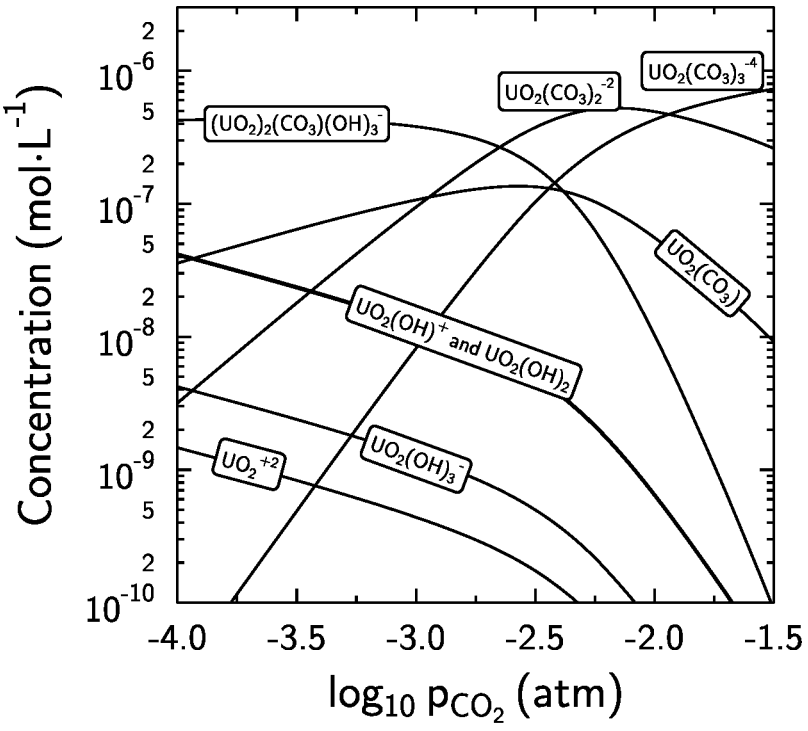

Figure 1-1. Uranium(VI) speciation as a function of the partial pressure of CO_2 in a 1 µM U(VI) solution in 0.1 M NaCl at pH 7 in the absence of Ca. Calculations were made with PHREEQC and the THERMOCHIMIE database (Giffaut et al. 2014).

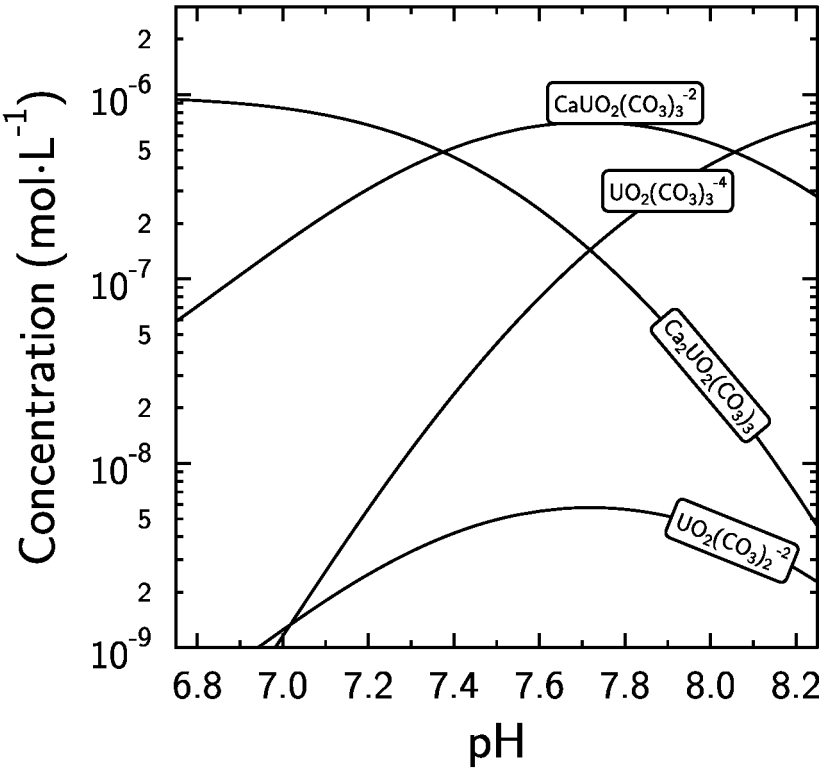

Figure 1-2. Uranium(VI) speciation as a function of pH in a 1 μM U(VI) solution in 0.1 M NaCl in equilibrium with a partial pressure of CO_2 at 1% and in equilibrium with calcite. Calculations were made with PHREEQC and the THERMOCHIMIE database (Giffaut et al. 2014).

The second major factor complicating a prediction of contaminant mobility in the EBS is the complex mineralogical structure of sodium-montmorillonite, the major component of bentonite in barrier systems, which affects both contaminant adsorption and diffusive transport behavior. Montmorillonite is a smectite, a 2:1-layer-type dioctahedral phyllosilicate with a large specific surface area (~750 $m^2 \cdot g^{-1}$) and cation exchange capacity (~1 $mol_c \cdot kg^{-1}$). Each montmorillonite layer has a thickness of ~1 nm and carries negative surface charges due to isomorphic substitutions of Al(III) for Si(IV) and Mg(II)/Fe(II) for Al(III) in its phyllosilicate framework (Brigatti et al. 2013). Due to its mineralogical structure, montmorillonite provides two types of surfaces and surface site types: (1) cation exchange sites with a permanent surface charge on basal planar surfaces, and (2) surface complexation sites, with variable surface charges as a function of pH, on edge surfaces of clay particles.

A fundamental understanding of U(VI) adsorption processes and the resulting U(VI) surface speciation on Na-montmorillonite is essential for an accurate prediction of uranium(VI) retardation and the magnitude of U(VI) diffusive fluxes across the EBS. As a result, many research groups have investigated the surface speciation of adsorbed U(VI) on montmorillonite with Extended X-ray Absorption Fine Structure (EXAFS) absorption spectroscopy (Dent et al. 1992; Chisholm-Brause et al. 1994; Giaquinta et al. 1997; Sylwester et al. 2000; Hennig et al. 2002; Catalano and Brown, 2005; Schlegel and Descostes, 2009; Marques Fernandes et al. 2012; Troyer et al. 2016). The analysis of the spectra obtained at various ionic strengths has revealed the presence of U(VI) outer-sphere complexes at low pH and/or low ionic strengths, and of U(VI) inner-sphere complexes at other conditions. These interpretations of EXAFS data are in qualitative agreement with the duality of adsorption mechanisms on montmorillonite surfaces, i.e. cation exchange on basal planar surfaces at low pH/ionic strength and surface complexation on edge surfaces at other conditions, as also evinced by other spectrometric techniques for a range of different

specifically adsorbed cations (Morris et al. 1994; Chisholm-Brause et al. 2001; Kowal-Fouchard et al. 2004; Wolthers et al. 2006).

The formation of inner-sphere bonds of U(VI) with surface groups at montmorillonite edge sites at neutral pH and high ionic strengths was deduced from the splitting of the U(VI) oxygen equatorial shell into two distinct contributions at ~2.3 Å and ~2.5 Å in EXAFS spectra. However, there is considerable uncertainty in the interpretation of second neighbor atoms involved in these surface complexes. Hennig et al. (2002) concluded that surface mononuclear bidentate complexes formed at aluminol sites. Schlegel and Descostes (2009) also proposed a U-Al shell, in agreement with Hennig et al. (2002). Additional Polarized-EXAFS (P-EXAFS) characterizations allowed them to conclude that the U complex was located on the particle edges and corresponded to a mononuclear bidentate complex. In contrast, Catalano and Brown (2005) suggested that the primary surface group second neighbors were Fe atoms, where Fe has substituted for Al in the octahedral sheets. In addition, Catalano and Brown (2005) fitted their data with a U-C shell and suggested that ternary uranyl-carbonato species formed at the surface in the presence of carbonate. However, more recently, Marques Fernandes et al. (2012) and Troyer et al. (2016) concluded that it was not possible to conclusively distinguish between Fe, Al, and Si as second neighbor atoms in U(VI) EXAFS spectra. Furthermore, Marques Fernandes et al. (2012) did not find spectroscopic evidence for uranyl-carbonato complexes at the montmorillonite surface, despite the fact that their surface complexation model included this species. Troyer et al. (2016) were not able to confirm the presence of ternary uranyl-carbonato surface complexes from their EXAFS data either, but made a strong conclusion about the presence of such species from laser-induced fluorescence spectroscopy (LIFS) data. The LIFS results, however, were obtained at very high U(VI) equilibrium concentrations and U(VI)/clay ratios. The total U(VI) concentration was 100 μM and solid-to-liquid ratio was 0.2 $g \cdot L^{-1}$, leading to an equilibrium U(VI) solution concentration of ~70 μM. Although it is not known, these conditions might have favored the formation of uranyl carbonate complexes driven by a high total uranium-carbonate ratio. In short, current results from spectroscopic sorption studies are still associated with a large degree of uncertainty regarding the relevance of ternary uranyl-carbonato surface complexes and the interpretation of second neighbor atoms involved in U(VI) surface complexes at montmorillonite edge sites.

Nevertheless, an accurate prediction of uranium mobility in clay-rich environments is dependent upon the development of adsorption models that can capture: (1) the complex uranium solution and surface speciation as a function of chemical solution conditions, and (2) the complexity of montmorillonite and its implications for the conceptual description of adsorption processes. Surface complexation models (SCMs) have the ability to directly link U(VI) adsorption behavior with U(VI) solution speciation based on existing thermodynamic data, which allows the models to predict changes in adsorption as a function of chemical solution conditions over time and space.

Several research groups have developed surface complexation models (SCMs) for the U(VI)-montmorillonite system (Pabalan and Turner 1996; Turner et al. 1996; Hyun et al. 2001; Bradbury and Baeyens 2005, 2011; Marques Fernandes et al. 2012). Surface complexation modeling studies predict that U(VI) adsorption decreases at alkaline pH when carbonate anions are present, due to the formation of strong uranyl-carbonato solution complexes (see Figure 1-1, and aqueous speciation diagrams in Davis et al. 2004 and Fox et al. 2006). The quantification of this effect was however dependent on the consideration, or not, of a retention mechanism of these uranyl-carbonato solution complexes on the clay surfaces. For example, in the model of Marques Fernandes et al. (2012), the authors found it necessary to include ternary uranyl-carbonato surface complexes to describe U(VI) adsorption onto montmorillonite in the presence of various concentrations of aqueous carbonate. Analogous U(VI) surface species have also been proposed on iron oxides and imogolite (Waite et al. 1994; Villalobos et al. 2001; Arai et al. 2006). For U(VI) adsorption on montmorillonite, however, in the absence of clear spectroscopic evidence, the need to add such additional surface complexes was solely guided by the quality of the fit between the model and the data. This fitting criterion may however be impaired by inadequate hypotheses in the modeling exercise. For example, the model of Marques Fernandes et al. (2012) was a non-electrostatic model, which means that the ionic nature of the sorbent and its interaction with the electrostatic potential field surrounding the montmorillonite particles is inherently not included. Given the complex U(VI)

solution speciation described above, it is important to take into account that the interactions of cationic, neutral or anionic U(VI) solution species with the surface electrostatic field is influenced by their charge. Hence, an electrostatic model is needed in order to test whether the importance of this electrostatic interaction is of first order to quantify U(VI) adsorption processes accurately, and whether it has an impact on the need to include ternary uranyl-carbonato surface complexes in the model.

However, currently available electrostatic surface complexation models for montmorillonite have mostly been based on the classical surface complexation models for oxides. These models include the hypothesis that surface charges are homogeneously distributed on a flat and infinite surface, which is invalid for clay minerals for the following two reasons. First, the edge surface is very different from a flat infinite surface in terms of its specific surface area and electrostatic surface potential. Second, the surface potential developed by the permanent charges of the basal surfaces interacts with the surface potential at the edge surfaces with pH-dependent charges (Tournassat et al. 2013, 2016a). This unique and relevant feature, called the 'spillover' effect, must be taken into account in the development of an electrostatic model for montmorillonite edge surfaces.

Given the current uncertainties associated with results from spectroscopic studies and the modeling needs described above, our goals with regards to U(VI) adsorption processes onto Na-montmorillonite were:

1) to improve the current mechanistic understanding of uranium(VI) adsorption onto montmorillonite as a function of chemical conditions, with a specific focus on the role of dissolved inorganic carbon; and
2) to develop an electrostatic surface complexation model that accounts for the impacts of the electric-double-layer (EDL) spillover effect on U(VI) surface reactions.

Besides U(VI) adsorption processes, the complexity of the montmorillonite structure will also affect the diffusive transport behavior of U(VI) in the EBS. For instance, the 'co-existence' of small interlayer pores within particles and larger macropores between clay particles can create two types of clay porosities and diffusion pathways. The relevance of the individual porosities and pathways is strongly dependent on system characteristics, such as the degree of bentonite compaction, chemical solution conditions, and the charge of contaminant species in solution. For example, a partial or full exclusion of anions from negatively charged clay interlayer spaces can change the effective 'anion-accessible' porosity and decrease the diffusive flux of these solutes under steady state conditions. As a result, diffusive fluxes can vary substantially between cations, anions and uncharged solutes. Furthermore, radionuclides that show dramatic changes in their chemical solution speciation as a function of pH, such as uranium(VI) are expected to show different diffusive transport behavior under varying chemical solution conditions.

Based on the literature we have reviewed, at present full or partial anion exclusion effects have not been clearly demonstrated experimentally for anionic uranium(VI) species, despite the theoretical understanding of the uranium(VI)-montmorillonite system described above. This is, at least in part, due to the difficulties associated with the experimental approach of so-called uranium(VI) through-diffusion experiments, which monitor the breakthrough and diffusive fluxes of uranium(VI) across a diffusion cell over the course of an experiment. Almost all previously reported uranium(VI)-montmorillonite/bentonite diffusion experiments were based on an evaluation of total uranium(VI) concentrations (dissolved plus sorbed concentrations) as a function of distance in the clay packing after the completion of experiments. While this approach still allows determining apparent uranium diffusion coefficients and sorption distribution coefficients (K_D values) based on the simulation of the concentration profile, the associated model parameters are less constrained, and direct observations of solute retardation, diffusive fluxes, and any potential kinetic effects are not possible.

Hence, our research goals with regard to U(VI) diffusion in Na-montmorillonite were:

(1) to provide clear, direct experimental evidence for U(VI) anion exclusion effects in through-diffusion experiments at alkaline pH conditions; and

(2) to complete a set of two, parallel uranium(VI) through-diffusion experiments, started during FY 2015, which also required a detailed, analytical characterization of the chemical composition of sample solutions in order to allow for a simulation of U(VI) solution speciation in later diffusion models.

In this report, we will first describe our experimental and modeling efforts regarding the investigation of uranium(VI) sorption behavior onto Na-montmorillonite, followed by a summary of experimental setups and results for U(VI) diffusion experiments. Finally, we will present our overall summary and conclusions and end with an outlook on planned future work.

2. DEVELOPMENT OF URANIUM(VI)-MONTMORILLONITE SURFACE COMPLEXATION MODEL

2.1 Materials and Methods

For the development of U(VI) surface complexation models, it is important to carefully characterize the compositions of experimental solutions, because various other solutes may affect U(VI) solution or surface speciation. Uranium(VI) adsorption onto Na-montmorillonite was investigated here as a function of total U(VI) and calcium concentrations and partial pressures of CO_2 (Table 2-1). Experimental blanks, standards and sample suspensions were analyzed for U(VI), calcium and dissolved inorganic carbon (DIC) concentrations, and monitored for elements that could indicate clay dissolution or inadequate solid-liquid phase separation (see Appendix for U(VI) and Ca background values; Si, Al, Fe, K, and Mg data not reported). Analysis of DIC concentrations in supernatant solutions was of particular importance in our experiments, given the relevance of carbonate for U(VI) speciation. Measured DIC concentrations allowed us to back-calculate actual pCO_2 values for all samples individually. In addition, analytical detection limits and experimental background values for DIC solution concentrations were determined as described in further detail below.

2.1.1 Materials

Glassware was cleaned by soaking in acid (10% (v/v) HCl) over 12 to 24 hours, followed by thorough rinsing with Nanopure water and air-drying. All aqueous solutions were prepared with Nanopure water (Barnstead ultrapure water system) using chemicals of reagent grade or better. Acids, bases and salt solutions used in adsorption experiments were of TraceSelect grade (Sigma Aldrich), in order to minimize calcium background concentrations in particular. Uranium(VI) solutions contained U-238, either from an in-house or a commercially available uranyl nitrate stock solution (1.30 mM stock provided by Drs. David Singer and Wayne Lukens at Lawrence Berkeley National Laboratory, or various dilutions of a 1000 µg U/mL Inorganic Ventures ICP-MS standard).

A well-characterized, standardized source clay (Na-montmorillonite, Standardized Na-montmorillonite source clay from Wyoming, provided by the Clay Minerals Society (SWy-2), Clay Minerals Society) was selected as the sorbent. Since this material is known to contain considerable impurities of quartz (8%), feldspars (16%) and calcite (Chipera and Bish 2001; Costanzo and Guggenheim 2001; Mermut and Cano 2001), it was pretreated to avoid uncontrolled impacts of calcite dissolution on U(VI) solution speciation during adsorption experiments. The major purification steps, which have been described in detail elsewhere (Tinnacher et al. 2016), included: (1) dissolution of calcite impurities in 1 M sodium acetate/0.564 M acetic acid solution at pH 5, (2) conversion of the clay into its Na form, (3) separation of quartz and feldspar impurities from the <2 µm clay fraction by centrifugation, and (4) oven-drying of the clay mineral phase at 45 °C. Afterwards, clay stock suspensions of 10 or 20 g L^{-1} were prepared in Nanopure water, and exact solid concentrations determined by weighing volume fractions before and after drying at 45 °C.

2.1.2 Batch Adsorption Experiments

Uranium(VI) adsorption onto Na-montmorillonite was characterized as a function of total U(VI) and calcium concentrations and "target" partial pressures of CO_2 (atmospheric CO_2, 2 % CO_2 and CO_2-free atmospheres). An overview of all experimental conditions is provided in Table 2-1.

Batch adsorption experiments were conducted at room temperature (22.5 – 23.5 °C) at an ionic strength of 0.1 M, and a Na-montmorillonite concentration of 0.5 g·L^{-1} (except for experiment 7 with a solid concentration, m_s, of 0.24 g·L^{-1}). The pH values ranged from 4.0 to 10.0. The reaction time was 48.5 hours, which closely approached or was sufficient to reach steady-state conditions (see discussion of kinetic adsorption data in Appendix). This reaction time is comparable to adsorption time-frames over 20-72 hours used in other, similar studies (Chisholm-Brause et al. 1994; Hyun et al. 2001; Bradbury and Baeyens, 2005; Schlegel and Descostes, 2009). Total calcium concentrations varied from low micromolar

background concentrations (see Table 2-1) to the higher concentration of 2.1 mM in the experiment with added Ca.

Table 2-1. Experimental conditions for U(VI) batch adsorption experiments.

.Exp.	Actual, total U(VI) conc. (µmol·L^{-1})	Target CO_2 partial pressures	Back-calculated range of CO_2 partial pressures [1]			Ca concentrations (µmol·L^{-1}) [2]
			log pCO_2 (atm)	pCO_2 (%)	pCO_2 (ppm)	
1	0.11	Laboratory air	-3.5 to -2.8	0.03 - 0.16	316 - 1585	6.7 - 8.5
2	0.96	Laboratory air	-3.6 to -3.1	0.03 - 0.08	251 - 794	6.4 - 1.9
3	2.6	Laboratory air	-3.5 to -2.8	0.03 - 0.16	316 - 1585	9.1 - 13
4	0.98	Laboratory air	-3.5 to -3.1	0.03 - 0.08	316 - 794	2100
5	1.1	Zero	-7 to -3.1	0.00 - 0.08	0 - 794	7.7 - 9.8
6	0.81	2% CO_2	-4 to -2	0.01 - 1.00	100 - 10000	10 - 27
7	0.98	2% CO_2	-2.7 to -2.1	0.20 - 0.79	1995 - 7943	10 - 13

[1] Based on back-calculation with measured DIC concentrations in sample solutions.
[2] Ca concentration in experiments 1 – 3 and 5 – 7 represent background values without any Ca additions (see Appendix).

Solutions were in contact with three different gas phases that varied in terms of their *target* partial pressures of CO_2: (1) atmospheric CO_2 in laboratory air (~0.04%, 400 ppm), (2) CO_2-"free" atmosphere (glove box, filled with 95% N_2/5% H_2 gas mixture), and (3) a *target* 2% CO_2 atmosphere. With respect to the last concentration, experiment 6 was conducted with a disposable Sigma Aldrich glove bag purged with certified 2% CO_2/balance nitrogen gas mixture. Experiment 7 was conducted in a COY anaerobic chamber filled with a 2% CO_2/98% nitrogen mix).

In the experiments performed under atmospheric or elevated CO_2 levels, additions of aliquots of $NaHCO_3$ solution were used to facilitate equilibration with the gas phases for samples with pH values of 7.0 or greater. Added aliquots of background electrolyte (NaCl) were decreased to account for the contributions of $NaHCO_3$ or $CaCl_2$ to the ionic strengths of the solutions. Fifty-mL polycarbonate centrifuge vials ('Oakridge centrifuge tubes') were used as sample vials to minimize U(VI) wall adsorption effects. In addition to samples containing Na-montmorillonite and U(VI) (1 replicate per pH condition), each experiment included experimental standards (in duplicate) to determine values of total, initial U(VI) solution concentrations. These standards had the same volume of U(VI) stock solution added to a vial in the absence of a mineral phase with the pH adjusted to 2.0. In addition, electrolyte blanks (in duplicate) containing 0.1 M NaCl but no U(VI) or solid were used to determine calcium and uranium-238 background concentrations in the absence of solid phases (see Appendix for these values).

The main steps in the batch adsorption experiments were: (1) pre-equilibration of Na-montmorillonite with a background electrolyte solution at the specified pH and chemical solution conditions, (2) U(VI) adsorption equilibration with the mineral phase, and (3) sampling and analysis of supernatant fractions after removal of the solid phase by centrifugation. At the beginning of experiments, aliquots of Nanopure water, Na-montmorillonite stock suspension, 1 M NaCl solution, and 1 M or 0.1 M $NaHCO_3$ solution were transferred into sample vials to yield the target solid concentrations and ionic strengths in the final sample volumes. pH values were adjusted with small volumes of HCl or NaOH solutions, and solutions were pre-equilibrated in closed sample vials by shaking for 12 to 24 hours.

After pre-equilibration with the electrolyte solution, aliquots of U(VI) stock solution were added to obtain the desired total U(VI) concentrations in the experiments. After re-adjustment of pH, the vials were shaken for 48.5 hours. Afterwards, final pH values were recorded while attempting to minimize gas exchange during pH measurements (discussed further below). Then, the sample suspensions were centrifuged to remove particles larger than approximately 50 nm from solution, as calculated based on Stokes law (Beckman Coulter Allegra 64R, F0850 rotor, centrifugation at 26 900 g for 61 minutes). Aliquots of supernatant solution were collected to analyze for metal concentrations by ICP-MS (Perkin-

Elmer SCIEX ICP-Mass Spectrometer ELAN DRC II, after sample acidification with TraceSelect grade HNO_3 (2% v/v)), and dissolved inorganic carbon (DIC) concentrations on a Shimadzu TOC-V_{CSH}.

Experimental results for batch adsorption experiments are reported in terms of distribution coefficients (K_D values, in $L \cdot kg^{-1}$) and fractions of U(VI) adsorbed ($f_{U(VI)_{adsorbed}}$ in %) after adsorption for 48.5 hours. Adsorbed U(VI) fractions and K_D values were computed based on concentration differences in supernatant solutions between experimental standards and samples:

$$f_{U(VI)_{adsorbed}} = \frac{U_{Std,supernat.} - U_{Sample,supernat.}}{U_{Std,supernat.}} \times 100 \quad (1)$$

$$K_D = \frac{f_{U(VI)_{adsorbed}} \times U_{Std,supernat.}}{100 \cdot m_s \cdot U_{Sample,supernat.}} \quad (2)$$

where $U_{supernat.}$ represents U(VI) concentrations in supernatant solutions for standards (subscript *Std*) and individual sample vials (subscript *Sample*), and m_S the solid concentration in kg L^{-1}.

2.1.3 Analytical Detection Limits and Background Values for Dissolved Inorganic Carbon

The manufacturer of the Shimadzu TOC-V_{CSH} instrument reports a detection limit of 4 $\mu g \cdot L^{-1}$ carbon. However, actual method detection limits are often dependent on the specific purity of water and reagents used to prepare calibration standards. Hence, following recommendations by the U.S. EPA (1995), the Method Detection Limit (MDL) and Minimum Level (ML) were determined for the specific setup of our DIC analysis on two separate days, as described in detail in the Appendix. The MDL represents the minimum DIC concentration that can be identified, measured and reported with a 99 % confidence that the concentration is greater than zero (U.S. EPA 1995). The ML is defined as the smallest measured concentration of a constituent that may be reliably reported using a given analytical method. Its value corresponds to the limit of quantitation (LOQ) established by the American Chemical Society, and is computed by multiplying the MDL by a factor of 3.18.

Furthermore, potential DIC contributions from various sources in the CO_2-"free" batch adsorption experiment, performed in a 95% N_2/5% H_2 glove box environment, were quantified as described in detail in the Appendix. In particular, as will be discussed later, it was necessary to understand if measured DIC concentrations had been present in solution during U(VI) adsorption equilibration, or if they represent a DIC contamination that was introduced into samples at a later point in time. For this particular experimental setup, potential sources of DIC contamination include: (1) DIC background concentrations in Milli-Q Water (MQW) (before and after purging with nitrogen gas) used for the later preparation of montmorillonite suspensions in the glove box, (2) handling of open sample vials in the glove box, if CO_2 was not fully excluded from the glove box atmosphere (maximum handling time for open vials estimated at 3-4 hours), (3) introduction of CO_2 into closed sample vials during centrifugation under atmospheric CO_2 outside the glove box, and (4) diffusion of atmospheric CO_2 into refrigerated, closed sample vials during a six-day storage period prior to DIC analysis.

2.1.4 Experimental Challenges in Experiments at Elevated CO_2 Partial Pressures

In experiment 6, it was difficult to create a controlled 2% CO_2 atmosphere using a disposable glove bag (Sigma Aldrich), which was repeatedly purged with a 2% CO_2/balance nitrogen gas mixture. In experiment 7, some of the problems associated with the disposable glove bag were avoided by using a Coy gas chamber. However, similarly to experiment 6, results from the DIC analysis of supernatant solutions suggest that samples were not fully equilibrated with the intended CO_2 partial pressure of 2% (see Experimental Results section 2.2 for details).

Despite these problems, DIC measurements in the final solutions allowed for an individual calculation of U(VI) aqueous speciation for each experimental sample. Although it was desired to have identical partial pressures of CO_2 for each series of vials in a particular experiment so that data could be illustrated and compared under identical conditions, DIC measurements showed that the solutions were not completely equilibrated with the respective gas phases, particularly for the elevated CO_2 atmospheres. Fortunately, for the purpose of creating an equilibrium geochemical model (and SCM) that describes the effect of dissolved carbonate on U(VI) speciation and adsorption, it was not necessary to have the same partial pressure of CO_2 in each vial. By measuring DIC in all sample solutions, including those from the laboratory air experiment, the equilibrium geochemical model determined the U(VI) aqueous speciation for each experimental data point rather than assuming a constant specific partial pressure of CO_2 in equilibrium with the aqueous phase. As will be discussed further below, this was very important in describing the observed U(VI) adsorption behavior in the SCM.

2.2 Experimental Results

2.2.1 Equilibration of Solutions with CO_2 in Gas Phases

2.2.1.1 Dissolved Inorganic Carbon Detection Limits and Background Contributions

Based on two analyses performed on different days, the Method Detection Limit (MDL) and Minimum Level (ML) were determined to be 0.051 and 0.161 $mg \cdot L^{-1}$ DIC (4.2E-6 and 1.3E-5 $mol \cdot L^{-1}$ DIC). Taking into account the offset due to DIC background concentrations in (MQW), calibration curves showed linearity down to the lowest concentration standard at 0.025 $mg \cdot L^{-1}$ (2.1E-6 $mol \cdot L^{-1}$) of added DIC.

The characterization of DIC background concentrations showed similar values for MQW before (0.121 $mg \cdot L^{-1}$, 1.0E-5 mol $mg \cdot L^{-1}$) and after (0.125 $mg \cdot L^{-1}$, 1.0E-5 mol L^{-1}) purging with nitrogen gas. The handling of open sample vials in the glove box atmosphere in the CO_2-"free" adsorption experiment, centrifugation of closed vials under atmospheric CO_2 conditions, and the refrigeration of closed vials outside the glove box prior to DIC analysis were each evaluated for their potential to increase measured DIC concentrations in N_2-purged MQW samples. Sample handling and centrifugation, which took place prior to supernatant sampling in the CO_2-"free" adsorption experiment, resulted in 0.344 and 0.277 $mg \cdot L^{-1}$ DIC (2.9E-5 and 2.3E-5 $mol \cdot L^{-1}$ DIC) concentrations during the test experiment. Storage of solutions in the refrigerator, which occurred after supernatant sampling in the adsorption experiments, resulted in a concentration of 0.331 $mg \cdot L^{-1}$ DIC (2.8E-5 $mol \cdot L^{-1}$ DIC) during testing.

Given the similarity of DIC contributions from these potential sources and the series of steps in the CO_2-"free" adsorption experiment, it can be assumed that open handling of sample solutions in the not-fully CO_2-"free" glove box atmosphere represented the major source of DIC contamination in the CO_2-"free" adsorption experiment. However, since most of the open handling of sample solutions occurred prior to the U(VI)-montmorillonite adsorption equilibration step in closed sample vials, we can further assume that measured DIC values represent actual DIC concentrations, present in sample suspensions during U(VI) sorption equilibration steps.

2.2.1.2 Measured DIC concentrations in batch adsorption experiments.

A detailed overview of measured DIC concentrations in the adsorption experiments is provided in the Appendix. A summary of measured DIC concentrations and calculated pCO_2 data are also plotted in Figure 2-1 (two bottom and top right panels). The calculations of pCO_2 were carried out with measured solution compositions (specifically DIC and pH) using PHREEQC v.3 (Parkhurst and Appelo, 2013) with the THERMOCHIMIE database (Giffaut et al. 2014). Experiments carried out in the presence of atmospheric CO_2 ($\sim 10^{-3.45}$ atm) resulted in measured DIC concentrations roughly in agreement with geochemical model calculations for this pCO_2. Samples from the CO_2-"free" glove box experiment had DIC concentrations similar to solutions observed under atmospheric conditions for pH< 6, suggesting CO_2 contamination as described above. However, in samples at pH>6 DIC concentrations, and

consequently the calculated pCO_2 values, were much lower than those under atmospheric conditions (Figure 2-1).

In experiments with a target value of 2% CO_2 in the gas phase (experiments 6 and 7), DIC results suggest that the gas bag or gas chamber was not sufficiently purged with the 2% CO_2/balance N_2 gas to achieve the intended 2% partial pressure. This was the case despite multiple purge volumes that were used to clear the bag and gas chamber in these experiments. In experiment 6, solutions up to a pH of 7.24 exhibited DIC concentrations that suggested equilibration with a gas phase composition closer to ~1% CO_2. Samples from supernatants at higher pH values had DIC concentrations consistent with even lower partial pressures of CO_2. This trend is most likely due to insufficient purging combined with a lack of fast CO_2 equilibration between the aqueous phase and the local atmosphere in the gas bag.

In experiment 7, the calculated low pCO_2 values at acidic pH suggest that the Coy gas chamber was also not sufficiently flushed to achieve the target CO_2 partial pressure. Although the solutions contained added $NaHCO_3$ such that they would be equilibrated with a 2% CO_2 gas phase, DIC data indicate that some CO_2 outgassed from solutions into the chamber atmosphere, driven by a pCO_2 value lower than 2%. Despite these problems, DIC measurements in the supernatant solutions allowed for an individual calculation pCO_2 values and U(VI) solution speciation in each sample.

2.2.2 U(VI) Adsorption Behavior under Varying Chemical Conditions

2.2.2.1 Effect of Variable pCO_2

Under atmospheric CO_2, U(VI)-montmorillonite K_D values varied over four orders of magnitude as a function of pH (Figure 2-1, left panel). At low pH, U(VI) adsorption is assumed to be limited due to its competition with protons at surface complexation sites (Stumm 1992). At high pH, low uranium adsorption is attributed to increasing carbonate concentrations, leading to weakly sorbing or non-sorbing aqueous U(VI)-carbonate complexes (Hsi and Langmuir 1985; Waite et al. 1994; Davis et al. 2004).

In the CO_2-"free" system, the shape of the U(VI) adsorption envelope is different compared to atmospheric CO_2 systems. In the low-pH region, U(VI) adsorption characteristics remain similar with comparable K_D values in the pH range from 4 to 6; above pH 6.5, however, U(VI) adsorption is much stronger at very low concentrations of CO_2. The greater U(VI) adsorption at high pH under low CO_2 conditions can be attributed to much lower concentrations of aqueous U(VI)-carbonate complexes that compete effectively with binary U(VI) surface complexation. A similar effect of the competition between aqueous carbonate and surface sites for U(VI) complexation is also observed when comparing U(VI) adsorption in systems at elevated at atmospheric CO_2 conditions, where U(VI) adsorption is lower at higher dissolved carbonate concentrations at pH values above 5.5 (Figure 2-1).

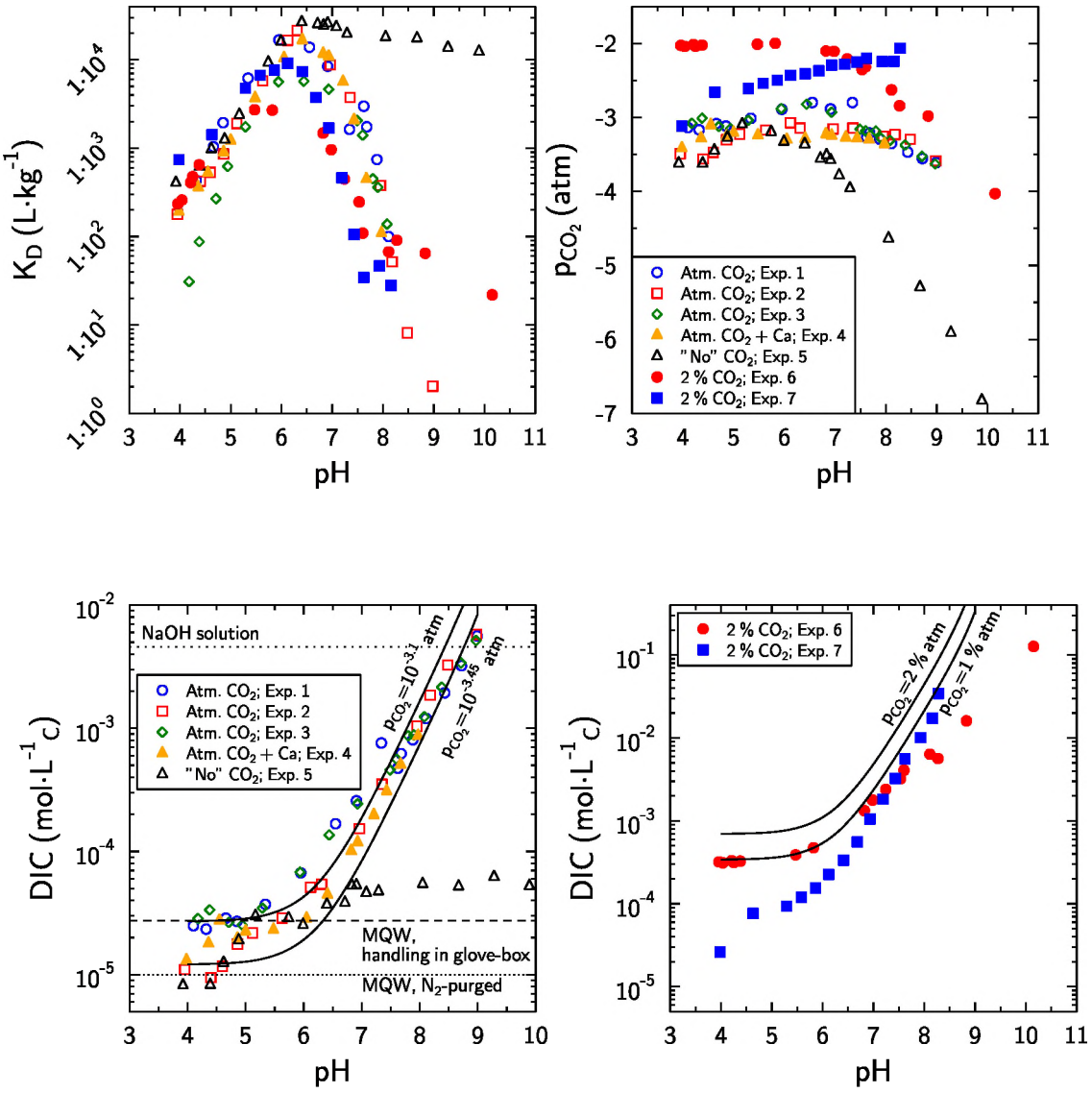

Figure 2-1. Top left: U(VI) adsorption as a function of pH and target pCO_2 partial pressures. Top right: Actual pCO_2 partial pressures calculated from DIC concentrations measured in supernatant samples as depicted in two bottom panels.

2.2.2.2 Effect of Variable Calcium Concentrations

Under atmospheric CO_2 conditions, U(VI) adsorption appeared to be approximately the same in the presence of 2.1 mM $CaCl_2$ compared to Ca background concentrations (Figure 2-1, left). At pH~8, the U(VI) K_D value appeared to be lower by approximately a half an order of magnitude (compare experiments 2 and 4 with similar total U(VI) concentrations). However, it is difficult to be certain of this effect because of differences in experimentally observed DIC concentrations. In this pH region, U(VI) aqueous speciation changes in the presence of 2 mM Ca concentrations, which leads to the formation of aqueous ternary Ca-U(VI)-carbonate complexes at pH>7.5 (Figure 2-2). This effect is evaluated further in the modeling section, where calculations are made at a constant pCO_2 partial pressure.

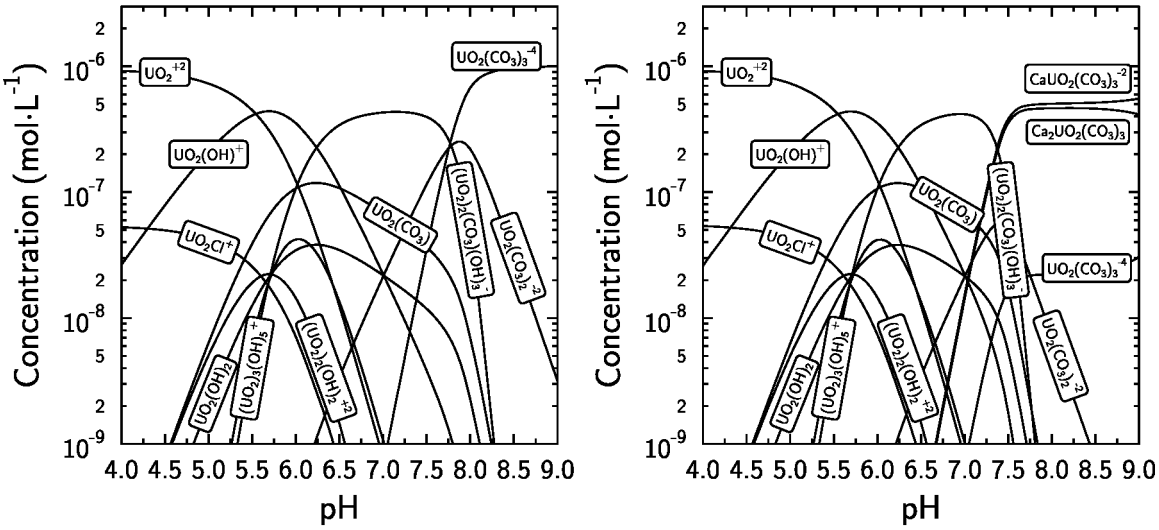

Figure 2-2. Aqueous speciation of a 1 µM U(VI) solution in 0.1 M NaCl in equilibrium with atmospheric CO_2 (log CO_2 = -3.45) in the absence (left) and presence of 2 mM Ca (right). Vertical axis is the negative log of the concentration of each U(VI) species.

2.3 Modeling and Discussion

2.3.1 Surface Complexation Modeling Strategy

An analysis of the literature shows that considerable uncertainty remains on the nature of inner-sphere complexes on montmorillonite edge surfaces. Surface complexation modeling cannot elucidate the nature of clay atoms present on surface sites, i.e., decipher the contributions of aluminol, silanol and Fe-substituted sites. However, modeling allows for an estimation of the likelihood of a reaction, such as the adsorption of uranyl carbonate complexes, and an understanding of the effect of Ca-CO_3-U(VI) solution complexes on the extent of U(VI) adsorption in calcium-rich environments. In the process, it is necessary to follow a parsimony rule, i.e., to build a model with the fewest adjustable parameters as possible in order to avoid correlations between fitting parameters. Accordingly, the chosen modeling strategy was based on a four-step approach, as follows. In a first step, U(VI) adsorption model parameters were fitted using experimental data from the CO_2-"free" experiment. In a second step, we applied these parameters to predict the data obtained in the other experiments: a good match of the prediction with experimental data would suggest that the adsorption of uranyl carbonate complexes is not important, while an underestimation of the adsorption extent would indicates that a uranyl carbonate complex must have formed at the surface (e.g., see the modeling approach of Waite et al. 1994). In a third step, we applied our model to a large range of data obtained from the literature in order to test its robustness. In a fourth and final step, factors influencing U(VI) adsorption, such as pCO_2 or Ca^{2+} concentrations, are discussed on the basis of predictive calculations using the model. A summary of experimental U(VI) batch sorption data from this study is provided in the Appendix in order to allow other researchers to test their modeling concepts.

2.3.2 Surface Complexation Model for Montmorillonite Edge Surfaces

The objective of the modeling work presented here was to develop a model that was as mechanistic as possible, but without adding too many fitting parameters. Accordingly, the speciation model for SWy-2 edge surfaces was directly taken from Tournassat et al. (2016a). This surface complexation model

explicitly takes into account the spillover effect of the basal surface potential on the edge surface potential. This effect is typical for layered minerals with structural charges and renders classical surface complexation models developed for oxide surfaces incorrect for modeling clay mineral edge surface properties (Bourg et al. 2007; Tournassat et al. 2013, 2015a, 2016a).

Briefly, the negative surface charge created by the isomorphic substitutions in the montmorillonite lattice creates a negative electrostatic potential field that interacts with the electrostatic field created by the amphoteric edge surface sites (Chang and Sposito 1994, 1996). Consequently, if the edge surface charge is zero, the edge surface potential remains negative. This effect can be adequately captured by setting the relationship between surface charge (Q_{edge} in C·m^{-2}) and surface potential (ψ_{edge} in V) to:

$$\frac{F\psi_{edge}}{RT} = A_1 \operatorname{asinh}\left(A_2\left(Q_{edge} + A_3\right)\right) \quad (3)$$

where A_1, A_2, and A_3 are fitted parameters, F is the Faraday constant (96485 C·mol^{-1}), R is the gas constant (8.314 J·K^{-1}·mol^{-1}) and T is the temperature (K). For montmorillonite at 25 °C, Tournassat et al. (2013) refined the values of these parameters to: A_1 = 1.4 -1.2 log I, A_2 = 11 + log I, and A_3 = -0.02 × (-log I)$^{1.60}$, where I refers to the ionic strength (unitless). This equation is comparable to the classic equation of the diffuse layer model (DLM) for oxides (Davis et al. 1978) that is implemented in most geochemical calculation codes (Steefel et al. 2015), but that is not adapted to model the properties of clay edge surfaces (Tournassat et al. 2013, 2015a, 2016a):

$$\frac{F\psi}{RT} = 2\operatorname{asinh}(B \cdot \sigma) \text{ with } B = \frac{1}{\sqrt{8\varepsilon\varepsilon_0 RT \cdot 1000 \cdot I}} \quad (4)$$

where $\varepsilon\varepsilon_0$ is the dielectric constant for water. The site densities, stoichiometries and protonation/deprotonation constants were taken from Tournassat et al. (2016a). Site densities were calculated from crystallographic considerations and structural formulas; protonation/deprotonation constants were obtained from the predictions of first-principle molecular dynamics calculations (Liu et al. 2013, 2014, 2015a, b).

Edge surfaces with different crystallographic orientations exhibit amphoteric sites of different natures and with different site densities (Tournassat et al. 2016a). Two kinds of edge surfaces can be found in this model, corresponding to the AC and B chains that were first described by White and Zelazny (1988). The relative proportions of these two kinds of surfaces (AC and B) on SWy-2 particle edges and the total edge specific surface area (~15 m^2·g^{-1}) were fitted from titration curves. The value of the edge specific surface area that was fitted by Tournassat et al. (2016a) compared well with the value measured by the low-pressure gas adsorption method (~19 m^2·g^{-1}) (Duc et al. 2005). This value, however, was different from the SWy-2 N_2-BET specific surface area value. Nitrogen-BET specific surface area measurements have been commonly used for the calibration of surface complexation models for clay minerals in the literature, even though these values are not representative of the edge specific surface area for the following reason. Nitrogen-BET measurements probe both edge and external basal surface areas of the particles, and the latter contribution always dominates over the first for montmorillonite particles (Tournassat et al. 2003, 2013, 2015a, 2016a; b).

None of the parameters of the above described surface model was changed during the modeling exercises, leaving only the speciation of U(VI) surface complexes and the related association constants as fitting parameters. Only U(VI) surface complexes on the B-chain surface type were considered in the model, in agreement with the results obtained with P-EXAFS on the orientation of the U(VI) surface complexes (Schlegel and Descostes, 2009; Marques Fernandes et al. 2012). In the absence of any supporting spectrometric evidence on the nature of the surface sites involved in U(VI)-specific adsorption, we hypothesized that the formation of U(VI) surface complexes took place on the most abundant, non-substituted Si_T-Al_{Oc}-Si_T edge sites, where subscripts T and Oc refer to the tetrahedral and octahedral sheets of the layer respectively (Table 2-2). Note that the influence of cation exchange reactions was

negligible under our experimental conditions, compared to the strong relevance of U(VI) surface complexation reactions for overall U(VI) adsorption behavior.

Table 2-2. U(VI) surface complexation reactions on SWy-2 particle edges and related association constants used for modeling[a]. The partial charges were calculated by adding up all bond valences of cations and anions from the clay structure that surround the surface site.

Edge surface areas	Total	15 $m^2 \cdot g^{-1}$
	Edge surface of B type	9 $m^2 \cdot g^{-1}$
Protonation/deprotonation reactions	Log K	
	Si_T-Al_{Oc}-Si_T	Si_T-Fe^{III}_{Oc}-Si_T
$>SiteH_4^+ = >SiteH_3^+ + H^+$	-3.1	-1.2
$>SiteH_3 = >SiteH_2^- + H^+$	-7	-5.1
$>SiteH_2^- = >SiteH^{2-} + H^+$	-7	-8.6
$>SiteH^{2-} = >Site^{3-} + H^+$	-8.3	-8.6
	Si_T-Mg_{Oc}-Si_T	Si_T-Fe^{II}_{Oc}-Si_T
$>SiteH_4^{+0.67} = >SiteH_3^{-0.33} + H^+$	-10.8	-6.6
$>SiteH_3^{-0.33} = >SiteH_2^{-1.33} + H^+$	-10.8	-10.2
$>SiteH_2^{-1.33} = >SiteH^{-2.33} + H^+$	-13.2	-10.2
$>SiteH^{-2.33} = >Site^{-3.33} + H^+$	N.A.	-11.2
	Al_T-Al_{Oc}-Si_T	
$>SiteH_4^{+0.75} = >SiteH_3^{-0.25} + H^+$	-4.9	
$>SiteH_3^{-0.25} = >SiteH_2^{-1.25} + H^+$	-7	
$>SiteH_2^{-1.25} = >SiteH^{-2.25} + H^+$	-8.5	
$>SiteH^{-2.25} = >Site^{-3.25} + H^+$	-15.1	
U(VI) adsorption reactions on Si_T-Al_{Oc}-Si_T sites		Log K
$>SiteH_3 + UO_2^{2+} = >SiteH_3UO_2^{2+}$		3.8
$>SiteH_3 + UO_2^{2+} = >SiteHUO_2 + 2\ H^+$		-5
$>SiteH_3 + UO_2^{2+} + 2\ H_2O = >SiteUO_2(OH)_2^{-3} + 5\ H^+$		-25.4

[a] The surface speciation model of Tournassat et al. (2016a) provides information on surface types and areas, site types and protonation/deprotonation constants.

An in-house version of PHREEQC, which was modified to handle Eq. (3), was used to carry out the calculations, together with the database THERMOCHIMIE v. 9b0 for thermodynamic parameters of solute species (Giffaut et al. 2014). This database is available in various formats including PHREEQC format at the following address: https://www.thermochimie-tdb.com/.

2.3.3 Calibration of the U(VI) Surface Complexation Model in the "Absence" of CO_2

Carrying out all the steps of an adsorption experiment in the complete absence of CO_2 is very difficult. The DIC measurements indicate that carbonate was not fully excluded from the solutions despite the

efforts to achieve this goal. Despite the observed carbonate contamination, the adsorption results from the CO_2-"free" experiments were qualitatively similar to other literature data for carbonate-free systems (Bradbury and Baeyens 2005; Marques Fernandes et al. 2012), i.e. showing a sharp increase in U(VI) adsorption from pH 4 to pH 6 and a limited decrease of U(VI) adsorption at pH>6 (Figure 2-1).

While actual DIC concentrations are usually not considered in CO_2-"free" U(VI) adsorption models in the literature, they were specifically taken into account in the model calculations discussed here. Only three edge surface reactions were necessary to reproduce the data (Figure 2-3 and Table 2-2). The effect of cation exchange was negligible because of the effective competition between Na^+ versus UO_2^{2+} for cation exchange sites under our experimental conditions (0.1 M NaCl background electrolyte). The calculation made with the same reference model parameters, but using a zero DIC value instead of the measured one, illustrates how sensitive the calculation is to the consideration of actual DIC values (dashed lines in Figure 2-3 represent the model predictions while assuming zero DIC; solid lines are based on the reference model using measured DIC values). Even at the low DIC concentrations observed in the CO_2-"free" experiment, dissolved carbonates provide highly competitive ligands for U(VI) complexation reactions relative to mineral surface sites.

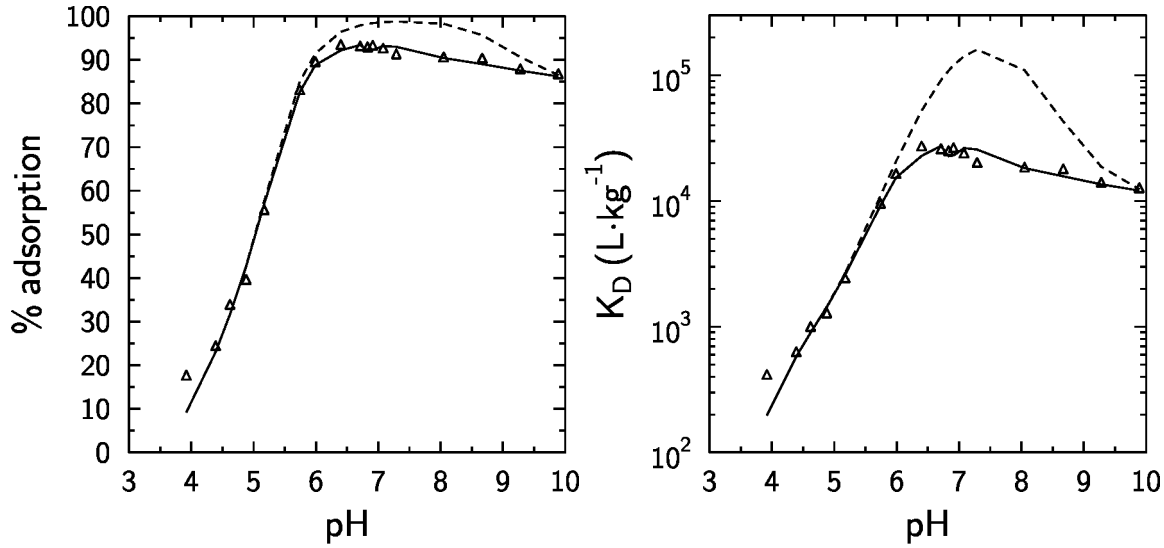

Figure 2-3. U(VI) adsorption results in the CO_2-"free" experiment (symbols: data; lines: model predictions) plotted as percentages of U(VI) adsorbed (left) and adsorption distribution coefficients (K_D, right). The reference model (solid line) was calculated taking into account individually measured DIC concentrations for each data point. The dashed line corresponds to a prediction using the same model parameters but while assuming zero DIC concentrations. Solid concentration = 0.52 g·L^{-1}, total U(VI) concentration = $1.1 \cdot 10^{-6}$ M, ionic strength=0.1 M NaCl.

2.3.4 Blind Prediction of U(VI) Adsorption in the Presence of CO_2

The minimal set of adsorption parameters obtained from the fitting of CO_2-"free" adsorption data were directly used to predict the results of experiments carried out at atmospheric CO_2 partial pressure (log pCO_2 ~ -3.45). Instead of assuming the expected pCO_2 value for every point in the calculations, however, the individually measured DIC concentrations were used to calculate the aqueous composition and U(VI) speciation. The blind prediction of U(VI) adsorption data was surprisingly good (Figure 2-4). Furthermore, in the experiment at $U(VI)_{tot}$ = 0.1 µM, the $NaHCO_3$ aliquot addition was twice of what it should have been for the sample at pH = 7.34, due to an experimental error (see point circled in left panel of Figure 2-4). The related decrease in U(VI) adsorption due to U(VI) aqueous complexation with carbonate was perfectly reproduced by the model, without a need for including the adsorption of uranyl carbonate complexes on the montmorillonite surface. This suggests that our doubts regarding the existence of such ternary surface complexes (on montmorillonite) under atmospheric pCO_2 conditions, triggered by the uncertainties associated with spectroscopic data, are probably justified. The experimental error in the $NaHCO_3$ addition for the sample at pH 7.34 also demonstrates that the solution was slow to re-equilibrate with the atmosphere outside of the closed sample vial, and confirms that measured DIC values correspond to DIC concentrations during U(VI) sorption equilibration.

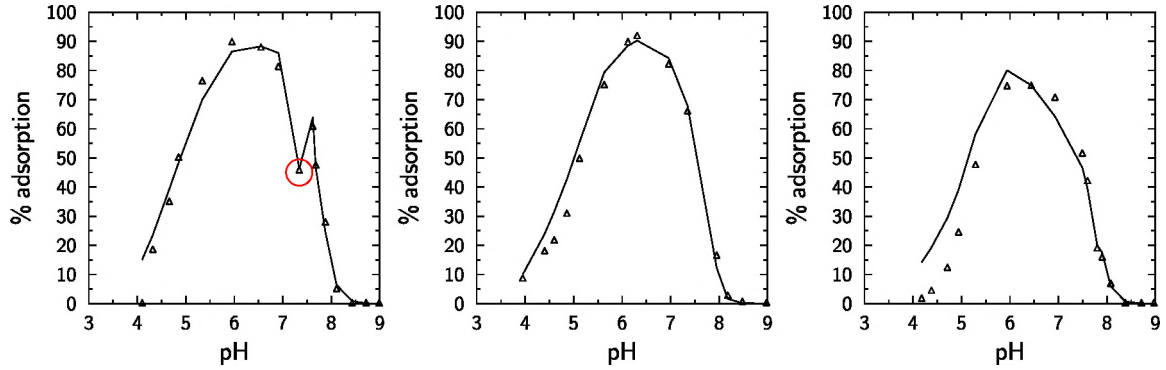

Figure 2-4. U(VI) adsorption results in the presence of atmospheric pCO_2 in a NaCl background electrolyte concentration of 0.1 M (symbols: data; line: model predictions). The model was calculated for each data point taking into account individually measured DIC concentrations. The solid concentration was ~0.52 $g \cdot L^{-1}$. From left to right, the total U(VI) concentration was $1.1 \cdot 10^{-7}$, $9.6 \cdot 10^{-7}$, or $2.6 \cdot 10^{-6}$ M. $NaHCO_3$ aliquot addition was twice of what it should have been for the sample at pH = 7.34 and $1.1 \cdot 10^{-7}$ M U(VI) (circled experimental point).The robustness of the model was further tested as a function of ionic strength, and, again, the model predicted the data well (Figure 2-5). Under the conditions of this experimental dataset, the influence of cation exchange reactions was negligible for pH >5. The apparent effect of ionic strength on the extent of U(VI) adsorption is due to the changes in electrostatic potential as a function of ionic strength, as well as to small changes in pH values (see Figure 2-5 caption).

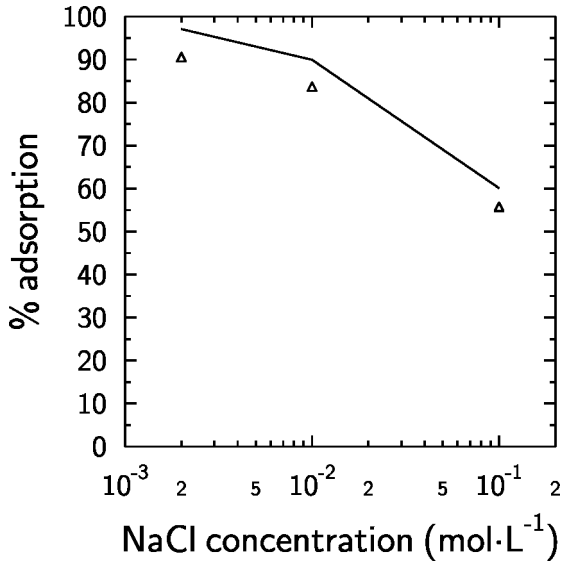

Figure 2-5. U(VI) adsorption as a function of ionic strength in the presence of atmospheric pCO_2 (symbols: data; line: model predictions). The model was calculated for each data point taking into account individually measured DIC concentrations and pH values (5.6, 5.4, 5.2 at 0.002, 0.01 and 0.1 M NaCl, respectively). The solid concentration was 0.52 $g \cdot L^{-1}$; the total U(VI) concentration $9.5 \cdot 10^{-7}$ M.

At greater DIC concentrations (due to pCO_2 values higher than atmospheric), U(VI) adsorption data were also correctly predicted by the model without changing fitting parameters, or adding new surface complexes. The model underpredicted the measured values in percent U(VI) adsorbed by 15% or less (Figure 2-6). However, it was not possible to enhance the quality of the fit by including a uranyl-carbonato surface complex without deteriorating the data fits obtained at atmospheric pCO_2 or CO_2-"free" conditions.

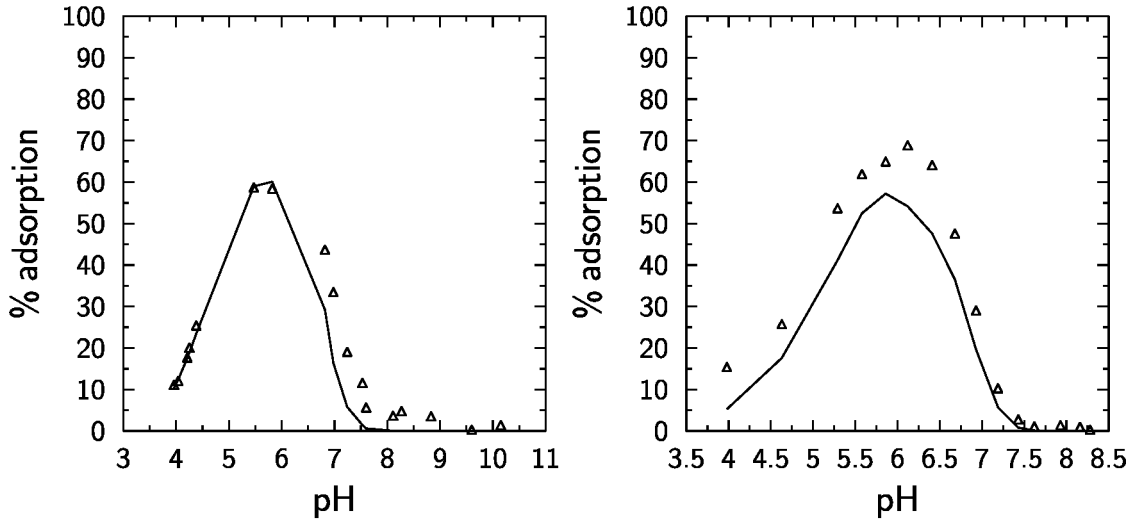

Figure 2-6. U(VI) adsorption in the presence of elevated pCO_2 (symbols: data; line: model predictions). The model was calculated for each data point taking into account individually measured DIC concentrations. Solid concentrations were 0.52 $g \cdot L^{-1}$ (left) or 0.24 $g \cdot L^{-1}$ (right). Total concentrations of U(VI) were $8.1 \cdot 10^{-7}$ M (left) and $9.8 \cdot 10^{-7}$ M (right).

2.3.5 Model Predictions of Literature Data

A wide range of literature data is available for U(VI) adsorption on montmorillonite (McKinley et al. 1995; Pabalan and Turner 1996; Turner et al. 1996; Hyun et al. 2001; Bradbury and Baeyens 2005; Marques Fernandes et al. 2015; Troyer et al. 2016). Thus, it was possible to test the predictive capabilities of the model over a wider range of conditions than those tested in the experiments described above. However, the limitations of this benchmarking approach are at least two-fold. First, the origin and preparation of the clay material (fine fraction separation and further chemical purification) can influence adsorption results because of variations in reactive surface area and surface chemistry. Second, DIC concentrations were not reported in previous studies, while the results presented here demonstrate the paramount importance of this parameter.

The following modeling and data presentation strategies were applied in order to avoid any misinterpretations regarding the quality of the model predictions. Data from the literature were first compared with a blind modeling prediction without any adjustment of model parameters given in Table 2-2 (reference model). In the case of experiments carried out under atmospheric conditions, a $\log_{10}(pCO_2)$ value of -3.45 was assumed for these reference calculations. In case of CO_2-"free" conditions, a $\log_{10}(pCO_2)$ value of -99 was applied. In a second step, various hypotheses were tested to achieve a better fit of the data, if necessary. In particular, as our reference model did not include cation exchange reactions, it was necessary to include these reactions to reproduce U(VI) adsorption data obtained at low ionic strength and low pH (pH<4) conditions.

2.3.5.1 Data of Troyer et al. (2016)

The data of Troyer et al. (2016) were acquired in the presence of atmospheric pCO_2 on a clay material similar to the one used in this study (< 2 µm fraction of SWy-2 montmorillonite), but in the presence of a 0.01M NaCl electrolyte, thus promoting cation exchange reactions compared to our conditions. We tested the model on the authors' three adsorption isotherms obtained at pH 4, 6 and 8. The error bands were based on adsorption data as follows:

$$\Delta C_{ads} = \frac{2}{m_{clay}}\sqrt{uC_{tot}{}^2 + uC_{eq}{}^2} = \frac{2}{m_{clay}}\sqrt{(0.02 \cdot C_{tot})^2 + \left(0.02 \cdot C_{eq}\right)^2} \qquad (5)$$

Data obtained at pH 6 could be adequately reproduced without changing any parameter from the reference model (Figure 2-7). Data obtained at pH 4 could be reproduced only by adding a cation exchange reaction to the reference model (Table 2-3). Data at pH 8 were not satisfactorily reproduced in the first calculations. However, a slight change in the pH value (7.8 instead of 8) or pCO_2 value (-3.7 instead of -3.45 in $\log_{10}$ value) made it possible to fit the data very well, again showing the great sensitivity of the system to pH/pCO_2 over this range of conditions.

Some data at high U(VI) surface coverage could not be predicted by the model, even after changing some of the parameters. The origin of this problem can be understood by comparing the measured U(VI) surface coverage with the maximum available surface site density. If we consider a site density of 2.06 sites·nm^{-2} (Bourg et al. 2007; Tournassat et al. 2016a) and a specific surface area of 15 m^2·g^{-1}, the maximum adsorption capacity for U(VI) complexes should be ~0.05 mol·kg^{-1}. If we further assume that no U multinuclear complexes form at the surface, this value decreases to ~0.025 mol·kg^{-1} (perfect ordering). This value is similar to the maximum adsorbed concentration value measured in Troyer et al. (2016) at pH 6, but far lower than the maximum value measured at pH 8. Hence, the much higher measured than simulated extent of U(VI) adsorption cannot be explained by the formation of isolated mononuclear bidentate U(VI) surface complexes alone. These data must include additional uptake processes that are not described in the model developed here, and are beyond the scope of this study, e.g. polymerization on the surface, or precipitation. The latter cannot be fully ruled out at elevated U(VI)

concentrations, since a supersaturation of schoepite was predicted at 1.3 and 62 µM U(VI) at pH 6 and pH 8 respectively, based on the U(VI) aqueous speciation model by Troyer et al. (2016).

Table 2-3. Cation exchange reaction parameters added to the reference model in order to reproduce literature data obtained at low ionic strength[a].

Surface reactions on montmorillonite basal surfaces	Log_{10} K	
$X^- + Na+ = XNa$	0	
Cation exchange reactions with U(VI) species (as a function of literature data)	Log_{10} K	CEC ($mol \cdot kg^{-1}$) [b]
Troyer et al. (2016), Hyun et al. (2001)		
$2\ XNa + UO_2^{2+} = X_2\ UO_2 + 2\ Na^+$	0.95	0.85
Pabalan and Turner (1996)		
$2\ XNa + UO_2^{2+} = X_2\ UO_2 + 2\ Na^+$	0.75	1.2
McKinley et al. (1995)		
$2\ XNa + UO_2^{2+} = X_2\ UO_2 + 2\ Na^+$	1.2	0.8
Turner et al. (1996)		
$2\ XNa + UO_2^{2+} = X_2\ UO_2 + 2\ Na^+$	0.9	0.41

[a] Cation exchange reactions were modeled with a classic diffuse layer model that was already calibrated for Na^+ and Ca^{2+} by Tinnacher et al. (2016). The total specific surface area for cation exchange reactions was set to the crystallographic surface area for montmorillonite, i.e. ~750 $m^2 \cdot g^{-1}$ (Tournassat and Appelo, 2011; Tournassat et al. 2011, 2015b; Tournassat and Steefel 2015).
[b] Values measured in the reference papers.

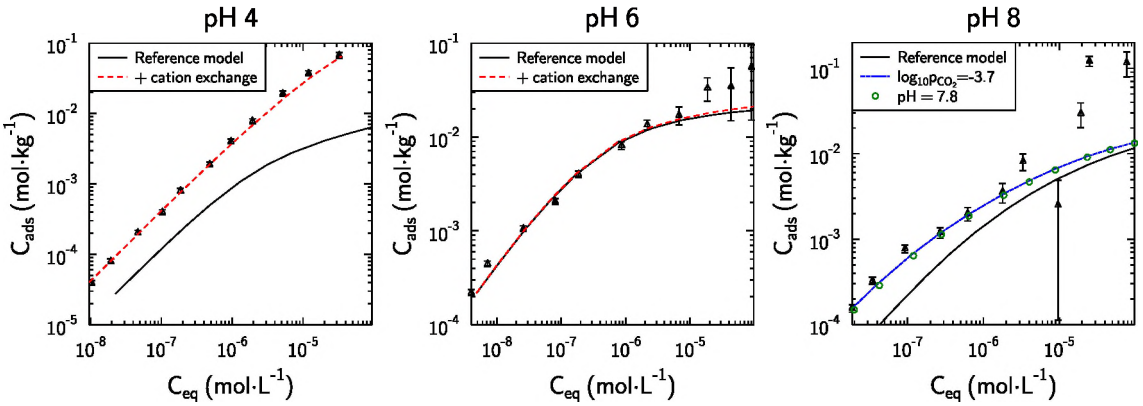

Figure 2-7. Comparison of model predictions with the U(VI) adsorption data on montmorillonite by Troyer et al. (2016).

2.3.5.2 Data of Hyun et al. (2001)

The data of Hyun et al. (2001) were also acquired in the presence of atmospheric pCO_2 on a clay material similar to the one used in this study (fine fraction of SWy-2 montmorillonite). Uranium(VI) adsorption was characterized at two fixed total U(VI) concentrations (10^{-7} and 10^{-5} mol·L^{-1}), with variable pH, and for two ionic strengths (I=0.001 and I=0.1), and at a relatively high solid concentration (~6-7 g·L^{-1}). The reference model provided a good prediction of the data (Figure 2-8).

At low ionic strength, the addition of cation exchange reactions, with the same parameters as for the study of Troyer et al. (2016), had almost no influence on the results. At pH 4 and low ionic strength, the high level of adsorption is mainly due to the increase in the surface potential value at edge surfaces. At high pH, the disagreement between experimental data and model predictions could be attributed to the fact that carbonate concentrations were not constrained experimentally (Hyun et al. 2001). Pabalan and Turner (1996) reported that, under some conditions, an equilibration period of ten days with the atmosphere was necessary to reach equilibrium between DIC and atmospheric CO_2. Insufficient time of equilibration with the atmosphere in the experiments of Hyun et al. (2001) could have led to pCO_2 values that were lower than the atmospheric value considered in the calculations: fitted value were log pCO_2 = -4.4 at pH 9 and -5.05 at pH 9.55 (blue line in Figure 2-8 right).

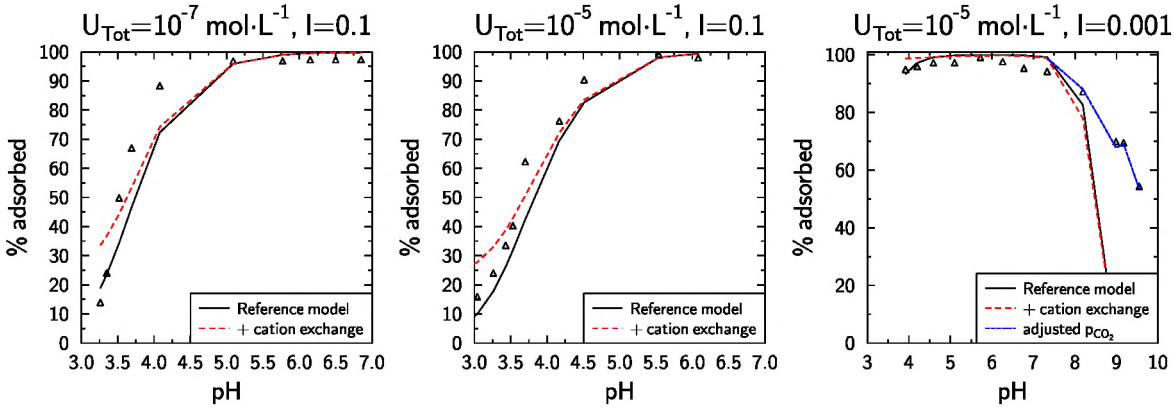

Figure 2-8. Comparison of model predictions with the U(VI) adsorption data on montmorillonite by Hyun et al. (2001).

2.3.5.3 Data of Pabalan and Turner (1996)

The data of Pabalan and Turner (1996) were obtained in the presence of atmospheric pCO_2 on a clay material, SAz-1, that was different from SWy-2. Experimental conditions were otherwise quite similar to those used in the present study. In particular, close equilibrium with atmospheric pCO_2 was ensured by the addition of bicarbonate to the solutions. Again, the predictions of the model were in very good agreement with the experimental data without any further adjustments (Figure 2-9), despite the different nature of the clay.

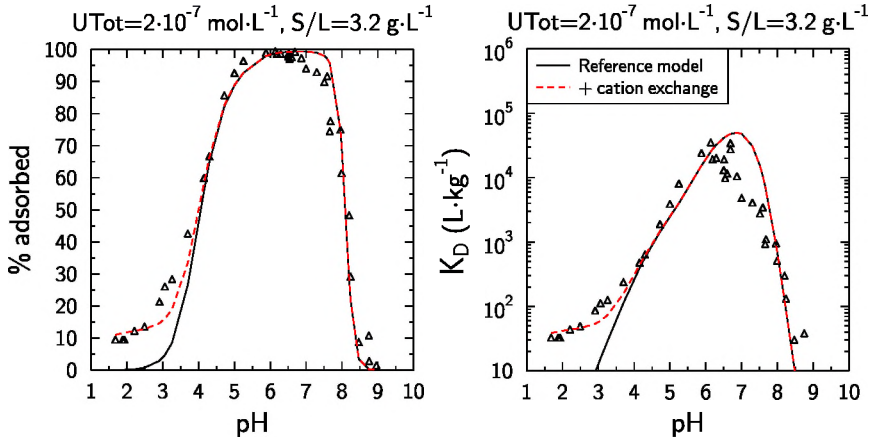

Figure 2-9. Comparison of model predictions with U(VI) adsorption data by Pabalan and Turner (1996). Cation exchange parameters are given in Table 2-3. Solid concentration = 3.2 $g \cdot L^{-1}$; total U(VI) concentration = $2 \cdot 10^{-7}$M. The results are presented in percentage adsorbed (left) and in $\log_{10} K_D$ values (right) for a better evaluation of model fits at low (left) and high (right) U(VI) adsorption.

2.3.5.4 Data of McKinley et al. (1995)

McKinley et al. (1995) reported U(VI) adsorption data on the <2 µm fraction of Swy-1 montmorillonite as a function of pH and ionic strength. At first sight, these data were not satisfactorily reproduced by the reference model (Figure 2-10). The addition of cation exchange reactions improved predictions at low pH, but U(VI) adsorption at pH>5.5 was still overestimated. However, these discrepancies can be satisfactorily explained by taking into account that the edge specific surface area of the Swy-1 sample from McKinley et al. (1995) was lower than the area of the Swy-2 sample, i.e. 10.5 $m^2 \cdot g^{-1}$ instead of 15 $m^2 \cdot g^{-1}$. Both values are within the range of montmorillonite edge surface area values reported in the literature, which vary from 5 $m^2 \cdot g^{-1}$ to 25 $m^2 \cdot g^{-1}$ (Tournassat et al. 2016a).

2.3.5.5 Data of Turner et al. (1996)

Turner et al. (1996) reported U(VI) adsorption data on the <2 µm fraction of a smectite isolate from a sedimentary rock fraction (Kenoma scmectite). Kenoma smectite is a beidellite, meaning that most of its structural charge originates from tetrahedral isomorphic substitutions, instead of octahedral substitutions for montmorillonite. Despite this difference, U(VI) adsorption data could be fitted equally well using the same approach as for the data of McKinley et al. (1995). Only U(VI) adsorption data obtained at very low ionic strength (I=0.001) were overestimated (Figure 2-11). Since the solid/liquid separation was achieved by centrifugation, it may be possible that finer particles were not completely removed from solution at this ionic strength, causing a lower apparent extent of U(VI) adsorption: at low ionic strength, separation of solids from solution based on density differences is more difficult, due to the increased intensity of electrostatic repulsive interactions between montmorillonite layers (Van Olphen 1992).

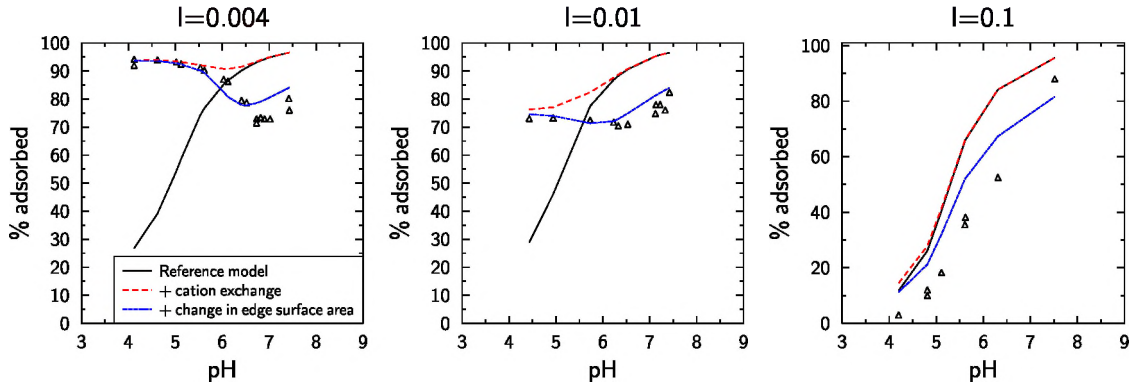

Figure 2-10. Comparison of model predictions with U(VI) adsorption data by McKinley et al. (1995). The edge surface area was set to 10.5 $m^2 \cdot g^{-1}$ instead of 15 $m^2 \cdot g^{-1}$ in the reference model. Cation exchange parameters are given in Table 2-3.

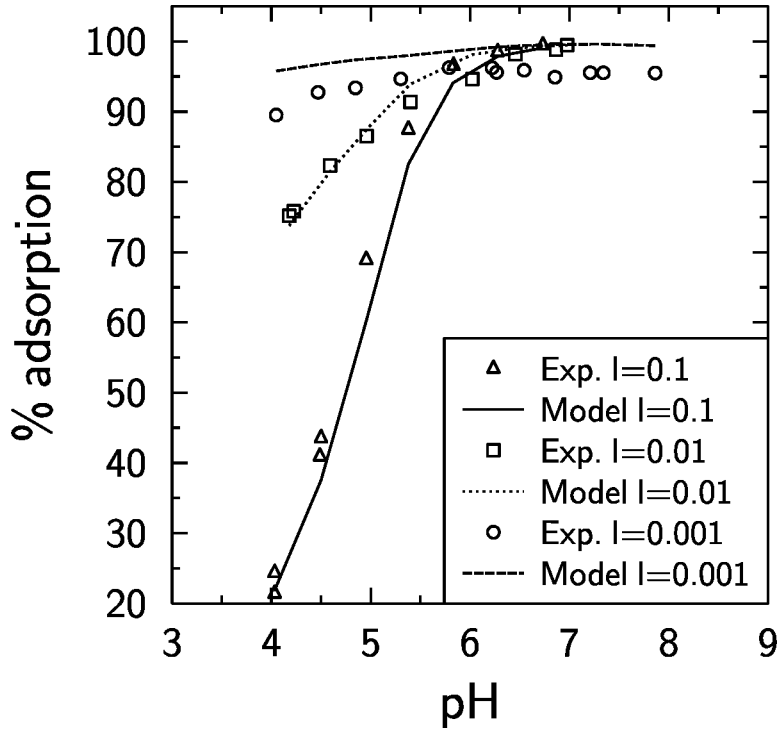

Figure 2-11. Comparison of model predictions (lines) with U(VI) adsorption data by Turner et al. (1996) (symbols). Cation exchange parameters are given in Table 2-3.

2.3.5.6 Data of Marques Fernandes et al. (2012)

Marques Fernandes et al. (2012) conducted U(VI) adsorption experiments on the <0.5 µm fraction of a SWy-1 montmorillonite over a wide range of pH and total U(VI) concentrations while varying pCO_2. Experimental data at pH>7, in the presence and absence of atmospheric pCO_2 (actual DIC concentrations were not measured), were predicted satisfactorily by the reference model without further modifications

(Figure 2-12). Experimental data obtained at lower pH, however, had higher adsorption than predicted by the reference model. The position of the pH adsorption edge could only be reproduced by increasing the edge surface area by a factor 10. This is obviously not a justifiable assumption, even if we consider that the authors used a finer clay fraction (<0.5 µm) than in most other reported studies (< 2 µm). With the large edge surface area, U(VI) adsorption was also greatly overestimated at pH>7 (Figure 2-12). The SWy-1 montmorillonite material of Marques Fernandes et al. (2012) thus exhibits U(VI) adsorption properties that are significantly different from the SWy-1 material studied by McKinley et al. (1995) and all other montmorillonite materials studied in the literature, given the otherwise good agreement between experimental data and our model predictions for a large number of other studies.

Based on the quality of fit, Marques Fernandes et al. (2012) attributed the very high adsorption affinity of SWy-1 montmorillonite to "strong sites", with a specific site density of ~2 mmol·kg^{-1}. However, if present, the influence of such strong sites should have been apparent in the many other studies discussed above, where the U(VI) to solid concentration ratio was lower than the putative "strong site" density. Hence, it appears that, for most other solid materials previously studied, these strong sites either do not exist or are present at a far lower site density than the reported value of ~2 mmol·kg^{-1} (Marques Fernandes et al. 2012). Differences in material preparation procedures could potentially explain this difference in reactivity; e.g., Marques Fernandes et al. (2012) acidified their clay sample to pH 3.5 to remove acid-soluble impurities, while pH 5 was used in this and other previous studies.

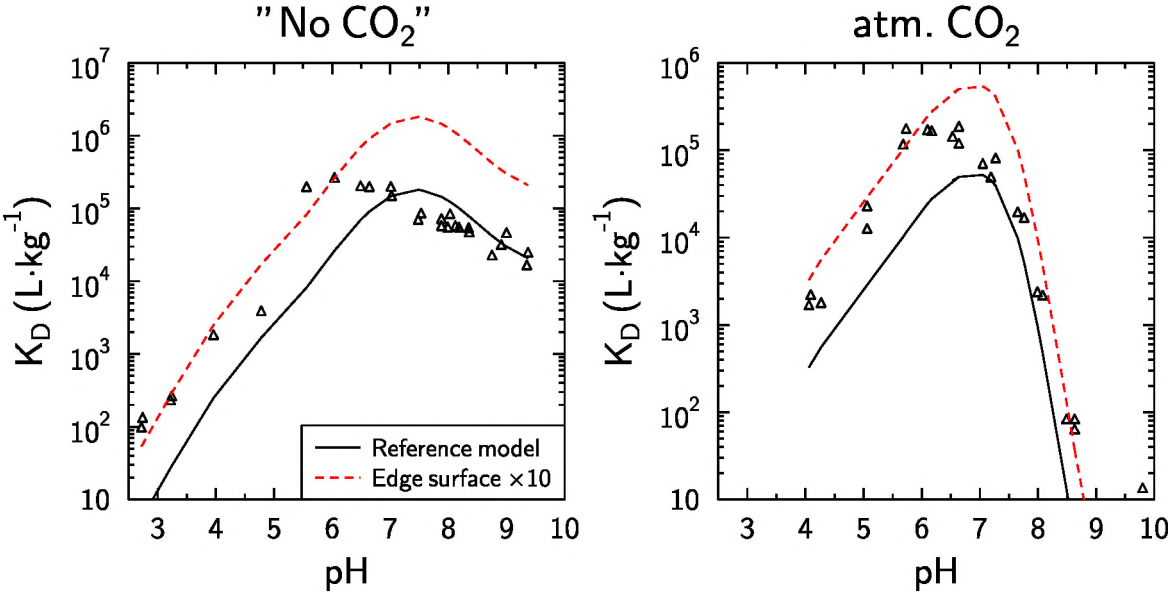

Figure 2-12. Comparison of model predictions (lines) with experimental U(VI) adsorption data on montmorillonite by Marques Fernandes et al. (2012) (symbols).

2.3.6 Summary of Modeling Results

The reference U(VI) adsorption model presented here is based on a state-of-the-art description of the reactivity of montmorillonite clay edges that specifically takes into account the spillover effect of the basal surface potential on the edge surface potential (Bourg et al. 2007; Tournassat et al. 2013, 2015a, 2016a). This model accurately predicts adsorption of U(VI) on montmorillonite surfaces over a wide range of experimental conditions, with only one specific adsorption site, three different U(VI) complexes at the surface, and one cation exchange reaction.

Within the limits of data accuracy, there was no need to include the formation of uranyl-carbonato surface complexes in the model to simulate the experimental data. Including such a species would only be

justified if: (1) the discrepancies between experimental data and model predictions (without including these surface complexes) were larger than the combined uncertainties associated with experimental errors and formation constants for aqueous U(VI)-carbonate complexes, and (2) if actual measurement data are available for all solution parameters, including DIC concentrations (or alternatively, alkalinity). Without these data, we consider the uncertainties of assumed pCO_2 values too large to draw any conclusions regarding the presence of ternary U(VI)-carbonato surface complexes.

For illustration, the effect of varying pCO_2 conditions on U(VI) adsorption is shown in Figure 2-13. Based on these calculations with the reference model, at pH>9 a "true" absence of CO_2 can be interpreted only if it can be demonstrated that actual pCO_2 values are lower than 10^{-6} atm. This partial pressure corresponds to 1 ppm CO_2 in the surrounding atmosphere, i.e., experimental conditions that could be met only with great difficulty in the laboratory, even in a specially equipped glove box. It can be concluded that an "absence of CO_2" at pH>9 (ideally corresponding to $pCO_2=10^{-99}$ atm in Figure 2-13), is, in fact, obtained because of slow gas exchange rates between degassed solutions and the surrounding atmosphere, and not a true equilibrium with atmospheric CO_2. Under these conditions, it is thus necessary to measure DIC concentrations to assess the exact concentrations in solutions exposed to low levels of pCO_2. To our knowledge, this type of measurement has never been performed in previously reported U(VI) adsorption studies on montmorillonite. Most likely, this has sometimes led to false assumptions that previous experiments were conducted at pCO_2 levels that did not impact U(VI) adsorption.

For example Schlegel and Descostes (2009) reported U(VI) adsorption results in the "absence of CO_2" that clearly show evidence of pCO_2 at higher values than ~10^{-5} atm (compare their Figure 1 with Figure 2-13 of this report). Even a precise interpretation of data obtained at atmospheric pCO_2 may be problematic. The value of atmospheric pCO_2 can fluctuate as a function of geographic location, season, and above all the presence of humans in an enclosed lab setting because of respiration and poor ventilation. Also, a slight change in pH after pre-equilibration of the clay, following for example the introduction of a mildly acidic U(VI) spike, can impact the final pCO_2 value if the time-frame of the pH re-adjustment is too short to allow for full gas-solution re-equilibration and the following sorption equilibration is performed in closed sample vials. A pCO_2 of $10^{-3.2}$ instead of $10^{-3.45}$ bar has a significant effect on the prediction of U(VI) adsorption at pH>7. Hence, even with a 'forced' pre-equilibration of background electrolyte solutions with $NaHCO_3$ buffer, the CO_2 exchange with the surrounding atmosphere and other experimental artefacts add a significant uncertainty to the modeling results, unless actual DIC concentrations are used during the model fitting process. This effect is well illustrated with the modeling of U(VI) adsorption data by Troyer et al. (2016) at pH~8 (Figure 2-11).

While actual values of DIC concentrations are critical parameters in the evaluation of U(VI) adsorption, the combined presence of Ca and carbonate further increases the level of complexity and uncertainty in the model calculations. This is due to the formation of aqueous calcium-uranyl-carbonate complexes (Meleshyn et al. 2009), with variable adsorption impacts (Fox et al. 2006). According to the reference model, the effect of the formation of this complex on U(VI) adsorption could be significant for Ca^{2+} concentrations larger than 2 mmol·L^{-1}, which is in agreement with our experimental results (Figure 2-14).

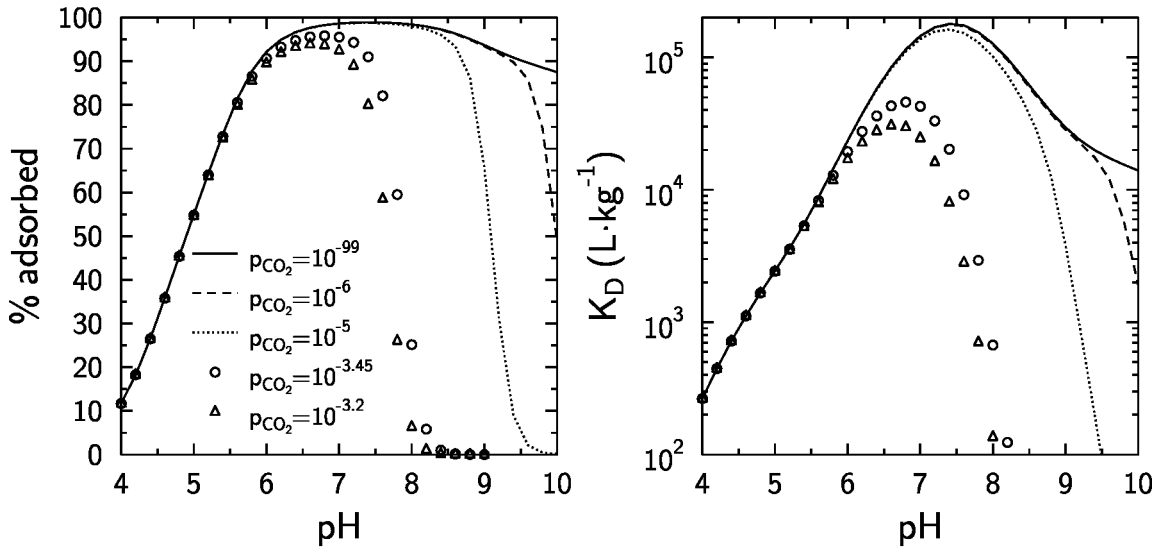

Figure 2-13. Predicted effect of pCO_2 on U(VI) adsorption onto montmorillonite using our reference model with a solid concentration of 0.5 g·L^{-1} , a 0.1M NaCl background electrolyte and a total U(VI) concentration of 10^{-7} M.

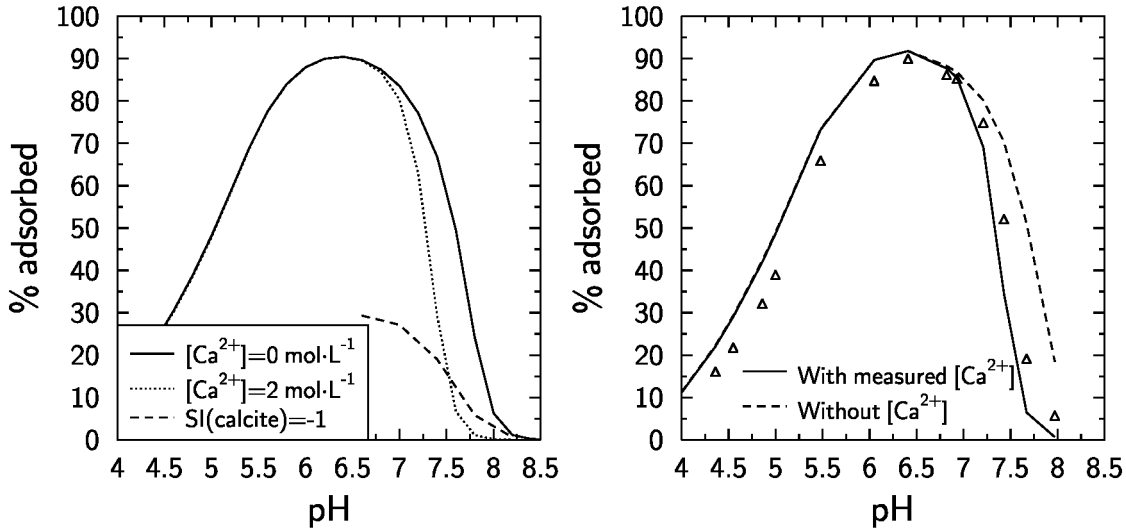

Figure 2-14. Left: Predicted effect of Ca^{2+} concentration on U(VI) adsorption using our reference model with a solid concentration of 0.5 g·L^{-1}, a 0.1 M NaCl background electrolyte, a total U(VI) concentration of 10^{-6} M, and a $pCO_2=10^{-3.2}$ bar. Solubility index (SI) for calcite is plotted for comparison. Right: Comparison of our experimental data with model results with and without taking into consideration the impact of Ca^{2+} on U(VI) solution speciation.

3. URANIUM(VI)-MONTMORILLONITE DIFFUSION EXPERIMENTS AT ALKALINE pH CONDITIONS

3.1 Materials and Methods

3.1.1 Chemicals and Solutions

All chemicals used in this study were reagent grade or better. Acids, bases, and salt solutions used in diffusion and batch kinetic sorption experiments were of TraceSelect grade (Sigma Aldrich) in order to minimize calcium background concentrations. Aqueous solutions were prepared with Nanopure water (ThermoScientific ultrapure water system). Glassware was cleaned by soaking in acid (10 % (v/v) HCl) for 12 to 24 hours, followed by thorough rinsing with Nanopure water and air-drying.

A U-233 stock solution provided by Dr. Heino Nitsche (Nuclear Sciences Division, Lawrence Berkeley National Laboratory, deceased) was utilized for these experiments. However, a purification of the stock solution was necessary in order to remove accumulated daughter products (Th-229, Ra-225, Ac-225), and to ensure that U-233 was present as uranium (VI) and in a known chemical solution matrix. The purification procedure was based on the separation of uranium from impurities using an Eichrom UTEVA resin column (2-mL cartridges, 50-100 µm UTEVA resin, Eichrom P/N: UT-R50-S), while largely following the recommendations provided in Method ACW02, Rev. 1.4 (Uranium in Water) by Eichrom Technologies, LLC. A detailed summary of the procedures is provided in the Appendix. Very briefly, the original U-233 stock solution (5 mL, 25 µCi total, nominal activity) was carefully dried in a Savillex PFA vial on a hot plate and, after a series of other steps, loaded onto the preconditioned resin column in 10 mL of 3 M nitric acid-1 M aluminum nitrate solution plus 1 mL of 3.5 M $NaNO_2$. After a series of additional steps (see Appendix for details), the purified U-233 was eluted from the column into three separate Savillex vials using 1 M HCl (twice) and 0.5 M HCl (once). Based on the weighing and liquid scintillation counting of the resulting, purified stock solutions, we estimated 100% recovery of U-233 after purification.

3.1.2 Montmorillonite

A commercially available, well-characterized, standardized Source Clay (Na-montmorillonite, SWy-2, Clay Minerals Society) was used as the solid material in all experiments. Given its known amounts of impurities in terms of quartz (8%), feldspars (16%) and calcite (Chipera and Bish 2001; Costanzo and Guggenheim 2001; Mermut and Cano 2001), the Source Clay was purified prior to its use in experiments, as described in detail elsewhere (Tinnacher et al. 2016).

Furthermore, dry, purified Na-montmorillonite was pre-equilibrated with the background electrolyte solutions at the specified pH-conditions (pH-8.75 and pH-8.95) in batch systems in order to accelerate the pH-equilibration in 0.1 M NaCl/$NaHCO_3$ background electrolyte prior to any diffusion experiments. The specific compositions of background electrolyte solutions at pH 8.75 and 8.95 and a total ionic strength of 0.1 M (pH-8.75: 9.52E-2 M NaCl, 4.32E-03 M $NaHCO_3$, 4.49E-4 M NaOH; pH-8.95: 9.22E-2 M NaCl, 7.05E-3 M $NaHCO_3$, 1.13E-03 M NaOH) were based on aqueous speciation calculations, taking into account the ionic strength contributions of the buffer (sodium bicarbonate) and the base (sodium hydroxide) to be added for initial pH adjustments.

Two-liter electrolyte solutions were prepared using high-purity chemicals (Fluka TraceSelect NaCl and NaOH; Alfa Aesar Puratronic $NaHCO_3$). After an initial equilibration of solutions with atmospheric CO_2 over two days, the pH was further adjusted by adding small volumes of high-purity HCl or NaOH. Then, six aliquots of approximately 1 gram of Na-montmorillonite were added to six acid-washed 40-mL polycarbonate centrifuge vials (Oakridge tubes). After adding 33 mL of pH-adjusted background electrolyte solutions to each vial (three vials per pH condition), the clay was first mixed by hand and then on a rotary shaker over four days. Afterwards, the pH values of the clay suspensions were recorded, and the clay separated from solutions in two consecutive centrifugation steps (Avanti J-E centrifuge, JA-17 rotor, 16,000 rpm; 31,511 average g-force, for 33 minutes each). After re-combining all clay fractions in the original polycarbonate vials, 20 mL of fresh background electrolyte solutions were added to each

individual vial, and the clay mixing and equilibration steps repeated for a total number of 10 steps over three weeks (individual equilibration times of 4, 0.8, 0.8, 1, 3.8, 0.9, 1, 0.9, 2.9, and 1 days). Afterwards, three pH fine-adjustments were performed by adding small volumes of HCl and NaOH solutions directly to the individual vials over three days, while allowing for system equilibration over about one day after each adjustment. An overview of the changing pH conditions after each equilibration or adjustment step is provided in the Appendix. The first and second pH values determined for pH-8.75 and pH-8.95 clay suspensions were pH 7.5 and 7.9, and pH 7.9 and 8.4, respectively. Over the course of the repeated exchange of electrolyte solutions and the pH fine-adjustments, the incremental increases in pH between equilibration steps became smaller. Over this time-frame, the pH values in electrolyte control solutions not in contact with clay remained stable. Pre-equilibrated clay samples were then isolated from solutions by centrifugation as described above, dried in a convection oven at 45 °C over five days, and ground on a Retsch MM 400 ball mill with tungsten-carbide balls (frequency of 30/sec for 2 minutes) prior to their use in experiments. No relevant changes in sample mineralogy were observed due to pH pre-equilibration, based on the elemental analysis of solid samples before and after (total digestion of ~1 gram of solids combined with XRF analysis and a Ca colorimeter measurement; see Appendix).

3.1.3 Uranium(VI) Through-Diffusion Experiments

3.1.3.1 Selection of Experimental Conditions

Uranium(VI) through-diffusion experiments were set up with the goal to investigate the effects of two processes on U(VI) diffusion at the same time: (1) the potential exclusion of anionic uranium(VI) solution species from montmorillonite interlayer spaces, and (2) U(VI) sorption onto montmorillonite. Given this goal, and to ensure U(VI) breakthrough within reasonable experimental time-frames, a careful selection of experimental conditions in terms of pH, total uranium(VI) concentration and degree of clay compaction was necessary.

With regard to pH, the selected target pH conditions had to ensure: (1) a predominance of negatively-charged uranium(VI) species in solution to evaluate potential anion exclusion effects, and (2) a sufficiently low U(VI) sorption affinity in order to avoid strong U(VI) retardation and unreasonably long experimental time-frames. For the latter, results from preliminary transport calculations indicated that log K_D values between 0.7 and 1 [L kg^{-1}] (K_D=5-10 [L kg^{-1}]) would be appropriate. The first requirement leads to the selection of alkaline pH conditions; the second further narrows the pH range to values between 8 and 9 based on previous U(VI) batch sorption experiments with the same solid (see sections above). Hence, we decided to perform two parallel through-diffusion experiments at target pH values of 8.75 and 8.95, with the expectation that clay interactions with the pH-adjusted electrolyte solutions could potentially further lower pH, given our experience from a previous diffusion experiment (Tinnacher et al. 2016).

We selected uranium-233 as the only uranium isotope to be used in these diffusion experiments due to its short half-life relative to other uranium isotopes. At a nominal total U(VI) concentration of 2.35×10^{-6} M, this allows for better detection limits of low uranium(VI) concentrations in solution, a relatively straight-forward and fast analysis by liquid scintillation counting, and hence a close and timely monitoring of diffusive fluxes over the course of diffusion experiments.

Last, a low degree of clay compaction (~ 0.8 kg dm^{-3}) was chosen to facilitate a reasonably fast diffusive transport of U(VI), and to allow for a simulation of Ca diffusion and its effects on U(VI) solution speciation, sorption and diffusive transport, if necessary, based on previous experimental Ca diffusion data at the same degree of compaction (Tinnacher et al. 2016). While we purified our solid material in order to avoid this additional level of complexity (see details above), the dissolution of trace calcite impurities in montmorillonite, or release of Ca from montmorillonite cation exchange sites, could still potentially lead to Ca solution concentrations affecting U(VI) sorption and transport behavior.

3.1.3.2 Experimental Setup and Procedure

Uranium(VI) through-diffusion experiments largely followed procedures previously described in the literature (Molera and Eriksen 2002; Van Loon et al. 2003a, b; Tinnacher et al. 2016). The experimental setup consists of a set of two diffusion cells, each connected to high- and low-concentration reservoirs with Teflon tubings, and a peristaltic pump circulating solutions over both ends of the diffusion cells (see figure A-9 in Appendix). These experiments include a series of steps which can be summarized as follows: (1) dry-packing of the pH-equilibrated montmorillonite samples into diffusion cells, (2) saturation of the initially dry clay packings with background electrolyte solutions at the specified, target pH, (3) a through-diffusion experiment with tritiated water (HTO) tracer to determine the total porosity of the clay packing in each cell, and (4) the uranium(VI) through-diffusion experiment, which is a HTO out-diffusion experiment at the same time.

At the beginning of the experiment, dry, pH-equilibrated Na-montmorillonite samples were packed into the diffusion cells (PEEK; D=1.0 cm, L=0.5 cm; Alltech 2 µm stainless-steel frits, P/N 721825) by hand with the goal to obtain a dry bulk density of approximately 0.8 kg dm^{-3}. The clay was carefully compacted with a custom-made PEEK rod, and then saturated with the individual background electrolyte solutions (0.1 M NaCl, pH-8.75 or pH-8.95; for exact composition see above) by circulating electrolyte solutions for about 3 ½ weeks (two 200-mL reservoirs per cell; estimated flow rate of 0.78 mL min^{-1}). Prior to their contact with the mineral phase, these electrolyte solutions had been repeatedly adjusted to the target pH values of pH 8.75 and 8.95 using small volumes of acid/base solutions (TraceSelect grade NaOH and HCl) while equilibrating with atmospheric CO_2. The exact dry densities of the clay packings (pH-8.75: 0.766 kg dm^{-3}; pH-8.95: 0.772 kg dm^{-3}) were calculated after determining the water content of dry, pH-equilibrated clay fractions from the same batches of solids used in diffusion experiments (drying at 150 °C for approximately five days).

After clay saturation, tracer tests with tritiated water (HTO) were initiated by replacing the reservoir solutions with 200 mL of background electrolytes at pH-8.75 or pH-8.95 containing ~24 nCi/mL (~890 Bq mL^{-1}) HTO (high-concentration reservoirs) on one end of each diffusion cell, and 20 mL reservoirs containing fresh, HTO-free electrolyte solutions (low-concentration reservoirs) on the opposite ends. Over the following weeks, the circulation of solutions was continued at the same flow rate. Electrolyte solutions in the low-concentration reservoirs were repeatedly replaced in order to maintain a nearly constant concentration gradient between the high- and low-concentration reservoirs. The exchanged low-concentration reservoir vials were weighed to correct for volume losses due to evaporation in the hood. Solutions were sampled for tritium analysis by liquid scintillation counting (PerkinElmer Liquid Scintillation Analyzer Tri-Carb 2900TR; Ultima Gold XR liquid scintillation cocktail), and their solution pH values were recorded. This procedure was continued until a series of data points had been collected under steady-state conditions for HTO diffusive fluxes.

The solutions in the high-concentration reservoirs were then replaced with HTO-free background electrolyte solutions at pH-8.75 and pH-8.95 containing a nominal concentration of 2.35×10^{-6} M uranium(VI) in the form of U-233 (exact concentrations were 2.36×10^{-6} M U-233 or 5.35 nCi mL^{-1} = 198 Bq mL^{-1} for pH-8.75, and 2.34×10^{-6} M U-233 or 5.30 nCi mL^{-1} = 196 Bq mL^{-1} for pH-8.95). Again, low-concentration reservoir solutions were continuously replaced, and uranium-233 and tritium activities analyzed (PerkinElmer Liquid Scintillation Analyzer Tri-Carb 2900TR; Ultima Gold XR liquid scintillation cocktail), with the goal to collect a sufficient number of data points under steady-state conditions for uranium(VI) diffusive fluxes in each system.

After the pH values in low-concentration reservoir solutions were recorded, solution fractions were collected for later ICP-MS analysis and alkalinity titrations. Metals analysis by ICP-MS (1:1 dilutions with 2% TraceSelect HNO_3, Perkin-Elmer SCIEX ICP-Mass Spectrometer ELAN DRC II) focused on elements that could either be relevant for uranium(VI) solution speciation (Ca, Mg) or indicate any potential montmorillonite degradation (Si, Al, Fe, etc.). Alkalinity titrations had the goal to constrain carbonate concentrations for later U(VI) solution speciation, sorption and transport modeling. For this purpose, Gran alkalinity titrations were performed on 5-ml fractions of selected low concentration

reservoir solutions using 0.02 eq/L sulfuric acid (Manufacturer: BDH). Precision reference standards (pH 4.000, 7.000 and 10.000, Ricca Chemical Company) were used for the calibration of the VWR pH meter. Since a pH drift to higher pH values was observed during initial titrations, possibly due to slow gas exchange with atmospheric CO_2, solutions were first titrated from the initial sample pH to a pH value of around 4, then allowed to reach pH stabilization over 27-46 hours. Afterwards, sample titrations were continued to the final end point at pH~3.2.

It is important to note that, with the replacement of HTO high-concentration reservoir solutions with HTO-free U-233 high-concentration reservoir solutions, we essentially started an 'out-diffusion' experiment for tritium. At the end of the tritium tracer test, and after reaching steady-state conditions, a linear HTO concentration profile had been established across the clay packing in the diffusion cell. By replacing the high-concentration reservoir with a HTO-free solution and continuously exchanging low-concentration reservoir solutions during the uranium(VI) diffusion experiments, new concentration gradients between HTO in the diffusion cells and the reservoir solutions are established. Hence, HTO diffuses out of the cells in both directions, and is accumulated in both, the high- and low-concentration reservoir solutions. As a result, low HTO concentrations are detected in low-concentration reservoir solutions during the uranium(VI) through-diffusion experiments. These 'out-diffusion' data for HTO (data not reported) allow us to further constrain total porosity values that are inferred from simulations of HTO through-diffusion data.

Furthermore, given the high importance of pH for U(VI) solution speciation and sorption behavior, we performed two additional types of pH measurements at two other points in the experimental setup during uranium(VI) diffusion experiments. First, a small pH probe was repeatedly immersed directly into the two high-concentration reservoir solutions containing U-233. In addition, we collected small volumes (3-5 mL) of 'flow-back' solutions directly from Teflon tubings. These samples represent high-concentration reservoir solutions that had been in contact with the clay packings in the diffusion cells, and were in the process of flowing back into the high-concentration reservoirs. After these pH measurements, collected solution fractions were returned to their respective reservoirs. These 'flow-back' solution measurements were taken in order to evaluate whether the pH values directly recorded in high-concentration reservoir solutions actually represented the pH conditions of solutions in contact with the clay packings. This consideration is based on the large dilution effect occurring in high-concentration reservoirs during the circulation of solutions (200 mL of reservoir volume versus 0.78 mL min^{-1} flow-rate for the circulating solution). However, both of these types of measurements were performed much less frequently than pH measurements of low-concentration reservoir solutions in order to minimize any potential disturbances to experiments.

Last, over the course of the 81-day uranium(VI) through-diffusion experiments, plastic tubings in the peristaltic pump were repeatedly replaced. Nonetheless, one of the tubings delivering high-concentration reservoir solution to the pH-8.95 diffusion cell failed, sometime after the sampling event on day 35. After the problem was noticed, the continuous flow of solutions was stopped for both cells in order to replace peristaltic tubings as well as the lost pH-8.95 high-concentration reservoir solution. The results reported in the following only cover time-frames (1) before the tubing failure, and (2) after the continuous flow of reservoir solutions was resumed and both systems stabilized again after the flow interruption.

3.2 Results and Discussion

3.2.1 pH Monitoring Data for High- and Low-Concentration Reservoir Solutions

In Figure 3-1, we show a summary of pH monitoring data recorded during the consecutive through-diffusion experiments with tritiated water (HTO), then uranium(VI), for both diffusion cells, set up at target pH values of pH 8.75 and 8.95. While a drop in pH was observed due to the contact of the background electrolyte solutions with the clay packings in both systems, pH conditions remained reasonably stable over the course of experiments. During U(VI) through-diffusion experiments, the average pH values measured in low-concentration reservoir solutions were calculated at pH 8.71 and 8.87 for the systems at target pH values of pH 8.75 and 8.95, respectively. Values of pH recorded in high-concentration and 'flow-back' solutions were generally in the same range than those measured in low-concentration reservoir solutions. Furthermore, no systematic differences in pH values between high-concentration reservoir and 'flow-back' solutions could be observed.

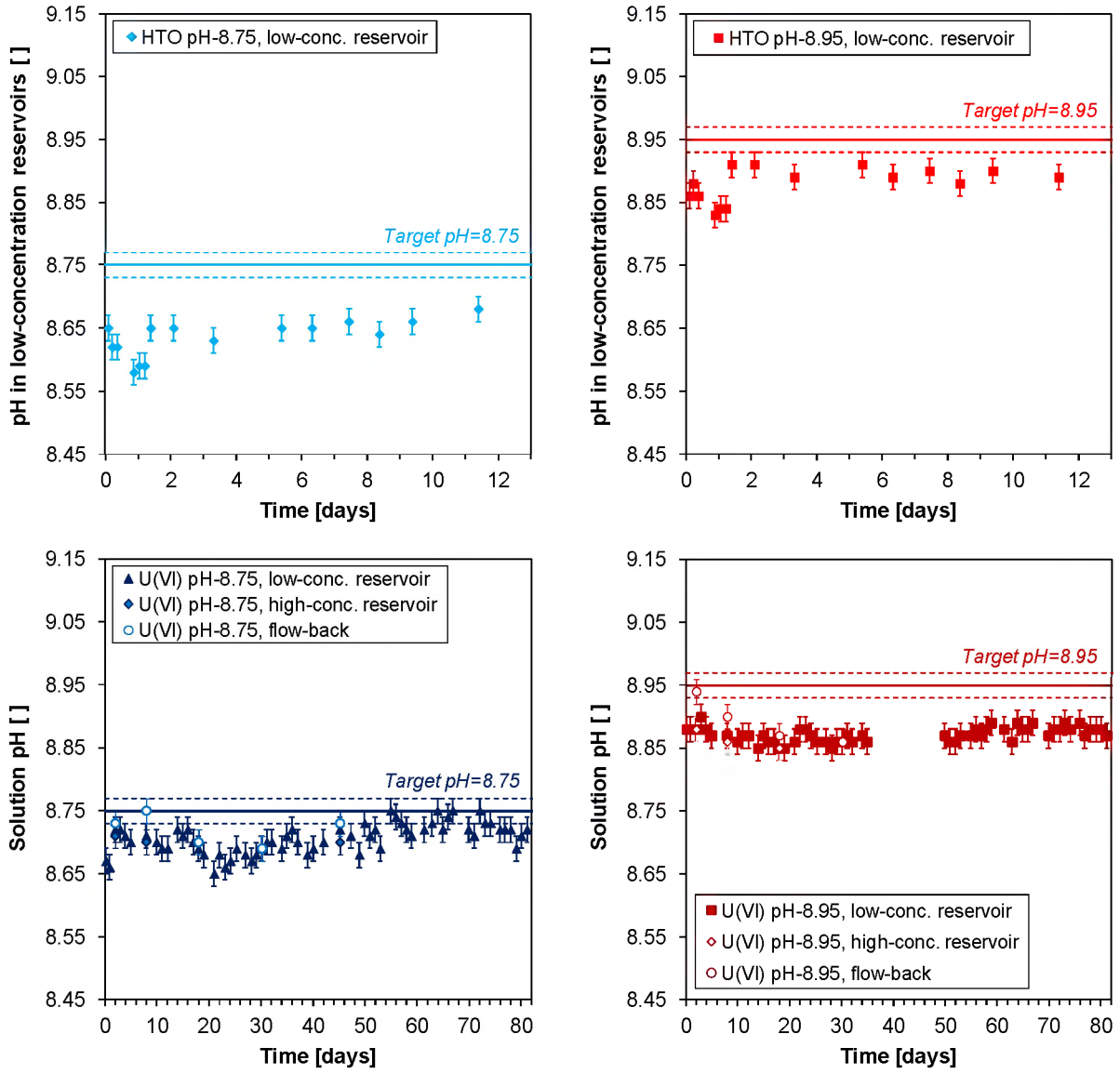

Figure 3-1. pH monitoring data for through-diffusion experiments with tritiated water (HTO, top) and uranium(VI) (bottom) in two, parallel diffusion cells set up at target pH values of pH 8.75 and 8.95. Data series include pH measurements for low-concentration reservoir, high-concentration reservoir and 'flow-back' solutions. High-concentration reservoir and 'flow-back' solutions were only analyzed at a few, selected time-points during U(VI) through-diffusion experiments. Measured pH values in 'flow-back' and high-reservoir solutions were the same, wherever data points for high-concentration reservoir solutions are not clearly visible.

3.2.2 Normalized Flux Data for Through-Diffusion Experiments with Tritiated Water

As described in last year's annual report, normalized mass flux densities reaching the low-concentration reservoir (J_N in m day^{-1}) were calculated with the following expression:

$$J_N = \frac{C_{low}}{C_{high}} \frac{V_{low}}{A\Delta t} \qquad (6)$$

where C_{low} is the concentration of the species of interest measured in the low-concentration reservoir at a sampling event, C_{high} is the constant concentration in the high-concentration reservoir, Δt is the time interval since the previous sampling event (in days), A is the cross sectional area available for diffusion (0.785 cm^2), and V_{low} is the volume of the low-concentration reservoir (about 20 mL).

Figure 3-2 depicts the results for normalized HTO fluxes recorded during the HTO through-diffusion experiments. Based on these data, the normalized HTO flux under steady-state conditions, and hence the total porosity of the clay packing, appear to be slightly higher in the pH-8.75 than the pH-8.95 system. This agrees well with our estimated dry density values for the two cells, with 0.766 and 0.772 kg dm^{-3} for the pH-8.75 and pH-8.95 systems, respectively. Slightly higher dry densities and degrees of clay compaction would result in slightly lower total porosities of the clay packing. A later simulation of both experimental data sets will allow us to determine the total porosity and water diffusion coefficients in each system.

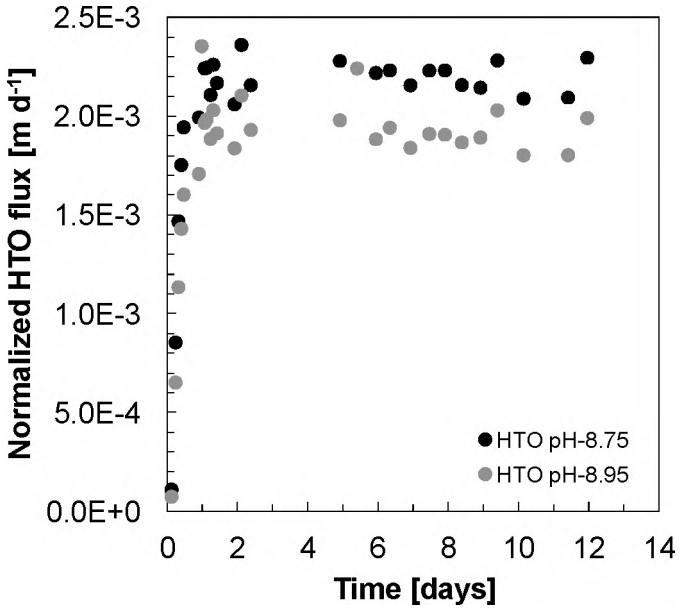

Figure 3-2. Normalized diffusive fluxes of tritiated water (HTO) during HTO through-diffusion experiments at target pH values of 8.75 and 8.95, which are used to determine the total porosities in each diffusion cell prior to U(VI) through-diffusion experiments.

3.2.3 Normalized Flux Data for Through-Diffusion Experiments with Uranium(VI)

Observed normalized fluxes for uranium(VI) are about one order of magnitude lower than fluxes for tritiated water (Figure 3-3). This difference in diffusive fluxes between a non-reactive tracer (HTO) and U(VI) provides direct, experimental evidence for a full or partial exclusion of anionic U(VI) solution species from montmorillonite interlayer spaces. This anion exclusion leads to a decrease in the diffusion-accessible porosity and normalized diffusive fluxes for U(VI) under steady-state conditions. This effect is expected to become even more relevant at the higher degrees of clay/bentonite compaction proposed for future nuclear waste repositories (dry density of ~1.65 kg dm^{-3}), than the one tested in this through-diffusion experiment (dry density of ~0.8 kg dm^{-3}). At high degrees of compaction, montmorillonite interlayer spaces will become the primary contributor to the total porosity in the clay packing. Hence, an exclusion of U(VI) from interlayer spaces effectively minimizes its overall diffusion-accessible porosity and diffusive fluxes.

Furthermore, under both pH conditions, uranium(VI) breakthrough is clearly retarded relative to the non-reactive tracer tritium due to U(VI) sorption onto montmorillonite. A greater U(VI) retardation is observed at target pH-8.75 than pH-8.95, given the different time-points of the initial breakthroughs of U(VI). The latter is in good agreement with uranium(VI) sorption data, which suggest higher uranium(VI)

sorption affinities and K_D values at pH-8.75 than pH-8.95. Uranium(VI) K_D values estimated from U(VI) through-diffusion data (2.0 L kg^{-1} for pH-8.75 and 1.3 L kg^{-1} for pH-8.95) following an approach by Van Loon et al. (2003b) are in the same range of values as would be expected from batch adsorption data (see Appendix, section A-5 for a summary of adsorption data).

Based on our newly developed surface complexation model, U(VI) adsorption onto montmorillonite is dominated by surface complexation reactions on montmorillonite edge sites, not cation exchange reactions on basal surfaces, under the chemical solution conditions tested in U(VI) through-diffusion experiments. This modeling result is further supported by the experimental results from the diffusion experiments. A strong influence of cation exchange reactions would most likely lead to higher U(VI) diffusive fluxes at steady-state conditions relative to the non-reactive tracer (HTO), similar to the diffusion behavior of Ca^{2+}, previously observed in a comparable system (Tinnacher et al. 2016). The latter is due to the 'surface diffusion' of cations along basal cation exchange sites, which are predominantly present within montmorillonite interlayer spaces. Our experimental U(VI) diffusion results, however, indicate a decrease and not an increase in U(VI) diffusive fluxes, compared to the non-reactive tracer.

Last, there appears to be a stronger kinetic limitation for uranium(VI) sorption reactions in the system at pH-8.75 than the one at pH-8.95 (Figure 3-3), since a longer time-frame seems to be required to reach steady-state conditions for U(VI) diffusive fluxes after the initial breakthrough. This indicates a potential overall rate dependence of U(VI) surface complexation reactions on the aqueous speciation of uranium(VI). For instance, the dissociation kinetics of different aqueous uranium(VI) complexes prior to the formation of uranium(VI) surface complexes at montmorillonite edge sites could be different. This hypothesis, however, is currently under further testing (data not reported), based on U(VI)-montmorillonite batch kinetic sorption experiments at the same chemical solution conditions.

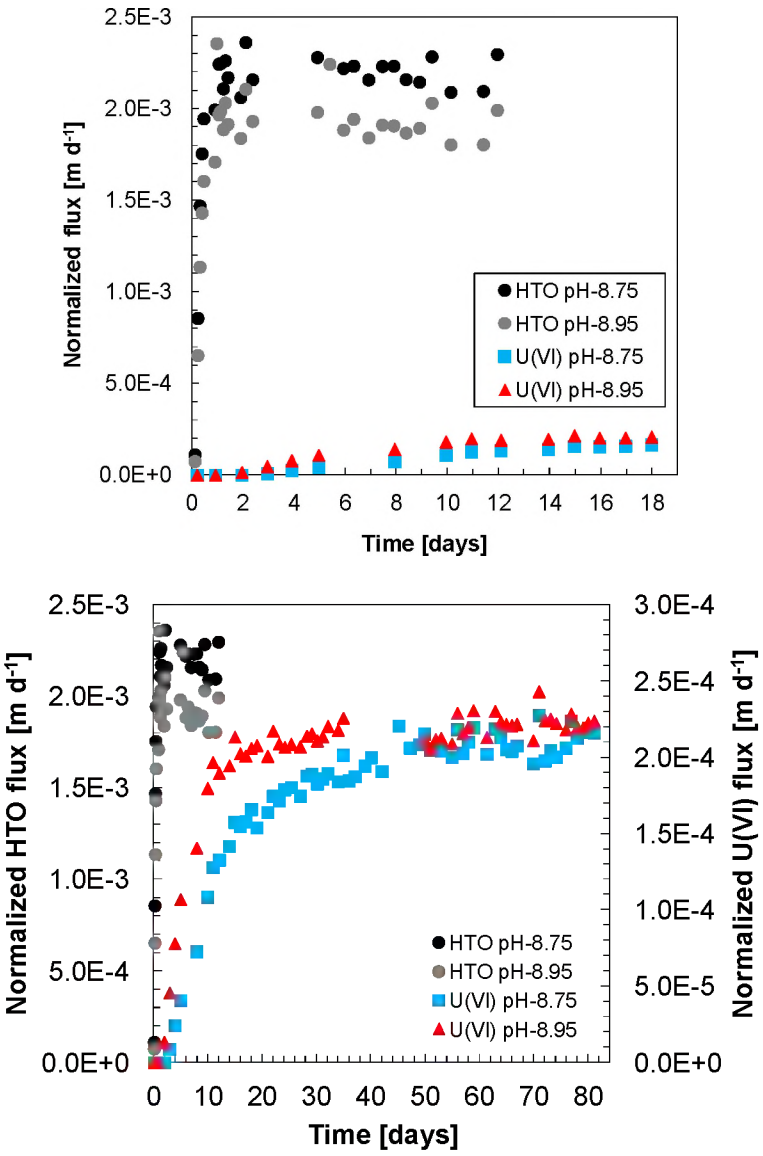

Figure 3-3. Comparison of normalized diffusive fluxes of tritiated water (HTO) and uranium(VI) observed during through-diffusion experiments at target pH values of 8.75 and 8.95 using the same (top) or different (bottom) scales for diffusive fluxes.

3.2.4 Characterization of Chemical Compositions of Low-Concentration Reservoir Solutions

The following results from the characterization of chemical compositions of low-concentration reservoir solutions will allow us to accurately compute U(VI) solution speciation in later simulations of U(VI) diffusion in these through-diffusion experiments. In this context, concentrations of dissolved inorganic carbon/carbonate alkalinity and metals directly affecting U(VI) solution speciation (Ca, Mg) are especially important.

Gran alkalinity titrations indicate stable carbonate concentrations in low-concentration reservoir solutions over the course of U(VI) through-diffusion experiments in both diffusion cell systems (Table 3-1). Alkalinity concentrations are consistently higher in solutions with the higher target pH value, as expected for systems in contact with atmospheric CO_2.

Table 3-1. Summary of results for Gran alkalinity titrations of low-concentration reservoir solutions in U(VI) through-diffusion experiments.

		pH-8.75		pH-8.95	
Sample ID	Time	Alkalinity	Alkalinity	Alkalinity	Alkalinity
[ ]	[days]	[meq/L]	[mg/L as CaCO3]	[meq/L]	[mg/L as CaCO3]
U-5	3.90	5.31	265.54	7.60	380.14
U-10	12.09	5.29	264.55	7.56	377.76
U-16	19.02	5.31	265.44	7.58	379.18
U-22	26.99	5.34	266.79	7.57	378.37
U-28	33.99	5.29	264.30	7.54	377.08
U-60	75.92	5.32	265.91	7.50	375.03
Average		**5.31**	**265.42**	**7.56**	**377.93**
Std. Dev.		**0.02**	**0.91**	**0.04**	**1.78**

Metal concentrations in low-concentration reservoir solutions, measured by ICP-MS analysis, are summarized in Figure 3-4. Based on previous U(VI) speciation calculations in the presence of Ca (Fox et al. 2006), we conclude at this point that Ca solution concentrations were not high enough to affect U(VI) solution speciation during our U(VI) through-diffusion experiments.

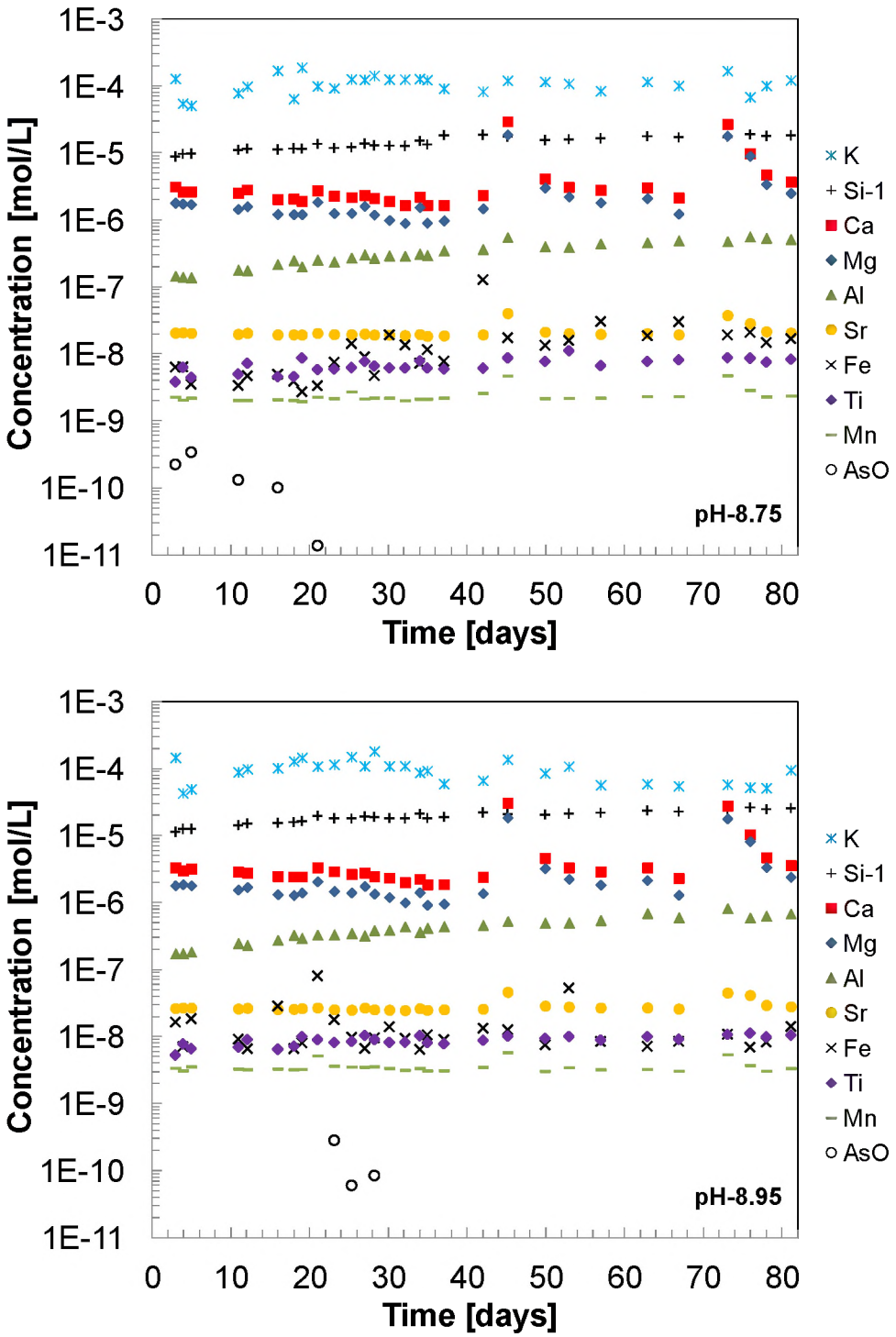

Figure 3-4. Metal concentrations observed in low-concentration reservoir solutions over the course of U(VI) through-diffusion experiments.

THIS PAGE INTENTIONALLY LEFT BLANK

4. SUMMARY AND CONCLUSIONS

With regard to our research on uranium(VI) adsorption onto Na-montmorillonite, we can summarize the major findings and implications as follows:

1. We developed a new surface complexation model (SCM) that specifically accounts for the 'spillover' of the electrostatic surface potential of basal cation exchange sites on the surface potential of neighboring edge sites. This model allows us to simulate U(VI) adsorption onto Na-montmorillonite over a wide range of chemical solution conditions with a lower number of fitting parameters than previous SCM concepts, and without including a second site type or the formation of ternary U(VI)-carbonato surface complexes. This SCM allows us to simulate U(VI) sorption onto montmorillonite as a function of chemical solution conditions, while minimizing the number of fitting parameters in subsequent uranium(VI) diffusion models.
2. Modeling results suggest that an accurate description of the unique characteristics of electrostatic surface potentials on montmorillonite edge sites is highly important, in order to accurately predict U(VI) sorption and transport behavior at larger field scales. Similar modeling approaches may also be useful for other charge-unbalanced, layered mineral phases.
3. Our modeling results further emphasize the strong influence of dissolved carbonate ligands on U(VI) sorption, which is driven by the competition between U(VI)-carbonate complexation reactions in solution and U(VI) surface complexation reactions on montmorillonite edge sites. As a consequence, predictive U(VI) transport models need to capture potential changes in dissolved inorganic carbon (DIC) concentrations over time and space, e.g. in case of variable contents in carbonate minerals along transport pathways and/or fluctuating pH conditions. For instance, calcite impurities in bentonite, the proposed buffer material at future nuclear waste repositories, may affect U(VI) sorption by providing a source of dissolved carbonate concentrations.
4. Lastly, a measurement of DIC concentrations appears to be crucial for accurate simulations of U(VI) aqueous speciation during the development and calibration of SCMs. Assumptions of a full exclusion of inorganic carbon from sample solutions in CO_2-"free" adsorption experiments, or a complete solution equilibration with atmospheric/elevated CO_2 levels in the local atmosphere, may often not be justified. This is due to the generally challenging nature of CO_2-"free" adsorption experiments, and the potentially slow CO_2 gas exchange between sample solutions and the local atmosphere under atmospheric/elevated CO_2 conditions. Hence, we recommend that DIC analysis or alkalinity titrations are included as routine measurements in future U(VI) adsorption studies. Furthermore, future experimental designs should also take into account the experimental challenges experienced in this study, with regards to achieving constant pCO_2 conditions across a series of sample solutions in a given adsorption experiment.

Our experimental results from U(VI)-montmorillonite diffusion experiments at alkaline pH can be briefly summarized as follows:

1. Our experimental data provide a first, direct experimental evidence of a full or partial exclusion of anionic U(VI) solution species from montmorillonite interlayer spaces in through-diffusion experiments at alkaline pH and low degrees of clay compaction. This anion exclusion effect results in a significant decrease in the U(VI) diffusion-accessible porosities and U(VI) diffusive fluxes by about one order of magnitude compared to a tritiated water tracer at a compaction of 0.8 kg dm^{-3}. At higher degrees of compaction, and with a larger relevance of clay interlayer spaces for the total porosity in the system, this phenomenon should be even further pronounced, possibly leading to extremely low diffusive fluxes of U(VI).
2. In addition, the U(VI) diffusion results further emphasize the importance of U(VI) adsorption reactions onto Na-montmorillonite in controlling U(VI) retardation during diffusive transport, even at fairly alkaline pH values, where U(VI) adsorption is typically low compared to more circum-neutral pH conditions.

3. Lastly, apparent kinetic limitations were observed for U(VI) sorption reactions in the diffusion cell at a target pH value of pH-8.75, compared to the system at pH-8.95. These apparent kinetic effects, however, need to be further evaluated experimentally and/or based on the simulation of U(VI) diffusion behavior. If relevant, they could affect the time-frames needed to reach full steady-state conditions for U(VI) diffusive fluxes across engineered barrier systems.

All of these results need to be taken into account for the conceptual development of U(VI)-montmorillonite adsorption and diffusion 'sub-models', as part of higher-level performance assessment models.

5. OUTLOOK ON FUTURE WORK

The following tasks are planned for the remaining time in this fiscal year (FY 2016):

(1) Submit a journal manuscript on the development of our new U(VI)-montmorillonite surface complexation model for publication.

(2) Evaluate the apparent kinetic limitations observed for U(VI) adsorption reactions in U(VI) diffusion experiments based on batch kinetic sorption experiments and/or during the simulation of U(VI) diffusive transport.

For the upcoming fiscal year (FY 2017), we plan to:

(1) Simulate the U(VI) diffusion behavior, observed at alkaline pH conditions and low degree of compaction in previous U(VI) through-diffusion experiments, while applying the newly developed U(VI)-montmorillonite surface complexation model to capture U(VI) adsorption processes.

(2) Test experimentally if U(VI) diffusion in Na-montmorillonite can be measured at the extremely low fluxes expected at alkaline pH and the high degrees of compaction (~1.65 kg dm^{-3}) proposed for nuclear waste repositories. If this is the case, then future performance assessment models could possibly rule out U(VI) as a potential contaminant of concern for a certain range of system conditions, e.g., at alkaline pH and high degrees of clay compaction.

Then, we would like to focus our efforts on bentonite samples from the second dismantling phase of the FEBEX heater test. These FEBEX samples represent unique, 'natural' samples with regards to realistic degrees of bentonite compaction (bentonite 'rock') and mineralogical impurities in the solid. The latter is expected to lead to a more complex chemical solution composition in the pore water, e.g. in terms of non-radioactive cations competing for cation exchange sites at low pH and ionic strength. Furthermore, these heat-treated samples also allow us to investigate the potential impacts of a ten-year bentonite exposure to moderate heat (at various water saturation levels) on mineralogical changes in bentonite and possible impacts on U(VI) sorption behavior. Hence, we plan the following experimental work with these FEBEX samples:

(1) Evaluate if U(VI) adsorption affinities onto bentonite have changed due to the heat treatment; and

(2) Characterize potential impacts of mineral impurities in bentonite on the overall diffusion-accessible porosities and U(VI) anion exclusion effects at alkaline pH.

6. ACKNOWLEDGEMENTS

This research was supported by the U.S. Department of Energy under Contract DE-AC02-05CH11231 under the auspices of the Used Fuel Disposition program (Office of Nuclear Energy) and by the French Geologic Survey (BRGM) through the Institut Carnot BRGM. The authors would like to thank Professor Jonsson and co-workers at the Applied Physical Chemistry, KTH, Sweden, for providing the diffusion cells used in this study.

7. REFERENCES

Adinarayana, K.N.V., Sasidhar, P., Balasubramaniyan, V., 2013. Modelling of calcium leaching and its influence on radionuclide migration across the concrete engineered barrier in a NSDF. *Journal of environmental radioactivity* 124, 93–100.

Arai, Y., McBeath, M., Bargar, J. R., Joye, J., and Davis, J. A., 2006. Uranyl adsorption and surface speciation at the imogolite-water interface: Self-consistent spectroscopic and surface complexation models. *Geochim. Cosmochim. Acta* 70, 2492-2509.

Bildstein, O., and Claret, F., 2015. Chapter 5- Stability of clay barriers under chemical perturbations. In: Tournassat, C., Steefel, C.I., Bourg, I.C., Bergaya, F. (Eds.), *Natural and Engineered Clay Barriers*, *Developments in Clay Science*. Elsevier, pp. 155–188.

Bourg, I.C., Sposito, G., Bourg, A.C.M., 2007. Modeling the acid-base surface chemistry of montmorillonite. *Journal of Colloid and Interface Science* 312, 297–310.

Bradbury, M.H., and Baeyens, B., 2003. Porewater chemistry in compacted re-saturated MX-80 bentonite. *Journal of Contaminant Hydrology* 61, 329–338.

Bradbury, M.H., and Baeyens, B., 2005. Modelling the sorption of Mn(II), Co(II), Ni(II), Zn(II), Cd(II), Eu(III), Am(III), Sn(IV), Th(IV), Np(V) and U(VI) on montmorillonite: Linear free energy relationships and estimates of surface binding constants for some selected heavy metals and actinides. *Geochimica et Cosmochimica Acta* 69, 875–892.

Bradbury, M.H., and Baeyens, B., 2011. Predictive sorption modelling of Ni(II), Co(II), Eu(IIII), Th(IV) and U(VI) on MX-80 bentonite and Opalinus Clay: A "bottom-up" approach. *Applied Clay Science* 52, 27–33.

Brigatti, M.F., Galán, E., Theng, B.K.G., 2013. Chapter 2 - Structure and Mineralogy of Clay Minerals. In: Bergaya, F., Lagaly, G. (Eds.), *Handbook of Clay Science*, *Developments in Clay Science*. Elsevier, pp. 21–81.

Catalano, J.G., and Brown, G.E. Jr., 2005. Uranyl adsorption onto montmorillonite: Evaluation of binding sites and carbonate complexation. *Geochimica et Cosmochimica Acta* 69, 2995–3005.

Chang, F.R.C., Sposito, G., 1994. The electrical double layer of a disked-shaped clay mineral particle: effect of particle size. *Journal of Colloid and Interface Science* 163, 19–27.

Chang, F.R.C., and Sposito, G., 1996. The electrical double layer of a disked-shaped clay mineral particle: effect of electrolyte properties and surface charge density. *Journal of Colloid and Interface Science* 178, 555–564.

Chipera, S. J. and Bish, D. L., 2001. Baseline studies of The Clay Minerals Society Source Clays: Powder X-ray diffraction analyses. *Clay Clay Min.* 49, 398-409.

Chisholm-Brause, C., Conradson, S.D., Buscher, C.T., Eller, P.G., Morris, D.E., 1994. Speciation of uranyl sorbed at multiple binding sites on montmorillonite. *Geochimica et Cosmochimica Acta* 58, 3625–3631.

Chisholm-Brause, C.J., Berg, J.M., Matzner, R.A., Morris, D.E., 2001. Uranium (VI) sorption complexes on montmorillonite as a function of solution chemistry. *Journal of Colloid and Interface Science* 233, 38–49.

Choppin, G.R., 2006. Actinide speciation in aquatic systems. *Marine Chemistry* 99, 83–92.

Costanzo, P. A. and Guggenheim, S., 2001. Baseline studies of The Clay Minerals Society Source Clays: Preface. *Clay Clay Min.* 49, 371-371.

Curtis, G. P., Davis, J. A., and Naftz, D. L., 2006. Simulation of reactive transport of uranium(VI) in groundwater with variable chemical conditions. *Water Resources Research* 42.

Davis, J.A., James, R.O., Leckie, J.O., 1978. Surface ionization and complexation at the oxide/water interface: I. Computation of electrical double layer properties in simple electrolytes. *Journal of Colloid and Interface Science* 63, 480–499.

Davis, J.A., Meece, D.E., Kohler, M., Curtis, G.P., 2004. Approaches to surface complexation modeling of Uranium(VI) adsorption on aquifer sediments. *Geochimica et Cosmochimica Acta* 68, 3621–3641.

Dent, A.J., Ramsay, J.D., Swanton, S.W., 1992. An EXAFS study of uranyl ion in solution and sorbed onto silica and montmorillonite clay colloids. *Journal of colloid and interface science* 150, 45–60.

Duc, M., Gaboriaud, F., Thomas, F., 2005. Sensitivity of the acid-base properties of clays to the methods of preparation and measurement: 2. Evidence from continuous potentiometric titrations. *Journal of Colloid and Interface Science* 289, 148–156.

Fox, P.M., Davis, J.A., Zachara, J.M., 2006. The effect of calcium on aqueous uranium (VI) speciation and adsorption to ferrihydrite and quartz. *Geochimica et Cosmochimica Acta* 70, 1379–1387.

Gaboreau, S., Claret, F., Crouzet, C., Giffaut, E., Tournassat, C., 2012a. Caesium uptake by Callovian–Oxfordian clayrock under alkaline perturbation. *Applied Geochemistry* 27, 1194–1201.

Gaboreau, S., Lerouge, C., Dewonck, S., Linard, Y., Bourbon, X., Fialips, C.I., Mazurier, A., Pret, D., Borschneck, D., Montouillout, V., Gaucher, E.C., Claret, F., 2012b. In-Situ Interaction of Cement Paste and Shotcrete with Claystones in a Deep Disposal Context. *American Journal of Science* 312, 314–356.

Gaucher, E.C., and Blanc, P., 2006. Cement/clay interactions - A review: Experiments, natural analogues, and modeling. *Waste Management* 26, 776–788.

Giaquinta, D., Soderholm, L., Yuchs, S., Wasserman, S., 1997. The speciation of uranium in a smectite clay: evidence for catalysed uranyl reduction. *Radiochimica Acta* 76, 113–122.

Giffaut, E., Grivé, M., Blanc, P., Vieillard, P., Colàs, E., Gailhanou, H., Gaboreau, S., Marty, N., Madé, B., Duro, L., 2014. Andra thermodynamic database for performance assessment: ThermoChimie. *Applied Geochemistry* 49, 225–236.

Hartmann, E., Baeyens, B., Bradbury, M.H., Geckeis, H., Stumpft, T., 2008. A Spectroscopic Characterization and Quantification of M(III)/Clay Mineral Outer-Sphere Complexes. *Environmental Science & Technology* 42, 7601–7606.

Hennig, C., Reich, T., Dähn, R., Scheidegger, A., 2002. Structure of uranium sorption complexes at montmorillonite edge sites. *Radiochimica Acta* 90, 653–657.

Hsi, C.D., and Langmuir, D., 1985. Adsorption of uranyl onto ferric oxyhydroxides: application of the surface complexation site-binding model. *Geochimica et Cosmochimica Acta* 49, 1931–1941.

Hursh, J., Spoor, N., 1973. Data on man. In: *Uranium· Plutonium Transplutonic Elements*. pp. 197–239.

Hyun, S.P., Cho, Y.H., Hahn, P.S., Kim, S.J., 2001. Sorption mechanism of U(VI) on a reference montmorillonite: binding to the internal and external surfaces. *Journal of Radioanalytical and Nuclear Chemistry* 250, 55–62.

Joseph, C., Schmeide, K., Sachs, S., Brendler, V., Geipel, G., and Bernhard, G., 2011. Sorption of uranium(VI) onto Opalinus Clay in the absence and presence of humic acid in Opalinus Clay pore water. *Chem. Geol.* 284, 240-250.

Kerisit, S. and Liu, C. X., 2010. Molecular simulation of the diffusion of uranyl carbonate species in aqueous solution. *Geochim. Cosmochim. Acta* 74, 4937-4952.

Kowal-Fouchard, A., Drot, R., Simoni, E., Ehrhardt, J.J., 2004. Use of spectroscopic techniques for uranium(VI)/montmorillonite interaction modeling. *Environmental Science & Technology* 38, 1399–1407.

Ma, R., Zheng, C., Prommer, H., Greskowiak, J., Liu, C., Zachara, J., and Rockhold, M., 2010. A field-scale reactive transport model for U(VI) migration influenced by coupled multirate mass transfer and surface complexation reactions. *Water Resources Research* 46.

Liu, X., Cheng, J., Sprik, M., Lu, X., Wang, R., 2014. Surface acidity of 2:1-type dioctahedral clay minerals from first principles molecular dynamics simulations. *Geochimica et Cosmochimica Acta* 140, 410–417.

Liu, X., Cheng, J., Sprik, M., Lu, X., Wang, R., 2015a. Interfacial structures and acidity of edge surfaces of ferruginous smectites. *Geochimica et Cosmochimica Acta* 168, 293–301.

Liu, X., Lu, X., Cheng, J., Sprik, M., Wang, R., 2015b. Temperature dependence of interfacial structures and acidity of clay edge surfaces. *Geochimica et Cosmochimica Acta* 160, 91–99.

Liu, X., Lu, X., Sprik, M., Cheng, J., Meijer, E.J., Wang, R., 2013. Acidity of edge surface sites of montmorillonite and kaolinite. *Geochimica et Cosmochimica Acta* 117, 180–190.

Marques Fernandes, M., Baeyens, B., Dähn, R., Scheinost, A.C., Bradbury, M.H., 2012. U(VI) sorption on montmorillonite in the absence and presence of carbonate: A macroscopic and microscopic study. *Geochimica et Cosmochimica Acta* 93, 262–277.

Marques Fernandes, M., Ver, N., Baeyens, B., 2015. Predicting the uptake of Cs, Co, Ni, Eu, Th and U on argillaceous rocks using sorption models for illite. *Applied Geochemistry* 59, 189–199.

McKinley, J.P., Zachara, J.M., Smith, S.C., Turner, D.R., 1995. The influence of uranyl hydrolysis and multiple site-binding reactions on adsorption of U(VI) to montmorillonite. *Clays and Clay Minerals* 43, 586–598.

Meleshyn, A., Azeroual, M., Reeck, T., Houben, G., Riebe, B., Bunnenberg, C., 2009. Influence of (calcium-) uranyl- carbonate complexation on U (VI) sorption on Ca-and Na-bentonites. *Environmental science & technology* 43, 4896–4901.

Mermut, A. R. and Cano, A. F., 2001. Baseline studies of The Clay Minerals Society Source Clays: Chemical analyses of major elements. *Clay Clay Min.* 49, 381-386.

Milodowski, A.E., Norris, S., Alexander, W.R., 2016. Minimal alteration of montmorillonite following long-term interaction with natural alkaline groundwater: Implications for geological disposal of radioactive waste. *Applied Geochemistry* 66, 184–197.

Molera, M., and Eriksen, T., 2002. Diffusion of $^{22}Na^{+}$, $^{85}Sr^{2+}$, $^{134}Cs^{+}$ and $^{57}Co^{2+}$ in bentonite clay compacted to different densities: experiments and modeling. *Radiochim. Acta* 90, 753–760.

Morris, D.E., Chisholm-Brause, C.J., Barr, M.E., Conradson, S.D., Eller, P.G., 1994. Optical spectroscopic studies of the sorption of UO22+ species on a reference smectite. *Geochimica et Cosmochimica Acta* 58, 3613–3623.

Muurinen, A., Lehikoinen, J., 1999. Porewater chemistry in compacted bentonite. *Engineering Geology* 54, 207–214.

NIH, 2016. U.S. National Library of Medicine, TOXMAP classic Environmental Health Maps: http://toxmap-classic.nlm.nih.gov/toxmap/superfund/mapControls.do; accessed on 05-24-2016.

Pabalan, R.T., Turner, D.R., 1996. Uranium (6+) sorption on montmorillonite: Experimental and surface complexation modeling study. *Aquatic Geochemistry* 2, 203–226.

Parkhurst, D.L., and Appelo, C.A.J., 2013. Description of Input and Examples for PHREEQC Version 3–a Computer Program for Speciation, Batch-reaction, One-dimensional Transport, and Inverse Geochemical Calculations.

Savage, D., Bateman, K., Hill, P., Hughes, C., Milodowski, A.E., Pearce, J.M., Rae, E., Rochelle, C.A., 1992. Rate and mechanism of the reaction of silicates with cement pore fluids. *Applied Clay Science* 7, 33–45.

Schlegel, M.L., and Descostes, M., 2009. Uranium uptake by hectorite and montmorillonite: a solution chemistry and polarized EXAFS study. *Environmental science & technology* 43, 8593–8598.

Steefel, C.I., Appelo, C.A.J., Arora, B., Jacques, D., Kalbacher, T., Kolditz, O., Lagneau, V., Lichtner, P.C., Mayer, K.U., Meeussen, J. C. L., Molins, S., Moulton, D., Shao, H., Šimunek, J., Spycher, N., Yabusaki, S.B., Yeh, G.T., 2015. Reactive transport codes for subsurface environmental simulation. *Computational Geosciences* 19, 445–478.

Stumm, W., 1992. Chemistry of the solid-water interface: processes at the mineral-water and particle-water interface in natural systems. John Wiley & Son Inc.

Sylwester, E.R., Hudson, E.A., Allen, P.G., 2000. The structure of uranium (VI) sorption complexes on silica, alumina, and montmorillonite. *Geochimica et Cosmochimica Acta* 64, 2431–2438.

Tinnacher, R.M., Holmboe, M., Tournassat, C., Bourg, I.C., Davis, J.A., 2016. Ion adsorption and diffusion in smectite: molecular, pore, and continuum scale views. *Geochimica et Cosmochimica Acta* 177, 130–149.

Tournassat, C., and Appelo, C.A.J., 2011. Modelling approaches for anion-exclusion in compacted Na-bentonite. *Geochimica et Cosmochimica Acta* 75, 3698–3710.

Tournassat, C., Bizi, M., Braibant, G., Crouzet, C., 2011. Influence of montmorillonite tactoid size on Na-Ca cation exchange reactions. *Journal of Colloid and Interface Science* 364, 443–454.

Tournassat, C., Bourg, I.C., Steefel, C.I., Bergaya, F., 2015a. Chapter 1 - Surface Properties of Clay Minerals. In: Tournassat, C., Steefel, C.I., Bourg, I.C., Bergaya, F. (Eds.), *Natural and Engineered Clay Barriers*, *Developments in Clay Science*. Elsevier, pp. 5–31.

Tournassat, C., Davis, J A, Chiaberge, C., Grangeon, S., Bourg, I.C., 2016a. Modeling acid/base properties at montmorillonite edge surfaces: A review. *Environmental Science* In review.

Tournassat, C., Gaboreau, S., Robinet, J.-C., Bourg, I.C., Steefel, C.I., 2016b. Impact of microstructure on anion exclusion in compacted clay media. *CMS Workshop lecture series* 21, 137–149.

Tournassat, C., Grangeon, S., Leroy, P., Giffaut, E., 2013. Modeling specific pH dependent sorption of divalent metals on montmorillonite surfaces. A review of pitfalls, recent achievements and current challenges. *American Journal of Science* 313, 395–451.

Tournassat, C., Neaman, A., Villiéras, F., Bosbach, D., Charlet, L., 2003. Nanomorphology of montmorillonite particles: Estimation of the clay edge sorption site density by low-pressure gas adsorption and AFM observations. *American Mineralogist* 88, 1989–1995.

Tournassat, C., Steefel, C., Bourg, I., Bergaya, F., 2015b. Natural and Engineered Clay Barriers. Elsevier.

Tournassat, and C., Steefel, C.I., 2015. Ionic transport in nano-porous clays with consideration of electrostatic effects. *Reviews in Mineralogy and Geochemistry* 80, 287–330.

Tournassat, C., Vinsot, A., Gaucher, E.C., Altmann, S., 2015c. Chapter 3 - Chemical conditions in clay-Rocks. In: Tournassat, C., Steefel, C.I., Bourg, I.C., Bergaya, F. (Eds.), *Natural and Engineered Clay Barriers*, *Developments in Clay Science*. Elsevier, pp. 71–100.

Troyer, L.D., Maillot, F., Wang, Z., Wang, Z., Mehta, V.S., Giammar, D.E., Catalano, J.G., 2016. Effect of phosphate on U (VI) sorption to montmorillonite: Ternary complexation and precipitation barriers. *Geochimica et Cosmochimica Acta* 175, 86–99.

Turner, G.D., Zachara, J.M., McKinley, J.P., Smith, S.C., 1996. Surface-charge properties and UO_2^{2+} adsorption of a subsurface smectite. *Geochimica et Cosmochimica Acta* 60, 3399–3414.

U.S. Environmental Protection Agency, 1995; https://nepis.epa.gov/Exe/ZyNET.exe/9101IMKK.TXT?ZyActionD=ZyDocument&Client=EPA&Index=1995+Thru+1999&Docs=&Query=&Time=&EndTime=&SearchMethod=1&TocRestrict=n&Toc=&TocEntry=&QField=&QFieldYear=&QFieldMonth=&QFieldDay=&IntQFieldOp=0&ExtQFieldOp=0&XmlQuery=&File=D%3A%5Czyfiles%5CIndex%20Data%5C95thru99%5CTxt%5C00000033%5C9101IMKK.txt&User=ANONYMOUS&Password=anonymous&SortMethod=h%7C-&MaximumDocuments=1&FuzzyDegree=0&ImageQuality=r75g8/r75g8/x150y150g16/i425&Display=hpfr&DefSeekPage=x&SearchBack=ZyActionL&Back=ZyActionS&BackDesc=Results%20page&MaximumPages=1&ZyEntry=1&SeekPage=x&ZyPURL; accessed on 08-19-2016. Development of Compliance Levels From Analytical Detection and Quantitation Levels.

U.S. Environmental Protection Agency, 2001; http://nepis.epa.gov/Exe/ZyPDF.cgi?Dockey=30006644.txt; accessed on 05-25-2016. Radionuclides Rule: A Quick Reference Guide.

Van Loon, L.R., Soler, J.M., Bradbury, M.H., 2003a. Diffusion of HTO, $^{36}Cl^-$ and $^{125}I^-$ in Opalinus Clay samples from Mont Terri: Effect of confining pressure. *J. Contam. Hydrol.* 61, 73–83.

Van Loon, L.R., Soler, J.M., Jakob, A., Bradbury, M.H., 2003b. Effect of confining pressure on the diffusion of HTO, 36Cl- and 125I- in a layered argillaceous rock (Opalinus Clay): diffusion perpendicular to the fabric. *Appl. Geochem.* 18, 1653–1662.

Van Olphen, H., 1992. Particle associations in clay suspensions and their rheological implications. In: Güven, N., Pollastro, R.M. (Eds.), *Clay-water interface and its rheological implications*. The clay minerals society, pp. 191–210.

Villalobos, M., Trotz, M.A., Leckie, J.O., 2001. Surface complexation modeling of carbonate effects on the adsorption of Cr (VI), Pb (II), and U (VI) on goethite. *Environmental science & technology* 35, 3849–3856.

Waite, T.D., Davis, J.A., Payne, T.E., Waychunas, G.A., Xu, N., 1994. Uranium (VI) adsorption to ferrihydrite: Application of a surface complexation model. *Geochimica et Cosmochimica Acta* 58, 5465–5478.

Wersin, P., 2003. Geochemical modelling of bentonite porewater in high-level waste repositories. *Journal of Contaminant Hydrology* 61, 405–422.

Wersin, P., Curti, E., Appelo, C.A.J., 2004. Modelling bentonite–water interactions at high solid/liquid ratios: swelling and diffuse double layer effects. *Applied Clay Science* 26, 249–257.

White, G.N., and Zelazny, L.W., 1988. Analysis and implications of the edge structure of dioctahedral phyllosilicates. *Clays and Clay Minerals* 36, 141–146.

Wolthers, M., Charlet, L., Tournassat, C., 2006. Reactivity of bentonite. An additive model applied to uranyl sorption. In: Lützenkirchen, J. (Ed.), *Surface complexation modelling*. Elsevier.

World Health Organization, 2004. Uranium in drinking-water – Background document for development of WHO guidelines for drinking-water quality. Available at http://www.who.int/water_sanitation_health/dwq/chemicals/en/uranium.pdf.

Yabusaki, S. B., Fang, Y., and Waichler, S. R., 2008. Building conceptual models of field-scale uranium reactive transport in a dynamic vadose zone-aquifer-river system. *Water Resources Research* 44.

APPENDIX

A-1 Background Concentrations of Uranium-238 and Calcium

Uranium. Most electrolyte blanks had U-238 background concentrations below the ICP-MS detection limits (<0.005 µg/L, <2.1E-11 M U-238). The highest background concentration was measured at 6.2E-10 M U-238, which represented 0.04% of the total U(VI) concentration (1.52E-6 M) in that particular experiment. Hence, dissolved concentrations of U(VI) were not corrected for U(VI) background concentrations.

Calcium. Figure A-1 illustrates total Ca concentrations versus the concentrations released from the pre-treated Na-montmorillonite. The latter were calculated based on average Ca concentrations in electrolyte blanks and U(VI) standards (containing no mineral phase).

Without taking into account experiment 4, where calcium was specifically added to solutions, the average calcium contributions from background electrolyte solutions ranged from 7.4E-7 to 7.2E-6 M Ca, which represents between 5.6% to 79.8% of the total Ca in solution. The addition of sodium bicarbonate buffer may slightly add to Ca background levels, but cannot fully explain the observed increase in Ca concentrations at higher pH. (At a 99.998% degree of purity for $NaHCO_3$ and assuming that all impurities in the bicarbonate buffer are due to Ca, the buffer addition at pH 10 would increase Ca background levels by around 3.0E-6 M Ca.) Instead, the pH trend may indicate an enhanced Ca release from the solid in the presence of carbonate ligands in solution. This hypothesis is further supported by lower Ca concentrations found in solutions in contact with atmospheric CO_2/CO_2-"free" gas phases compared to solutions in contact with elevated CO_2 levels.

Furthermore, comparable low concentrations of Ca are released from montmorillonite during all experiments without any specific calcium additions. In contrast, a small uptake of Ca was observed in experiment 4, where a concentration of 2.1 mM Ca was added. In experiments without specific calcium additions, total Ca concentrations (6.4 – 27 µM) were not high enough to affect U(VI) solution speciation in terms of the formation of ternary aqueous U(VI)-Ca-carbonate complexes.

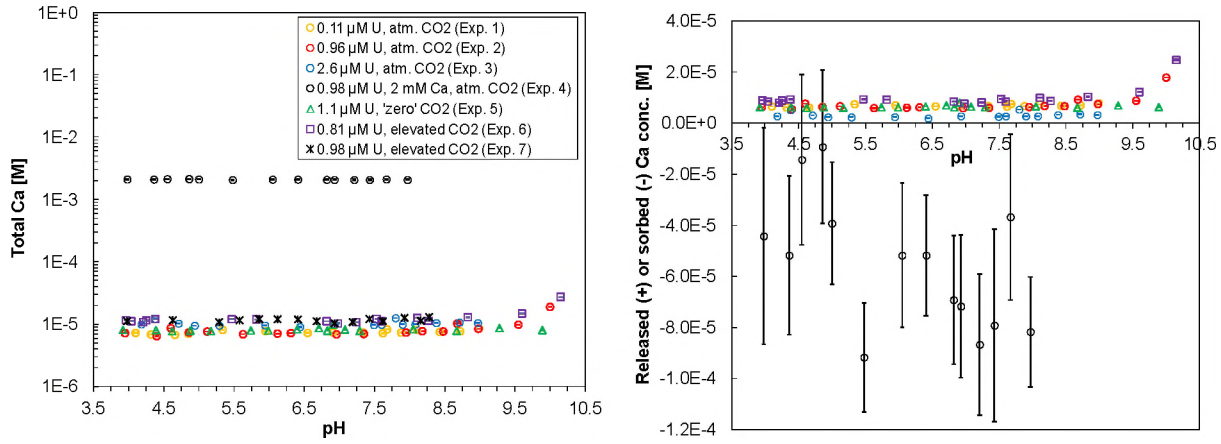

Figure A-1. Total (left) and released (+)/adsorbed (-) (right) concentrations of calcium determined in U(VI) adsorption experiments with Na-montmorillonite under various chemical solution conditions. Data symbols are identical for both figures. Calcium was specifically added only in experiment 4. Error bars represent analytical uncertainties with invisible error bars being smaller than data points.

A-2 Batch U(VI) Adsorption Kinetic Experiment

Experimental Setup

Uranium(VI) adsorption behavior was characterized as a function of time based on the repeated sampling of the same clay suspension at specified time-points. The experiment was set up at room temperature (22.5 – 23.5 °C), with a nominal total U(VI) concentration of 10^{-6} M and a Na-montmorillonite concentration of 0.5 g/L. Solutions were in contact with atmospheric CO_2 (~0.04%, 400 ppm) at a total ionic strength of 0.1 M NaCl and a target pH value of pH-5, without any pH buffering. The standard concentration, representing 100% of U(VI) in solution in the absence of a mineral phase, was calculated based on direct ICP-MS analysis of duplicate 5-µL aliquots of the U(VI) stock solution.

The experiment consisted of two main steps: (1) the pre-equilibration of a U(VI) solution and a separate Na-montmorillonite suspension at pH-5 and 0.1 M NaCl; and (2) the time-dependent adsorption of U(VI) onto the clay, which was characterized by repeated sampling of the montmorillonite suspension. On the first day, a 43.8-mL U(VI)-electrolyte solution and clay-electrolyte suspension were prepared by combining Milli-Q water with 1 M NaCl, and an aliquot of either the U(VI) stock solution or Na-montmorillonite stock suspension. After adjusting the pH to pH 5 with small volumes of HCl and NaOH (1, 0.1, 0.01, 0.001 M), the vials were set up on a shaking table for pre-equilibration overnight.

On the next day, a second pH check/adjustment was performed for both vials individually. Then, the kinetic experiment was started by pouring the clay suspension into the Nalgene bottle containing the U(VI) solution at the same pH and ionic strength. After a brief mixing by hand, four 1-mL volume fractions were transferred into four 2-mL centrifugation vials. (Suspension volumes of 1 mL in 2-mL centrifugation vials allowed us to minimize the height of liquid levels, sample centrifugation times, and hence, the minimum time-frames required in between sampling events.) The remaining sample suspensions were set up for continuous adsorption equilibration under shaking. Sampled suspensions were centrifuged in order to remove >50 nm clay particles, based on calculations using Stokes law (Beckman Coulter Allegra 64R, F3602 rotor, 11 minutes at 26,000 g / 16,335 rpm). After centrifugation, two 0.75-mL supernatant fractions were combined twice to give two 1.5-mL sample solutions for ICP-MS analysis.

The same sampling/centrifugation procedure was followed for the rest of the kinetic experiment, but only one 1.5-mL ICP-MS sample was created per sampling event. In addition, on the first and last day of the experiment a similar procedure was applied to collect supernatant solutions for dissolved inorganic carbon (DIC) analysis on a Shimadzu TOC-V. Last, pH values of sample suspensions were recorded every couple of days in order to monitor for potential changes in pH over time.

Results

Uranium(VI) shows a fast initial uptake, followed by slower apparent adsorption kinetics (Figure A-2), which resulted in a slight increase in U(VI) adsorption distribution coefficients (K_D values) from 1709 L/kg (2.0 days) to 2479 L/kg (13.2 days) over time. Dissolved inorganic carbon (DIC) concentrations remained fairly constant throughout the experiment with values of 0.34 ± 0.02 and 0.28 ± 0.02 mg/L DIC on the first and last sampling days. In contrast, pH appears to consistently increase over time (Figure A-3), from pH 5.00 to pH 5.19 and pH 5.25 after 1.0, 7.4, and 13.2 days into the experiment.

In order to evaluate if the slight increase in U(VI) K_D values in the kinetic experiment is driven by slow adsorption processes or the shift to higher pH conditions, we draw a comparison between batch kinetic data and adsorption results determined in a batch adsorption experiment after 48.5-hours reaction time under the same chemical conditions (see manuscript for experimental details). First, at a pH value between 5.00 and 5.07, the U(VI) K_D value determined in the kinetic experiment after 2.0 days (1709 L/kg) compares well with the adsorption distribution coefficient from the 48.5-hour adsorption

experiment (1,892 L/kg, pH 5.12, 0.262 ± 0.001 mg/L DIC). Hence, the slightly different experimental setups had no apparent effect on U(VI) adsorption results. Second, at the longest reaction time in the kinetic experiment (13.2 days), we computed a U(VI) K_D value of 2479 L/kg at pH 5.25. A directly comparable data point at the same pH value is not available from the adsorption experiment with a 48.5-hour reaction time. However, a graphical interpolation between neighboring data points (data not reported) results in estimated 48.5-hour U(VI) K_d values between 2,523 and 2,784 L/kg.

Based on these results, the observed increase in U(VI) K_d values in the kinetic experiment is most likely due to changing pH conditions, and not driven by secondary slow U(VI) adsorption processes under the given set of experimental conditions. Hence, under these conditions, distribution coefficients determined at adsorption equilibration times of 48.5 hours are most likely at, or close to, values determined under steady-state conditions.

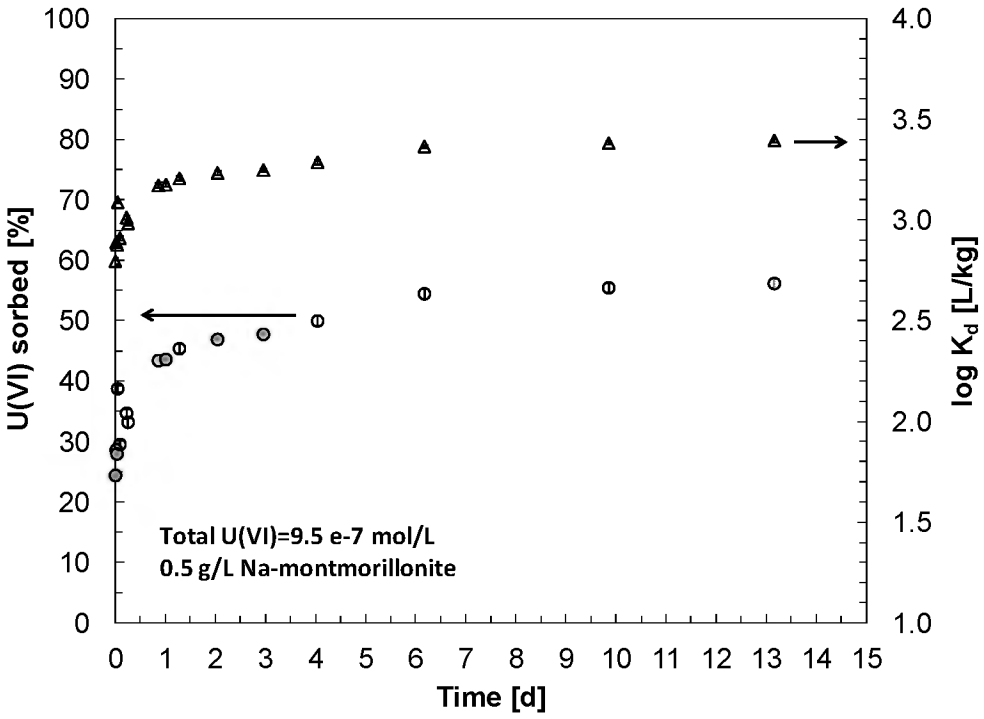

Figure A-2. Adsorption of 9.5 × 10-7 M U(VI) as a function of time, at a target pH of 5, I=0.1 M NaCl, in a 0.5 g/L Na-montmorillonite suspension equilibrated with atmospheric CO2. Error bars represent analytical uncertainties, which are smaller than data points.

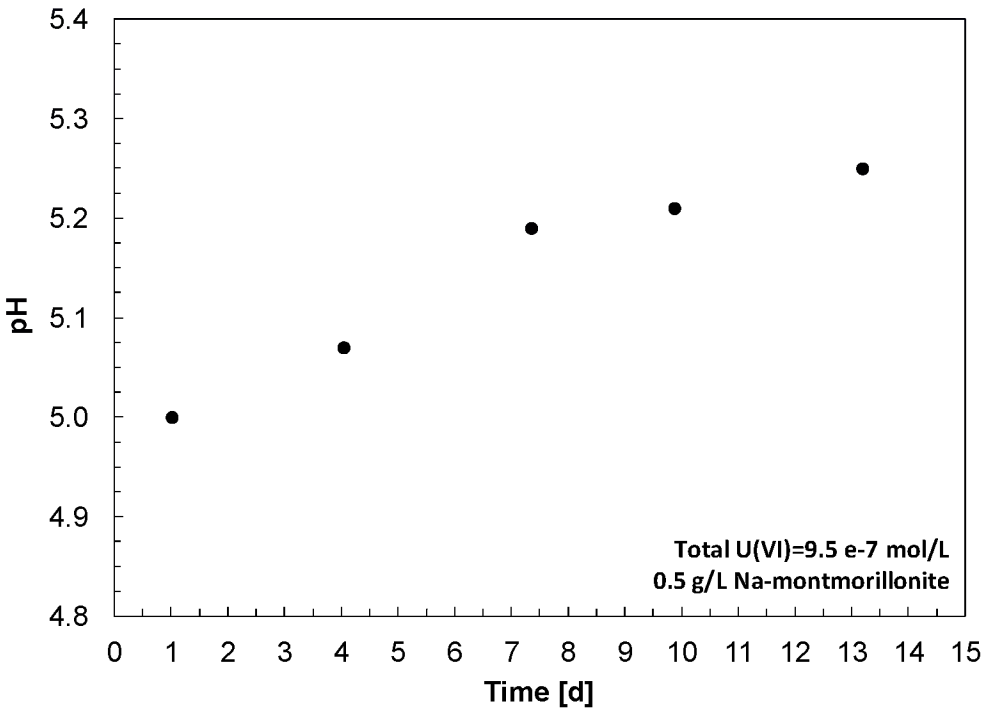

Figure A-3. Changes in pH as a function of time during the U(VI) batch kinetic experiment at a target pH of 5, I=0.1 M NaCl, in a 0.5 g/L Na-montmorillonite suspension equilibrated with atmospheric CO_2.

A-3 Experimental Procedure for Quantification of Analytical Detection Limits and Background Values for Dissolved Inorganic Carbon

Following recommendations by the U.S. EPA (1995), the Method Detection Limit (MDL) and Minimum Level (ML) were determined for the specific setup of our DIC analysis, on two separate days. Both limits were based on a nonconsecutive analysis of seven Milli-Q water (MQW) blanks after establishing a MQW blank-corrected DIC calibration curve with the same MQW as solution matrix (standard concentrations of 0, 0.025, 0.05, 0.1, 0.5, 1 and 5 $mg \cdot L^{-1}$ DIC, corresponding to 0, 2.1E-6, 4.2E-6, 8.3E-6, 4.2E-5, 8.3E-5 and 4.2E-4 mol L^{-1} DIC). The MDL represents the minimum DIC concentration that can be identified, measured and reported with a 99 % confidence that the concentration is greater than zero (U.S. EPA, 1995). It is calculated from the standard deviation of DIC concentrations in seven replicate MQW blanks multiplied by the Student t-value for the 99 % confidence level with six degrees of freedom (3.14). The ML is defined as the smallest measured concentration of a constituent that may be reliably reported using a given analytical method. Its value corresponds to the limit of quantitation (LOQ) established by the American Chemical Society, and is computed by multiplying the MDL by a factor of 3.18.

Furthermore, in order to determine potential sources of DIC contamination in the CO_2-"free" batch adsorption experiment, approximately one liter of heated MQW was sparged with N_2(g) using a glass sparger and a 20 µm tube-fitting filter for approximately 20 hours. Inside a glove box filled with 5% H_2/95% N_2 gas, samples were prepared to provide DIC background values for the N_2-purged MQW (in triplicates), plus a series of samples with known, added concentrations of $NaHCO_3$ (nominal concentrations of 0.031, 0.063, 0.125, 0.250, 0.500 and 1.000 $mg \cdot L^{-1}$ DIC, corresponding to 2.6E-6, 5.2E-6, 1.0E-5, 2.1E-5, 4.2E-5 and 8.3E-5 mol L^{-1} DIC). Exact volumes of added 0.001 M $NaHCO_3$ solution and N_2-purged MQW were determined by weight. The same procedure was also applied to volume fractions of the same N_2-purged MQW after: (1) centrifuging solutions in the same manner as during the CO_2-"free" batch adsorption experiments, (2) storage of N_2-purged MQW solutions in open 50 ml polycarbonate vials in the glove box for 22.6 hours (about 5-times the time-frame estimated for the actual CO_2-"free" adsorption experiment), and (3) storage in closed glass vials in the fridge for approximately seven days.

A-4. Overview of Measured Dissolved Inorganic Carbon Concentrations

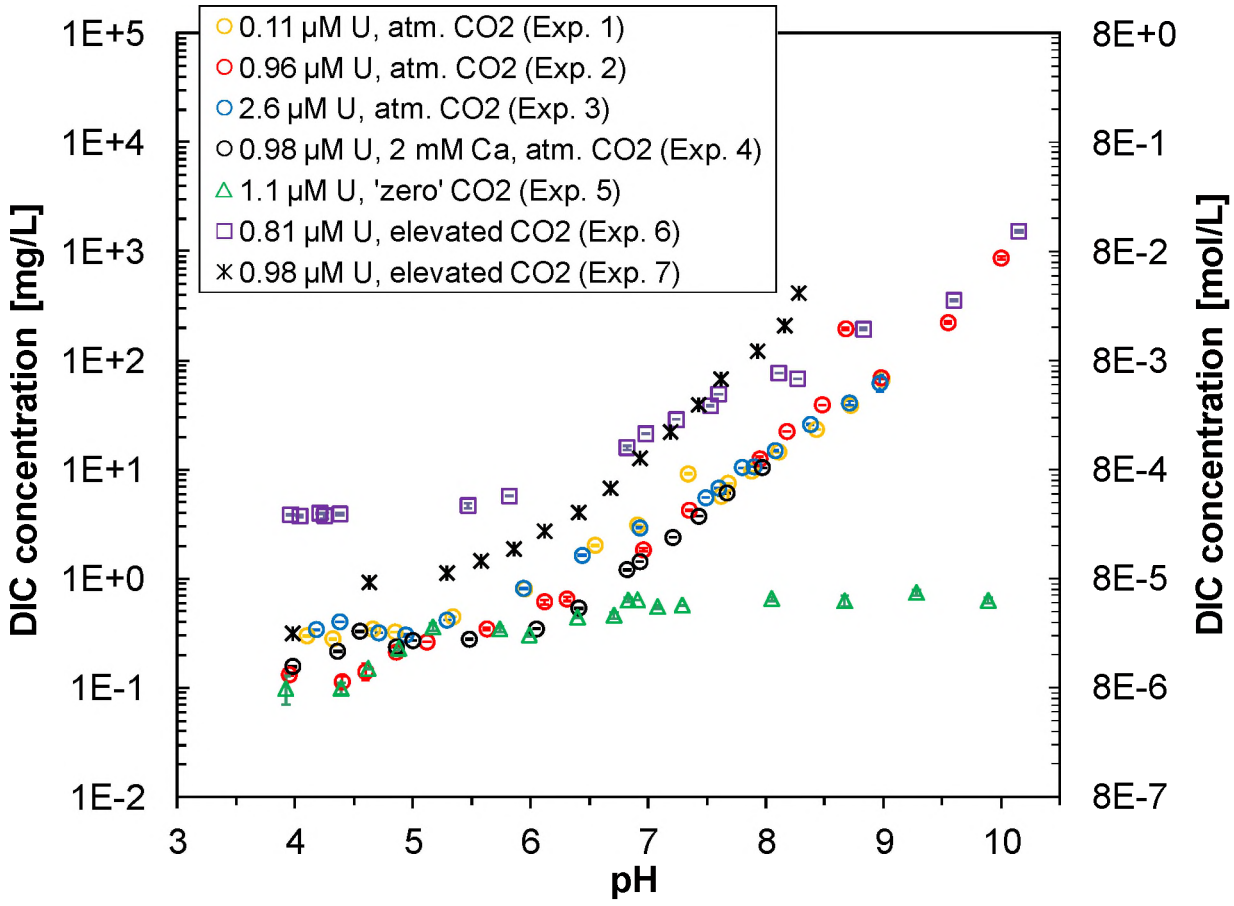

Figure A-4. Dissolved inorganic carbon (DIC) concentrations measured in supernatant solutions during U(VI) adsorption experiments as a function of pH at I=0.1 M NaCl and 0.5 g/L Na-montmorillonite.

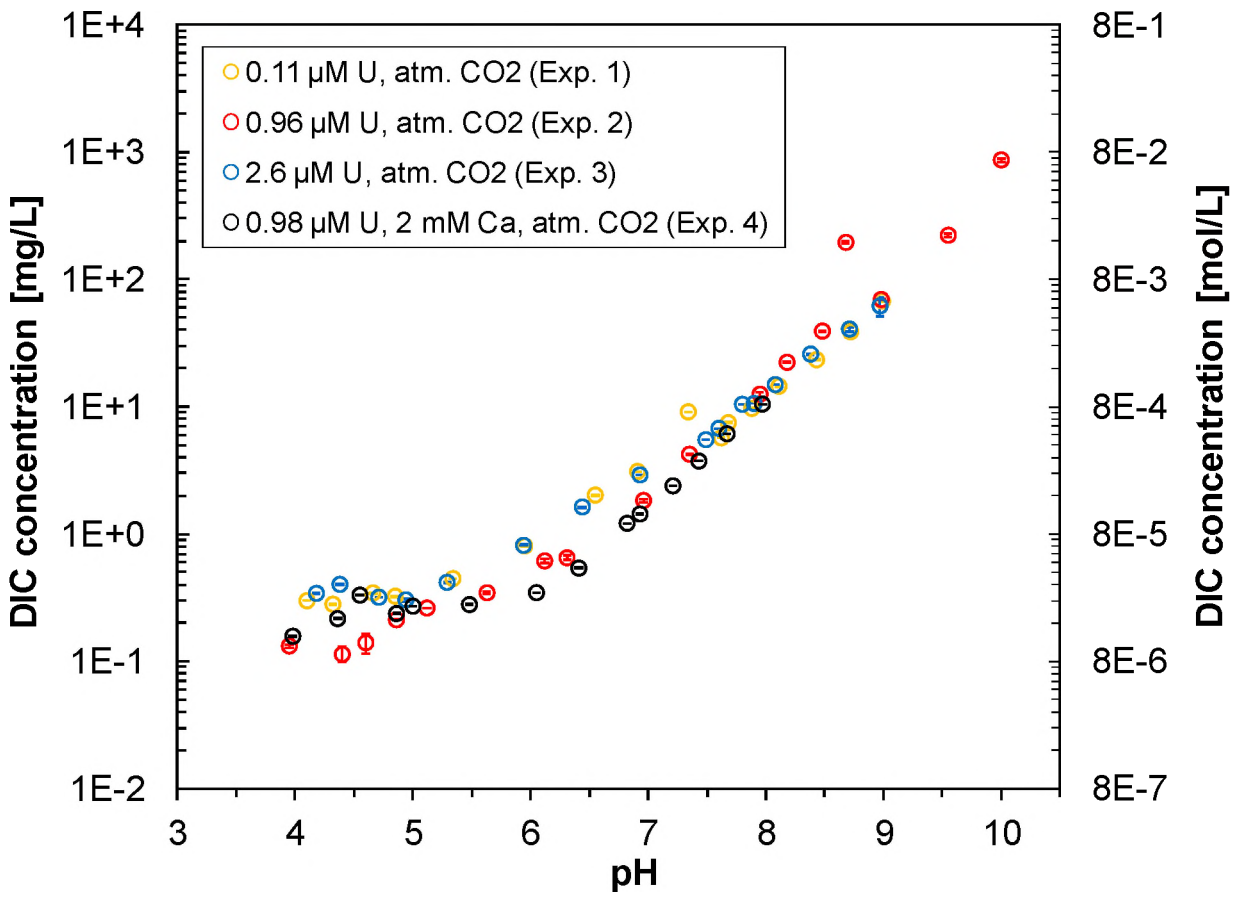

Figure A-5. Comparison of dissolved inorganic carbon (DIC) concentrations measured in supernatant solutions during U(VI) adsorption experiments at atmospheric CO2 conditions, I=0.1 M NaCl and 0.5 g/L Na-montmorillonite.

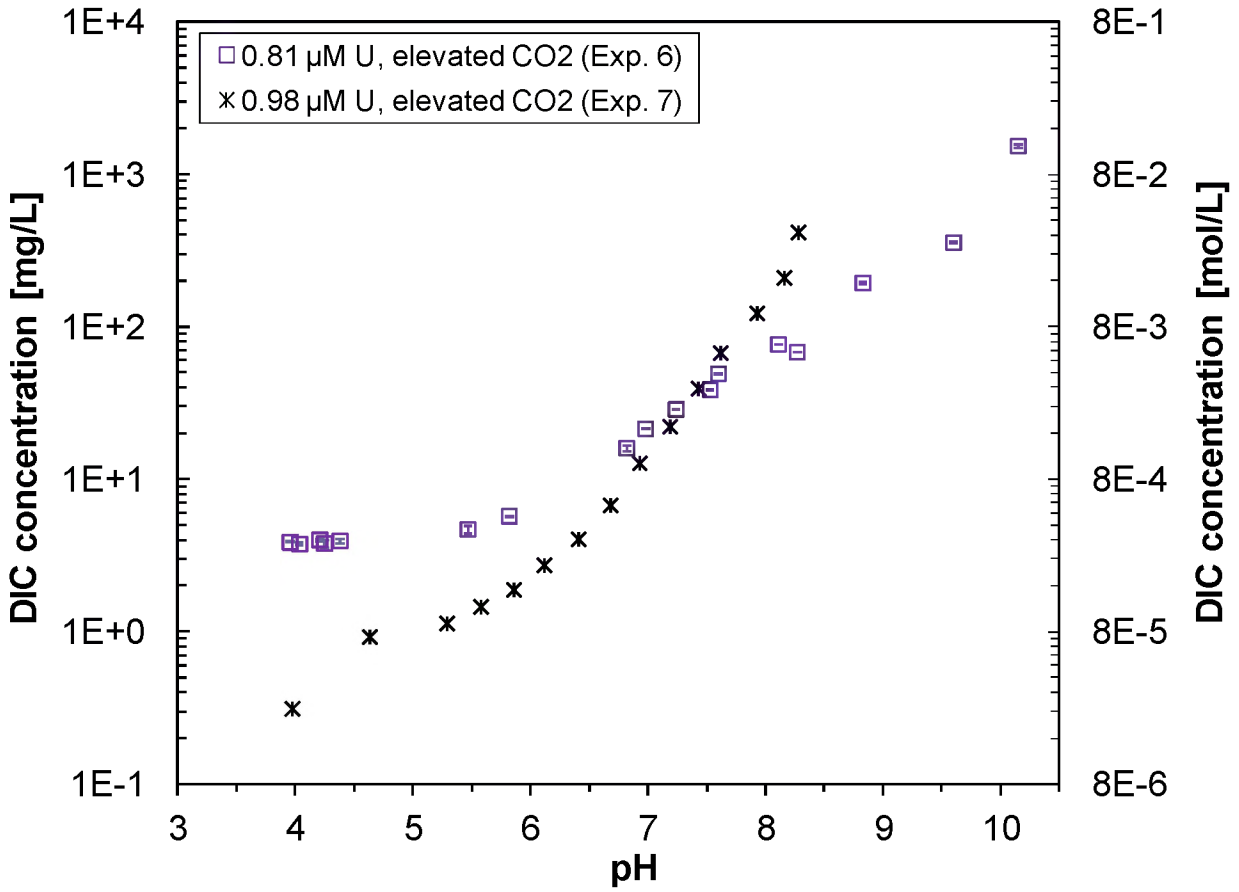

Figure A-6. Comparison of dissolved inorganic carbon (DIC) concentrations measured in supernatant solutions during U(VI) adsorption experiments at elevated CO_2 conditions, I=0.1 M NaCl and 0.5 g/L Na-montmorillonite.

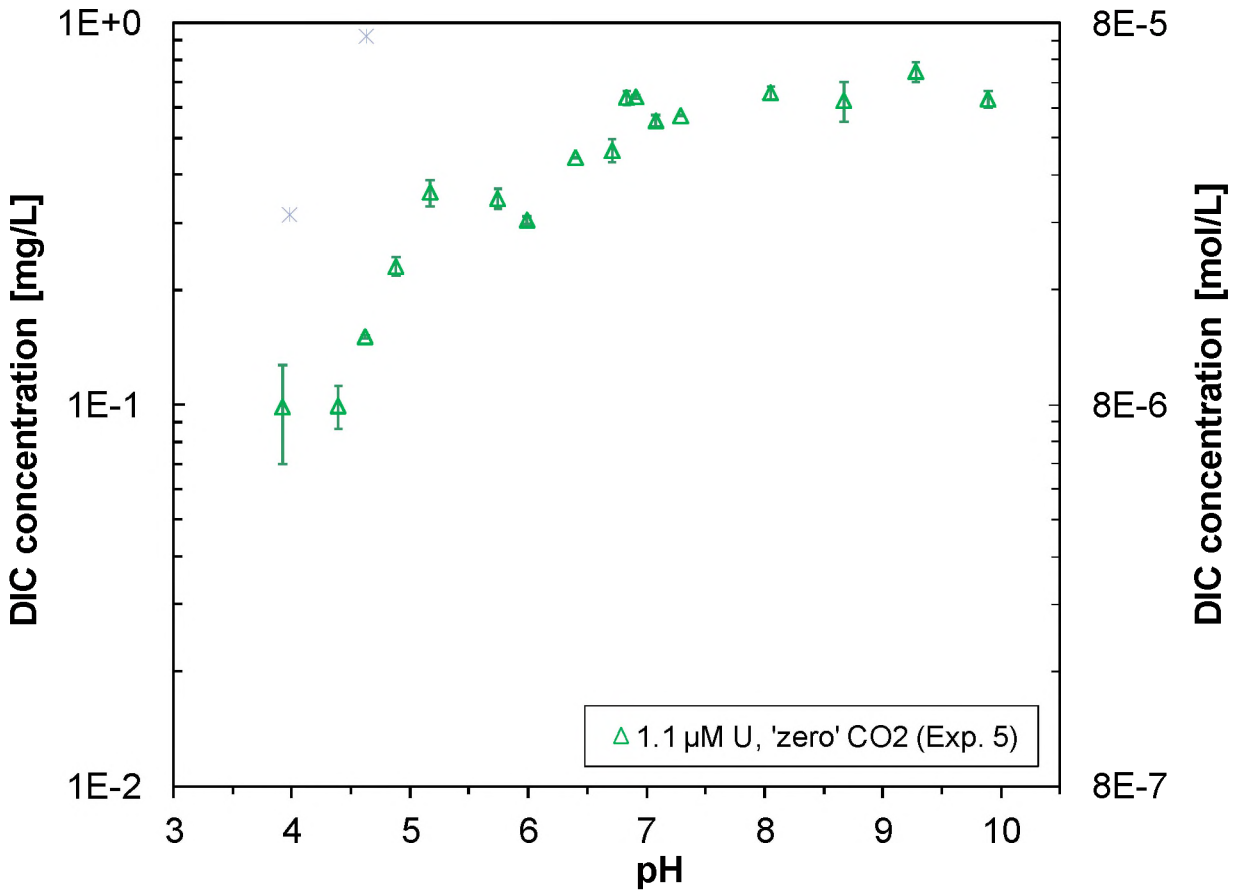

Figure A-7. Dissolved inorganic carbon (DIC) concentrations measured in supernatant solutions during 'CO2-free' U(VI) adsorption experiment at I=0.1 M NaCl and 0.5 g/L Na-montmorillonite.

A-5 Summary of Batch U(VI) Adsorption Data

Experiment 1: 1.11E-7 M U(VI) total, atmospheric CO_2, no Ca added

Sample no.	Clay conc.	pH	Total concentrations			Supernatant concentrations				Calc. pCO_2
			Na	Cl	U	Ca	Mg	U	TIC	
[ ]	[g/L]	[ ]	[mol/L]	[mol/L]	[mol/L]	[mol/L]	[mol/L]	[mol/L]	[mol/L]	[atm]
1	0.5161	4.10	1.01E-01	1.00E-01	1.11E-07	7.23E-06	5.50E-06	1.02E-07	2.49E-05	
2	0.5161	4.32	1.01E-01	1.00E-01	1.11E-07	6.83E-06	5.31E-06	8.97E-08	2.34E-05	
3	0.5161	4.66	1.01E-01	1.00E-01	1.11E-07	6.74E-06	5.25E-06	7.13E-08	2.87E-05	
4	0.5161	4.85	1.01E-01	1.00E-01	1.11E-07	7.02E-06	5.26E-06	5.43E-08	2.70E-05	
5	0.5161	5.34	1.01E-01	1.00E-01	1.11E-07	8.07E-06	5.23E-06	2.43E-08	3.72E-05	
6	0.5161	5.95	1.01E-01	1.00E-01	1.11E-07	7.69E-06	5.21E-06	8.91E-09	6.70E-05	
7	0.5161	6.55	1.01E-01	1.00E-01	1.11E-07	7.24E-06	5.21E-06	1.25E-08	1.68E-04	
8	0.5085	6.91	9.97E-02	9.85E-02	1.11E-07	7.33E-06	5.07E-06	1.94E-08	2.58E-04	
9	0.5133	7.34	1.01E-01	9.95E-02	1.11E-07	7.33E-06	5.10E-06	5.93E-08	7.59E-04	
10	0.5161	7.62	1.01E-01	9.98E-02	1.11E-07	7.14E-06	5.17E-06	4.24E-08	4.74E-04	
11	0.5166	7.68	1.01E-01	9.98E-02	1.11E-07	8.20E-06	5.28E-06	5.70E-08	6.23E-04	
12	0.5161	7.88	1.01E-01	9.95E-02	1.11E-07	7.32E-06	5.13E-06	7.94E-08	8.07E-04	
13	0.5164	8.11	1.01E-01	9.91E-02	1.11E-07	8.04E-06	5.18E-06	1.05E-07	1.20E-03	
14	0.5161	8.43	1.01E-01	9.84E-02	1.11E-07	7.49E-06	5.02E-06	1.18E-07	1.94E-03	
15	0.5180	8.72	1.02E-01	9.78E-02	1.11E-07	7.65E-06	4.89E-06	1.23E-07	3.22E-03	
16	0.5319	8.99	1.05E-01	9.76E-02	1.11E-07	8.52E-06	4.90E-06	1.26E-07	5.62E-03	

In this and all following, related tables, Na and Cl concentrations take into account additions of NaCl, NaOH and HCl to sample solutions.

Experiment 2: 9.6E-7 M U(VI) total, atmospheric CO_2, no Ca added

Sample no.	Clay conc.	pH	Total concentrations			Supernatant concentrations				Calc. pCO_2
			Na	Cl	U	Ca	Mg	U	DIC	
[ ]	[g/L]	[ ]	[mol/L]	[mol/L]	[mol/L]	[mol/L]	[mol/L]	[mol/L]	[mol/L]	[atm]
1	0.5166	3.95	1.00E-01	1.00E-01	9.56E-07	7.16E-06	7.44E-06	8.75E-07	1.10E-05	
2	0.5166	4.40	1.00E-01	1.00E-01	9.56E-07	6.42E-06	7.17E-06	7.85E-07	9.45E-06	
3	0.5166	4.60	1.00E-01	1.00E-01	9.56E-07	8.63E-06	7.57E-06	7.48E-07	1.17E-05	
4	0.5166	4.86	1.00E-01	1.00E-01	9.56E-07	7.35E-06	7.05E-06	6.62E-07	1.77E-05	
5	0.5166	5.12	1.00E-01	1.00E-01	9.56E-07	7.60E-06	7.04E-06	4.81E-07	2.18E-05	
6	0.5166	5.63	1.00E-01	1.00E-01	9.56E-07	6.88E-06	6.88E-06	2.37E-07	2.88E-05	
7	0.5166	6.12	1.00E-01	1.00E-01	9.56E-07	7.04E-06	6.86E-06	9.85E-08	5.12E-05	
8	0.5166	6.31	1.00E-01	1.00E-01	9.56E-07	7.18E-06	6.70E-06	7.60E-08	5.41E-05	
9	0.5166	6.96	1.00E-01	1.00E-01	9.56E-07	6.86E-06	8.83E-06	1.70E-07	1.53E-04	
10	0.5166	7.35	1.00E-01	9.98E-02	9.56E-07	6.94E-06	8.12E-06	3.25E-07	3.52E-04	
11	0.5166	7.95	1.00E-01	9.95E-02	9.56E-07	7.31E-06	8.79E-06	7.99E-07	1.04E-03	
12	0.5166	8.18	1.00E-01	9.91E-02	9.56E-07	7.71E-06	6.61E-06	9.31E-07	1.86E-03	
13	0.5166	8.48	1.00E-01	9.84E-02	9.56E-07	7.62E-06	6.52E-06	9.52E-07	3.26E-03	
14	0.5166	8.68	1.14E-01	9.71E-02	9.56E-07	1.02E-05	1.17E-05	9.62E-07	1.62E-02	
15	0.5166	8.98	1.00E-01	9.47E-02	9.56E-07	8.43E-06	6.23E-06	9.55E-07	5.78E-03	
16	0.5166	9.55	1.05E-01	8.16E-02	9.56E-07	9.80E-06	5.65E-06	9.65E-07	1.85E-02	
17	0.5166	10.00	1.36E-01	2.48E-02	9.56E-07	1.89E-05	8.09E-06	9.77E-07	7.22E-02	

Experiment 3: 2.55E-6 M U(VI) total, atmospheric CO_2, no Ca added

Sample no.	Clay conc.	pH	Total concentrations			Supernatant concentrations				Calc. pCO_2
			Na	Cl	U	Ca	Mg	U	DIC	
[ ]	[g/L]	[ ]	[mol/L]	[mol/L]	[mol/L]	[mol/L]	[mol/L]	[mol/L]	[mol/L]	[atm]
1	0.5158	4.18	1.01E-01	1.00E-01	2.55E-06	9.94E-06	6.33E-06	2.51E-06	2.85E-05	
2	0.5158	4.38	1.01E-01	1.00E-01	2.55E-06	1.23E-05	6.43E-06	2.43E-06	3.35E-05	
3	0.5158	4.71	1.01E-01	1.00E-01	2.55E-06	1.02E-05	6.11E-06	2.24E-06	2.65E-05	
4	0.5158	4.94	1.01E-01	1.00E-01	2.55E-06	9.50E-06	5.72E-06	1.93E-06	2.53E-05	
5	0.5158	5.29	1.01E-01	1.00E-01	2.55E-06	9.49E-06	5.80E-06	1.33E-06	3.47E-05	
6	0.5158	5.94	1.01E-01	9.99E-02	2.55E-06	9.57E-06	5.69E-06	6.29E-07	6.78E-05	
7	0.5158	6.44	1.01E-01	9.99E-02	2.55E-06	9.05E-06	5.57E-06	6.29E-07	1.36E-04	
8	0.5158	6.93	1.01E-01	9.99E-02	2.55E-06	9.93E-06	5.62E-06	7.37E-07	2.43E-04	
9	0.5158	7.49	1.01E-01	9.98E-02	2.55E-06	9.74E-06	5.67E-06	1.23E-06	4.59E-04	
10	0.5159	7.60	1.01E-01	9.97E-02	2.55E-06	9.86E-06	5.61E-06	1.47E-06	5.62E-04	
11	0.5159	7.80	1.02E-01	1.00E-01	2.55E-06	1.25E-05	5.75E-06	2.07E-06	8.69E-04	
12	0.5162	7.90	1.02E-01	9.96E-02	2.55E-06	9.89E-06	5.59E-06	2.14E-06	8.82E-04	
13	0.5162	8.08	1.02E-01	9.91E-02	2.55E-06	9.90E-06	5.57E-06	2.37E-06	1.24E-03	
14	0.5162	8.38	1.02E-01	9.84E-02	2.55E-06	1.04E-05	5.46E-06	2.86E-06	2.16E-03	
15	0.5282	8.71	1.05E-01	9.97E-02	2.55E-06	1.07E-05	5.38E-06	2.78E-06	3.39E-03	
16	0.5311	8.97	1.05E-01	9.75E-02	2.55E-06	1.04E-05	5.23E-06	2.77E-06	5.15E-03	

Experiment 4: 1.52E-6 M U(VI) total, atmospheric CO_2, 2.1 mM Ca added

Sample no.	Clay conc.	pH	Total concentrations			Supernatant concentrations				Calc. pCO_2
			Na	Cl	U	Ca	Mg	U	DIC	
[ ]	[g/L]	[ ]	[mol/L]	[mol/L]	[mol/L]	[mol/L]	[mol/L]	[mol/L]	[mol/L]	[atm]
1	0.516625	3.98	9.74E-02	1.02E-01	1.52E-06	2.10E-03	1.20E-05	8.91E-07	1.31E-05	
2	0.516625	4.36	9.70E-02	1.01E-01	1.52E-06	2.09E-03	1.26E-05	8.23E-07	1.80E-05	
3	0.516625	4.55	9.70E-02	1.01E-01	1.52E-06	2.13E-03	1.16E-05	7.60E-07	2.75E-05	
4	0.516625	4.86	9.70E-02	1.01E-01	1.52E-06	2.13E-03	1.28E-05	6.60E-07	1.97E-05	
5	0.516625	5.00	9.70E-02	1.01E-01	1.52E-06	2.10E-03	1.12E-05	5.92E-07	2.25E-05	
6	0.516625	5.48	9.70E-02	1.01E-01	1.52E-06	2.05E-03	1.16E-05	3.07E-07	2.32E-05	
7	0.516625	6.05	9.70E-02	1.01E-01	1.52E-06	2.09E-03	1.12E-05	1.21E-07	2.87E-05	
8	0.516625	6.41	9.70E-02	1.01E-01	1.52E-06	2.09E-03	1.10E-05	8.07E-08	4.48E-05	
9	0.516625	6.82	9.70E-02	1.01E-01	1.52E-06	2.07E-03	1.70E-05	1.23E-07	1.01E-04	
10	0.516625	6.93	9.70E-02	1.01E-01	1.52E-06	2.07E-03	1.13E-05	1.33E-07	1.19E-04	
11	0.516625	7.21	9.70E-02	1.01E-01	1.52E-06	2.05E-03	1.13E-05	2.38E-07	1.98E-04	
12	0.516625	7.43	9.70E-02	1.01E-01	1.52E-06	2.06E-03	1.39E-05	4.66E-07	3.10E-04	
13	0.516625	7.67	9.70E-02	1.01E-01	1.52E-06	2.11E-03	1.14E-05	7.90E-07	5.08E-04	
14	0.516625	7.97	9.73E-02	1.01E-01	1.52E-06	2.06E-03	1.12E-05	9.28E-07	8.69E-04	

Experiment 5: 1.12E-6 M U(VI) total, 'zero' CO_2, no Ca added

Sample no.	Clay conc.	pH	Total concentrations			Supernatant concentrations				Calc. pCO_2
			Na	Cl	U	Ca	Mg	U	DIC	
[ ]	[g/L]	[ ]	[mol/L]	[mol/L]	[mol/L]	[mol/L]	[mol/L]	[mol/L]	[mol/L]	[atm]
1	0.5166	3.92	1.00E-01	1.01E-01	1.12E-06	8.01E-06	7.50E-06	9.24E-07	8.20E-06	
2	0.5166	4.39	1.00E-01	1.00E-01	1.12E-06	7.96E-06	7.72E-06	8.48E-07	8.26E-06	
3	0.5166	4.62	1.00E-01	1.00E-01	1.12E-06	7.69E-06	9.86E-06	7.42E-07	1.25E-05	
4	0.5166	4.88	1.00E-01	1.00E-01	1.12E-06	7.87E-06	6.72E-06	6.74E-07	1.91E-05	
5	0.5166	5.17	1.00E-01	1.00E-01	1.12E-06	7.72E-06	6.70E-06	4.97E-07	3.00E-05	
6	0.5166	5.74	1.00E-01	1.00E-01	1.12E-06	7.93E-06	7.14E-06	1.88E-07	2.88E-05	
7	0.5166	5.99	1.00E-01	1.00E-01	1.12E-06	7.89E-06	7.08E-06	1.16E-07	2.54E-05	
8	0.5166	6.40	1.00E-01	1.00E-01	1.12E-06	8.24E-06	7.01E-06	7.22E-08	3.70E-05	
9	0.5166	6.71	1.00E-01	1.00E-01	1.12E-06	8.66E-06	7.62E-06	7.61E-08	3.85E-05	
10	0.5166	6.83	1.00E-01	1.00E-01	1.12E-06	7.86E-06	8.80E-06	7.97E-08	5.31E-05	
11	0.5166	6.91	1.00E-01	1.00E-01	1.12E-06	9.80E-06	9.06E-06	7.48E-08	5.33E-05	
12	0.5166	7.08	1.00E-01	1.00E-01	1.12E-06	8.18E-06	9.13E-06	8.14E-08	4.62E-05	
13	0.5166	7.29	1.00E-01	1.00E-01	1.12E-06	7.82E-06	1.21E-05	9.76E-08	4.76E-05	
14	0.5166	8.05	1.00E-01	1.00E-01	1.12E-06	8.27E-06	8.97E-06	1.04E-07	5.46E-05	
15	0.5166	8.67	1.00E-01	1.00E-01	1.12E-06	7.80E-06	7.32E-06	1.09E-07	5.21E-05	
16	0.5166	9.28	1.00E-01	1.00E-01	1.12E-06	8.61E-06	7.65E-06	1.37E-07	6.21E-05	
17	0.5166	9.89	1.00E-01	1.00E-01	1.12E-06	8.00E-06	4.21E-06	1.49E-07	5.26E-05	

Experiment 6: 8.1E-7 M U(VI) total, '2%' CO_2, no Ca added

Sample no.	Clay conc.	pH	Total concentrations			Supernatant concentrations				Calc. pCO_2
			Na	Cl	U	Ca	Mg	U	DIC	
[ ]	[g/L]	[ ]	[mol/L]	[mol/L]	[mol/L]	[mol/L]	[mol/L]	[mol/L]	[mol/L]	[atm]
1	0.5166	4.04	1.00E-01	1.01E-01	8.05E-07	1.12E-05	7.50E-06	7.07E-07	3.12E-04	
2	0.5166	3.96	1.00E-01	1.00E-01	8.05E-07	1.16E-05	7.66E-06	7.13E-07	3.21E-04	
3	0.5166	4.21	1.00E-01	1.00E-01	8.05E-07	1.08E-05	7.44E-06	6.60E-07	3.32E-04	
4	0.5166	4.25	1.00E-01	1.00E-01	8.05E-07	1.15E-05	7.44E-06	6.41E-07	3.14E-04	
5	0.5166	4.38	1.00E-01	1.00E-01	8.05E-07	1.20E-05	7.34E-06	5.95E-07	3.27E-04	
6	0.5166	5.47	1.00E-01	1.00E-01	8.05E-07	1.20E-05	7.24E-06	3.25E-07	3.89E-04	
7	0.5166	5.82	1.00E-01	1.00E-01	8.05E-07	1.19E-05	7.41E-06	3.24E-07	4.75E-04	
8	0.5166	6.82	1.00E-01	9.94E-02	8.05E-07	1.11E-05	7.39E-06	4.50E-07	1.33E-03	
9	0.5166	6.98	1.00E-01	9.93E-02	8.05E-07	1.03E-05	7.04E-06	5.34E-07	1.78E-03	
10	0.5166	7.24	1.00E-01	9.92E-02	8.05E-07	1.08E-05	7.07E-06	6.49E-07	2.39E-03	
11	0.5166	7.53	1.01E-01	9.89E-02	8.05E-07	1.21E-05	7.14E-06	7.11E-07	3.21E-03	
12	0.5166	7.60	1.01E-01	9.85E-02	8.05E-07	1.11E-05	7.05E-06	7.60E-07	4.08E-03	
13	0.5166	8.11	1.01E-01	9.78E-02	8.05E-07	1.26E-05	7.07E-06	7.76E-07	6.37E-03	
14	0.5166	8.27	1.01E-01	9.65E-02	8.05E-07	1.13E-05	6.95E-06	7.67E-07	5.65E-03	
15	0.5166	8.83	1.01E-01	9.41E-02	8.05E-07	1.30E-05	6.71E-06	7.79E-07	1.61E-02	
16	0.5166	9.60	1.05E-01	8.10E-02	8.05E-07	1.48E-05	6.39E-06	8.07E-07	2.96E-02	
17	0.5166	10.15	1.25E-01	2.41E-02	8.05E-07	2.74E-05	8.99E-06	7.96E-07	1.27E-01	

Experiment 7: 9.8E-7 M U(VI) total, '2%' CO_2, no Ca added

Sample no.	Clay conc.	pH	Total concentrations			Supernatant concentrations				Calc. pCO_2
			Na	Cl	U	Ca	Mg	U	DIC	
[ ]	[g/L]	[ ]	[mol/L]	[mol/L]	[mol/L]	[mol/L]	[mol/L]	[mol/L]	[mol/L]	[atm]
1	0.2400	3.98	1.00E-01	1.00E-01	9.86E-07			8.37E-07	2.61E-05	
2	0.2400	4.63	1.00E-01	1.00E-01	9.86E-07			7.35E-07	7.67E-05	
3	0.2400	5.29	1.00E-01	1.00E-01	9.86E-07			4.60E-07	9.34E-05	
4	0.2400	5.58	1.00E-01	1.00E-01	9.86E-07			3.79E-07	1.20E-04	
5	0.2400	5.86	1.00E-01	1.01E-01	9.86E-07			3.49E-07	1.55E-04	
6	0.2400	6.12	1.00E-01	1.00E-01	9.87E-07			3.10E-07	2.26E-04	
7	0.2400	6.41	1.00E-01	1.00E-01	9.86E-07			3.57E-07	3.35E-04	
8	0.2400	6.68	1.00E-01	9.95E-02	9.86E-07			5.20E-07	5.58E-04	
9	0.2400	6.93	1.00E-01	9.89E-02	9.86E-07			7.03E-07	1.05E-03	
10	0.2400	7.19	1.00E-01	9.80E-02	9.86E-07			8.88E-07	1.83E-03	
11	0.2400	7.43	1.00E-01	9.63E-02	9.87E-07			9.62E-07	3.25E-03	
12	0.2400	7.62	1.00E-01	9.35E-02	9.87E-07			9.78E-07	5.57E-03	
13	0.2400	7.93	1.00E-01	8.81E-02	9.86E-07			9.76E-07	1.01E-02	
14	0.2400	8.16	1.00E-01	7.88E-02	9.86E-07			9.80E-07	1.73E-02	
15	0.2400	8.28	1.00E-01	6.20E-02	9.87E-07			9.96E-07	3.44E-02	

A-6 Purification of Uranium-233 Stock Solution

We selected uranium-233 as the tracer for uranium(VI) diffusion experiments due to its short half-life relative to other uranium isotopes. This allows for better detection limits of low uranium(VI) concentrations in solution, a relatively straight-forward and fast analysis by liquid scintillation counting, and hence a close and timely monitoring of diffusive fluxes over the course of diffusion experiments. As commercially available U-233 was too expensive, we utilized an existing in-house U-233 stock solution provided by Dr. Heino Nitsche (Nuclear Sciences Division, Lawrence Berkeley National Laboratory, deceased). However, a purification of this in-house stock was necessary in order to remove accumulated daughter products (Th-229, Ra-225, Ac-225), and to ensure that U-233 was present as uranium(VI) and in a known chemical solution matrix.

The purification procedure was based on the separation of uranium from impurities using an Eichrom UTEVA resin column (2-mL cartridges, 50-100 µm UTEVA resin, Eichrom P/N: UT-R50-S), while largely following the recommendations provided in Method ACW02, Rev. 1.4 (Uranium in Water) by Eichrom Technologies, LLC. During the procedure, resin columns were positioned in an Eichrom column rack (P/N AC-103) and connected to 2-mL NORM-JECT Luer sterile syringes, serving as solution reservoirs.

All acids and other chemicals used in the procedure were of TraceSelect Grade. New, acid-washed Savillex PFA vials were used to contain acids and other solutions. Furthermore, a nitric acid (3 M)-aluminum nitrate (1 M) solution was purified from known impurities of natural uranium in aluminum nitrate prior to its use in the procedure, as described in the following. A 2-mL UTEVA resin column was first conditioned with 7 mL of 3 M nitric acid in small volume increments (1 or 2 mL). Then, the nitric acid (3 M)-aluminum nitrate (1 M) solution was loaded onto the conditioned column in 2 mL increments and the purified solution, drained by gravity, collected in a fresh clean vial.

The original U-233 stock solution (5 mL, 25 µCi total, nominal activity) was carefully dried in a Savillex PFA vial on a hot plate. The glass vial, previously containing the original stock, was rinsed with 4 mL, and then 2-times 3 mL of 5 M nitric acid. After each rinse, the individual rinse solutions were dried in the same Savillex vial. Then, U-233 was redissolved in 10 mL of 5 M nitric acid, and dried again. Finally, U-233 was dissolved in 10 mL of 3 M nitric acid-1 M aluminum nitrate solution plus 1 mL of 3.5 M $NaNO_2$. The latter was added to ensure a +6 oxidation state of U-233 in the final, purified stock.

A new 2-mL UTEVA resin column was preconditioned with 4-times 2 mL of 3 M nitric acid. Then, the solution containing U-233 was loaded onto the column in 2 mL increments, and the column effluent, which is expected to contain Ra-225, Ac-225 and possibly other impurities, collected as waste. Up to the loading of the U-233 solution, all solutions were eluted from the resin column by gravity. However, after this step, gravity-based flow-rates decreased and solutions had to be gently loaded by hand with syringes (2-mL NORM-JECT Luer sterile syringes), while ensuring sufficiently slow flow-rates (~1 mL/min.).

Next, the Savillex vial, used to dry the original U-233 stock, was rinsed with 3-times 2 mL of 3 M HNO_3, and the rinse solutions loaded onto the UTEVA column as well. This was followed by column rinses with three different types of solutions, all added in small volume increments: (1) 5 mL of 3 M HNO_3, (2) 15 mL of 8 M HNO_3, and (3) 5 mL of 9 M HCl. With the last rinse, the column resin was converted to the chloride system, and some Np and Th is expected to be removed in the process. During all of these rinses, column effluents were collected as waste. In the next step, Th-229 was removed from the column by eluting with 7-times 3 mL of 5 M HCl-0.05 M oxalic acid.

Finally, the purified U-233 was eluted from the column into three separate Savillex vials, using 5-times 2 mL of 1 M HCl (stock #1), 5-times 2 mL of 1 M HCl (stock #2), 5-times 2 mL of 0.5 M HCl (stock #3). Exact volumes of the eluted stock solutions were calculated based on weight differences before and after filling of the vials. Liquid scintillation counting (PerkinElmer Liquid Scintillation Analyzer Tri-Carb 2900TR; Ultima Gold XR liquid scintillation cocktail) of small volumes of each stock (5, 10 and 15 µL)

determined specific activities of 0.61 µCi/mL (stock #1), 1.61 µCi/mL (stock #2) and 0.30 µCi/mL (stock #3) of U-233. The recovery of U-233 during the purification procedure was estimated at 100%.

A-7. Montmorillonite Pre-Equilibration with pH Conditions

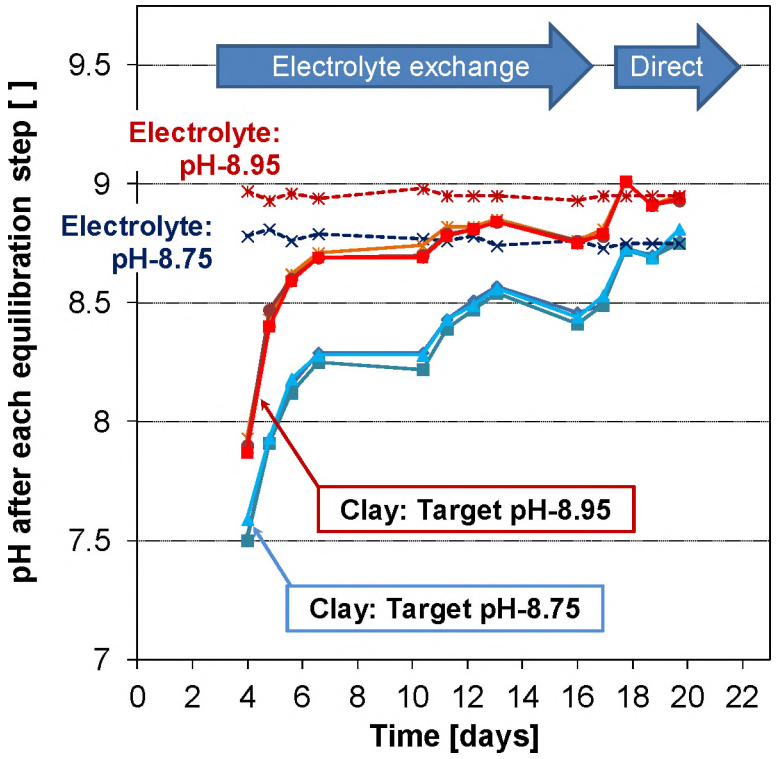

Figure A-8. Overview of pH-equilibration of Na-montmorillonite in preparation for uranium(VI) experiments. Large, blue arrows indicate changes in the equilibration procedure from the exchange of background electrolyte solutions to a direct pH adjustment with HCl and NaOH solutions. Dashed lines show pH conditions in solid-free electrolyte control solutions during the pre-equilibration procedure.

A-8 Elemental Composition of Na-Montmorillonite (SWy-2) Before and After Purification and pH Pre-Equilibration

Oxide	Composition (wt %)			
	Original SWy-2	Purified SWy-2	Purified SWy-2, pH-8.75	Purified SWy-2, pH-8.95
SiO_2	59.1	56.8	52.6	52.2
Al_2O_3	17.5	20.4	18.8	18.7
Fe_2O_3	3.60	4.11	3.83	3.81
MgO	2.3	2.3	2.2	2.1
CaO	1.5	n. d.	n. d.	n. d.
Na_2O	1.3	2.4	5.4	5.3
K_2O	0.66	0.17	0.68	0.83
TiO_2	0.13	0.09	0.08	0.08
P_2O_5	0.05	n. d.	n. d.	n. d.
MnO	0.02	n. d.	n. d.	n. d.

A-9 Schematic of Experimental Setup for Through-Diffusion Experiments

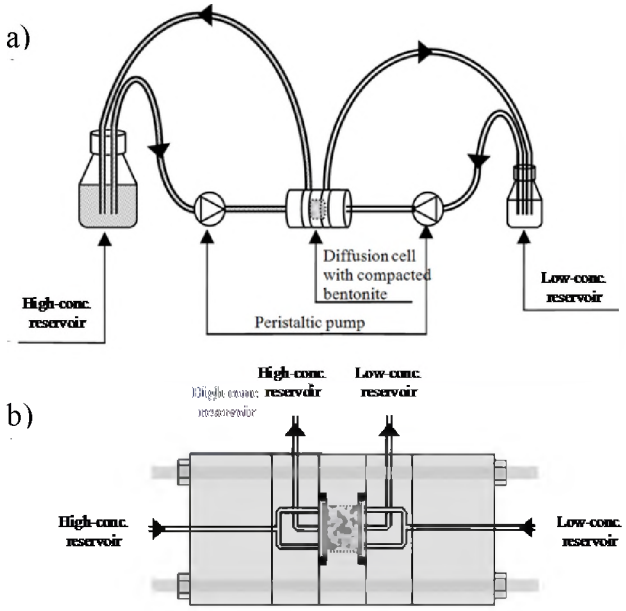

Figure A-9. Schematic of the experimental apparatus for uranium(VI) diffusion studies.